Effect of Indium and Niobium Segregation on the Surface vs. Bulk Chemistry of Titanium Dioxide (Rutile)

A thesis by

Armand Jason Atanacio

Submitted in partial fulfilment of the requirements for the degree of

Doctor of Philosophy (PhD)

Solar Energy Technologies Group
School of Computing, Engineering and Mathematics
University of Western Sydney, Australia
June 2013

"Take this to heart. Do what I tell you…live!
Sell everything and buy Wisdom! Forage for Understanding!
Don't forget one word! Don't deviate an inch!
Never walk away from Wisdom…she guards your life;
love her…she keeps her eye on you.
Above all and before all, do this: Get Wisdom!
Write this at the top of your list: Get Understanding!
Throw your arms around her…believe me, you won't regret it;
never let her go…she'll make your life glorious.
She'll garland your life with grace,
she'll festoon your days with beauty."

Proverbs 4:4-9 (msg)

Acknowledgements

I have come to realise that accomplishments cannot be attained without first being given opportunities to achieve. I am therefore sincerely thankful for all of the opportunities I have been given that have enabled me to accomplish this degree.

Firstly to my parents, Armando and Lydia, and sister, Marissa, who instilled in me the importance of education, a love of music, and have been a constant source of encouragement over the years. Without music as an outlet for my frustration and emotion, I probably would have lost my sanity a long time ago.

I dedicate this thesis to my beautiful wife, Myms, and daughters, Aria and Zoey. I'm sure that when Myms married me in 2008, she really didn't comprehend how much time this PhD (on top of full-time work) would occupy my nights and weekends. I could not have completed this thesis without the love, support and many sacrifices of my family which gave me the freedom to accomplish this goal.

I want to thank Prof Kathryn Prince for seeing enough potential in me as a young inexperienced scientist all those years ago to not only give me a job, but also supporting my request to undertake this PhD candidature whilst working in her group full-time. As well as training me to operate the SIMS, she has been the source of many insightful discussions during the writing of this thesis.

I would like to thank A/Prof Tad Bak for all the times he helped me process samples when my work commitments meant I couldn't get back to the lab at the required time. Without his assistance, I'm sure I would still be in the lab performing experiments right now instead of writing these acknowledgements! I am also grateful also for his invaluable input during the development of the defect chemistry models derived as part of this work.

Most of all, I'm indebted to my principal PhD supervisor Prof Janusz Nowotny for the opportunity to work as part of his group on this research topic. He generously shared his wealth of knowledge and experience with me and was crucial in the development and direction of this thesis. I sincerely appreciate his mentorship and willingness to give up so many of his Fridays and weekends to spend with me discussing page-upon-page of raw data, plots and manuscript drafts.

I am very grateful to my ANSTO colleagues, Mr Ed Stelcer, Dr Mihail Ionescu and Dr Rainer Siegele, for training me to operate the accelerator, as well as patiently answering my many questions about IBA data processing and interpretation.

I am thankful also to Dr Leigh Sheppard for his assistance with experimental set-up during the initial stages of my candidature, Dr David Nelson for SIMS analysis and, Dr Bill Gong for XPS analysis.

Last but not least, I would like to acknowledge the significant support of my employer the Australian Nuclear Science and Technology Organisation (ANSTO) for providing me with one day per week to work on this PhD.

Statement of Authentication

The work presented in this thesis is, to the best of my knowledge and belief, original except as acknowledged in the text. I hereby declare that I have not submitted this material, either in full or in part, for a degree at this or any other institution.

.....

Armand J. Atanacio

Table of Contents

List of Figures

List of Tables

List of Abbreviations

$[A^z], [D^z]$	The concentration of acceptor and donor defects with valency z, respectively
A, D	Acceptor, donor
BE	Binding energy [eV] (XPS analysis)
Φ_S	Spectrometer work function (XPS analysis)
c_o, c(x,t)	Initial surface concentration and, the concentration at depth x or time t
$C_{\perp}$, $C_{\|\|}$	Diffusion perpendicular to c-axis, diffusion parallel to c-axis
C_z	Concentration of element with atomic number Z (PIXE analysis)
D	Diffusion coefficient [m^2/s]
D_o	Diffusion a pre-exponential factor
D	Detector efficiency (XPS analysis)
$\sigma(\theta)$	Differential scattering cross section
σ	Photoelectron cross section (XPS analysis)
e^-, h^+	Electron, hole
ECE	Energy conversion efficiency
Erf, erfc	Error function and Error function compliment, respectively
E_a	Activation energy [kJ/mol]
E_g	Band gap [eV]
E_F	Fermi energy [eV]
E_{CB}, E_{VB}	Conduction band edge energy, valence band edge energy [eV]
E_A, E_D	Acceptor edge energy level, donor edge energy level
f	Enrichment factor (surface-to-bulk ratio)
F_{RSF}	Relative sensitivity factor
I, Y	Intensity (counts), Yield (counts)

I	Photoelectron peak area (XPS analysis)
$I_z(E_{K\alpha})$	Counts in principal K_α peak of element with atomic number Z (PIXE analysis)
J	X-ray flux (XPS analysis)
$J(E_{K\alpha})$	Sensitivity function (PIXE analysis)
KPP	Key performance properties
k	Kinematic factor (RBS analysis)
K_1	Equilibrium constant associated with the formation of $V_O^{\bullet\bullet}$
K_2	Equilibrium constant associated with the formation of $Ti_i^{\bullet\bullet\bullet}$
K_3	Equilibrium constant associated with the formation of $V_{Ti}^{''''}$
K_4	Equilibrium constant associated with the formation of $Ti_i^{\bullet\bullet\bullet\bullet}$
K_i	Equilibrium constant for intrinsic ionisation
L	Orbital symmetry factor (XPS analysis)
λ	Inelastic mean free path (XPS analysis)
m	Mass
m	Gradient
M	Total mass density of target (PIXE analysis)
MO	Metal oxide
$\mu_x(d)$	Chemical potential at distance, d
$\psi_x(d)$	Electrical potential at distance, d
Ω	Solid angle
n, p	Concentration of electrons and holes, respectively
N	Number of target atoms per unit volume (RBS analysis)
$\eta_x(d)$	Electrochemical potential at distance, d
PIXE	Proton induced x-ray emission
$p(O_2)$	Oxygen activity [Pa]

(PC), (SC)	Poly-crystal, single-crystal
R	Ideal gas constant
RBS	Rutherford backscattering
SIMS	Secondary ion mass spectrometry
[S]	Energy loss factor (RBS analysis)
T	Temperature [K]
T	Analyser transmission efficiency (XPS analysis)
t	Time
TGA	Thermal gravimetric analysis
V	Lattice vacancy
Q[C]	Charge collected during PIXE analysis
Q	Total incident projectiles (RBS analysis)
Δx	Target thickness (RBS analysis)
x	Distance or depth
XPS	X-ray photoelectron spectroscopy
XRD	X-ray diffraction

Abstract

Since the landmark paper in 1972 by Fujishima and Honda [1], TiO_2 has become one of the most promising candidates of a new generation of solar energy materials capable of generating clean hydrogen fuel using only sunlight (photo-electrochemically) to dissociate water.

TiO_2 has both bulk properties and surface properties which contribute to its functional performance. Considering that all of the electrochemical reactions induced by light occur at the surface of TiO_2, it becomes clear that understanding the surface properties of TiO_2 is of crucial importance for its performance; specifically the conversion of solar energy into chemical energy.

The surface phase of TiO_2 can be substantially different from that of the bulk phase as a result of a phenomenon known as segregation. Segregation involves the transport of certain lattice species from the bulk phase to the surface, driven by excess surface energy.

To date, developments in the understanding of TiO_2 solid solutions and related properties have mainly been centred on bulk properties. In comparison, relatively little work has been reported on segregation in TiO_2 solid solutions and its influence on functional properties, such as reactivity and photoreactivity.

The present work has studied the effect of indium (acceptor-type ion) and niobium (donor-type ion) segregation on the surface chemistry of well-defined In-doped and Nb-doped TiO_2 solid solutions. Specifically, examining the relationship between imposed sample processing conditions, such as the gas phase oxygen activity, on segregation-induced surface enrichment. This was achieved using a range of complimentary analysis techniques including X-ray photoelectron spectroscopy (XPS), secondary ion mass spectrometry (SIMS), Rutherford backscattering (RBS) and proton-induced X-ray emission (PIXE).

In-doped TiO_2

The incorporation of dopants in TiO_2 results in a change of Fermi level and related semiconducting properties. However, to achieve well-defined solid solutions, in which the dopant is homogeneously distributed throughout the bulk phase, requires knowledge of the dopant ion diffusion coefficients [2-7]. The present work included the determination of the self-diffusion coefficient of indium in TiO_2 single crystal (rutile) in the temperature range 1073 - 1573 K and p(O2) = 21 kPa.

$$D_{In-TiO_2} = 7.4\times10^{-4}\exp\left(\frac{-316\,kJ/mol}{RT}\right)\left[m^2 s^{-1}\right]$$

The determination of this new data enables us to predict the processing conditions required to incorporate In into the TiO_2 lattice.

The effect of oxygen activity on the segregation-induced surface concentration of indium in In-doped TiO_2 was studied for various annealing times, ranging between 5 h and 120 h, at 1273 K. It was shown that the equilibrium segregation of indium in oxidising conditions, $p(O_2)$ = 21 kPa, can be established within ~20 h. However, in highly reducing conditions, $p(O_2) = 10^{-10}$ Pa, equilibrium could not be established due to indium evaporation, which becomes substantial at $p(O_2) < 1.8x10^2$ kPa.

The present work examined the effect of indium (acceptor) segregation on the surface vs. bulk composition of In-doped TiO_2. The data determined that annealing of 0.3 at% In-doped TiO_2 at 1273 K in oxygen activity, $p(O_2)$ = 75 kPa and $p(O_2)$ = 10 Pa, resulted in an enrichment of the surface to the level of 2.95 at% In and 2.61 at% In, respectively. It was postulated that substantial In surface enrichment leads to the formation of a low-dimensional surface structure and a sub-surface layer resulting from the interactions of titanium vacancies and interstitial indium ions.

Nb-doped TiO_2

The present work also studied the effect of niobium (donor) segregation on the surface and near-surface composition of Nb-doped TiO_2 (0.18 at% Nb and 0.018 at% Nb). The data showed that 0.18 at% Nb-doped TiO_2 specimens annealed at 1273 K in oxidising conditions, $p(O_2)$ = 75 kPa and $p(O_2)$ = 10 Pa, resulted in segregation-enriched surface concentrations of 2.83 at% and 2.35 at%, respectively. However, annealing the same specimen in strongly reducing conditions, $p(O_2) = 10^{-10}$ Pa, resulted in a depletion of the surface to the level of 0.05 at% Nb (desegregation). The theoretical model postulated in this work considered the predominant driving force for niobium segregation in oxidising conditions is the negative surface charge associated with titanium vacancies formed in the surface layer. However, the effect of desegregation is induced by a positive surface charge related to a Magneli-type surface structure formed in strongly reducing conditions.

The present work provides new well-defined empirical data on segregation. The derived theoretical models describing the effect of processing conditions on indium and niobium segregation/desegregation can be used as a technology for the imposition of controlled surface composition. The related data can be used for imposition of a chemically-induced electric field required for charge separation and controlled surface composition that is required to achieve desired reactivity of TiO_2 as photocatalyst and photoelectrode for solar energy conversion.

References

(1) Fujishima, A.; Honda, K. "Electrochemical Photolysis of Water at a Semiconductor Electrode". Nature (1972), 238, 37-38.

(2) Akse, J. R.; Whitehurst, H. B. "Diffusion of titanium in slightly reduced rutile". J. Phys. Chem. Solids (1978), 39 [5], 457-465.

(3) Hoshino, K.; Peterson, N. L.; Wiley, C. L. "Diffusion and point defects in TiO_{2-x}". J. Phys. Chem. Solids (1985), 46 [12], 1397-1411.

(4) Lundy, T. S.; Coghlan, W. A. "Cation self diffusion in rutile". Journal de Physique Colloques (1973), C9, 299-302.

(5) Peterson, N. L.; Sasaki, J. Mechanisms of impurity diffusion in rutile. In Transport in Nonstoichiometric Compounds; Simkovich, G., Stubican, V. S., Eds.; Plenum Press: New York, (1985); pp 269-284.

(6) Sasaki, J.; Peterson, N. L.; Hoshino, K. "Tracer impurity diffusion in single-crystal rutile (TiO_{2-x})". J. Phys. Chem. Solids (1985), 46 [11], 1267-1283.

(7) Venkatu, D. A.; Poteat, L. E. "Diffusion of titanium of single crystal rutile". Materials Science and Engineering (1970), 5 [5], 258-262.

CHAPTER 1

Postulation of the Thesis

1.1 Why Titanium Dioxide (TiO_2)?

Titanium dioxide, TiO_2 (titania) is an extremely abundant material typically extracted from the naturally occurring minerals, rutile and ilmenite. It has most commonly been used in powder form as a white pigment or opacifier in a wide range of applications including paints, cosmetics, toothpaste and food. Australia in particular has a large amount of ilmenite sands and consequently supplies approximately 40% of the world's ilmenite and 25% of its rutile requirements.

In 1972 the pioneering research of Fujishima and Honda [1] identified TiO_2 as a promising candidate for a new generation of solar energy materials, and essentially paved the way for an entirely new range of applications for titania. Since then, TiO_2 has been the focus of intense research for applications including solar energy conversion [1-18], gas sensors [19-22], self-cleaning surfaces [6,23] and water purification [24-27].

The significant advantages of titania compared with other solar energy materials, include its low cost, owing to its abundance, and its resistance to corrosion and photo-corrosion in water.

1.2 Solar Energy Conversion Using TiO_2

Titania can be used for the conversion of solar energy into chemical energy via water oxidation (partial or total). Partial water oxidation results in the formation of active radicals, which have the capacity to remove microorganisms and organic contaminants from water. However, total water oxidation results in the generation of hydrogen, which can be used as an environmentally friendly fuel. Furthermore, unlike other available environmentally friendly energy sources, such as photovoltaics, wind and geothermal, which generate electricity that must

be used immediately as it is produced; hydrogen is a storable energy. This means that it can be stored, transported and used when required in a similar fashion to the way our society currently utilise fossil fuels. However, a significant hindrance to hydrogen is that it is not naturally available as a gas in nature. Consequently, hydrogen has to be extracted from hydrogen rich compounds, such as water. Unfortunately, while the extracted hydrogen is considered to be an environmentally friendly fuel, most of the current commercially available extraction methods for hydrogen are not. Therefore, the negative impact to the environment is not eliminated, but simply displaced from the point of use to the point of generation. The significant advantage of solar-hydrogen is that hydrogen can be obtained using only sunlight. Therefore, the race is on to optimise and commercialise solar-hydrogen technology as an alternative means of generating environmentally friendly fuel. TiO_2 is one of the most promising materials capable of extracting hydrogen cleanly and renewably by the direct photoelectrolysis of water using only sunlight.

The present work forms part of a wider research program in the Solar Energy Technologies Group at the University of Western Sydney. This program aims at increasing the efficiency with which TiO_2 converts solar energy into chemical energy by optimising several key-performance-related properties (KPP). It has been postulated that the KPPs are [5]:

- **Band gap.** TiO_2 exhibits a relatively large band gap of 3 eV. This limits its absorption of the solar spectrum to the ultraviolet wavelength. Much of the research effort has therefore been focused on trying to modify the properties of TiO_2 in such a way as to reduce the band gap from 3 eV to approximately 2 eV to increase visible light absorption.
- **Charge transport.** Pure titania is a good insulator. This results in high energy losses related to charge transport. Therefore, research is aimed at increasing charge transport and minimising the resistance-related energy losses.
- **Flat band potential.** The flat band potential (FBP) is related to the potential drop across the TiO_2/electrolyte interface, which results in charge separation. The FBP must be optimised in order to achieve maximised performance.
- **Surface properties.** The surface of TiO_2 must exhibit the required surface sites to form the active complexes necessary for water splitting. Therefore, studies are needed to understand the surface, in terms of defects, in order to optimise the reactivity between TiO_2 and H_2O.

It is important to note that these KPPs are also inter-related. Therefore, in order to optimise the KPPs to obtain maximum TiO_2 performance, knowledge of each KPP as well as their interdependence to the other KPPs must first be addressed.

So far, little is known about the surface properties that are needed to enhance the performance of TiO_2. Therefore, research is needed to increase the present level of understanding regarding the effect of surface modification, including structure, composition and electrical properties; on solar energy conversion performance.

1.2.1. Effect of Surface on Solar Energy Conversion

The properties of TiO_2 can be considered in terms of bulk properties and surface properties. While the bulk properties of TiO_2 have already been assessed at length in literature [28-40], the influence of surface properties and their effect on reactivity and photoreactivity is still unclear. However, when one considers that all of the electrochemical reactions induced by light take place on the surface of TiO_2, clearly the understanding of surface properties becomes crucially important for optimising the conversion of solar energy into chemical energy.

A frequently used strategy for modifying the properties of TiO_2 is based on the incorporation of aliovalent ions (doping). However, awareness is growing that doping can result in a different modification of the surface phase compared with the bulk phase. In other words, the properties of the surface can differ significantly from the bulk phase in terms of chemical composition, structure and related properties. The effect responsible for this difference is a phenomenon known as segregation [41-44].

Surface segregation refers to the diffusional transport of certain lattice elements, such as dopants or impurities; from the bulk to the surface during sample processing at elevated temperature. This phenomenon has already been extensively studied for metallic systems and the theory is now at a stage that experimental results can be predicted quite accurately with modelling software [45]. However, little is still understood about surface segregation in nonstoichiometric metal oxides, such as TiO_2. This is due to additional charge-related and gas phase complexities which are not present in metallic systems. Consequently, the effect of segregation in TiO_2, often unaccounted for in literature, could be a contributing factor in the frequent contradiction of the properties reported for doped-TiO_2.

It is important to note that segregation not only results in an enrichment of the topmost surface, but also forms a compositional concentration gradient in the near-surface (or sub-surface) layer. Consequently, these segregation-induced concentration gradients can result in the formation of chemically-induced electric fields, which may influence charge separation. Therefore, there is an urgent need to understand the phenomenon of segregation in oxides,

including TiO_2, and its effects on the surface and near-surface composition. The aim of this PhD research project is to address this need.

The overall aim of this PhD research project is to examine the largely unknown phenomena of cation segregation in TiO_2. It is believed that understanding the phenomenon of segregation induced surface enrichment is a critical step toward the formation of systems with enhanced performance.

The specific objective of the present work is to determine the effect of segregation on both donor- and acceptor-type dopants in terms of the surface and near-surface chemistry of TiO_2.

For this work niobium was selected as the donor-type cation. While the effect of niobium on the bulk properties of Nb-doped TiO_2 has already been reported [46-55], so far little is known of the effect of segregation on surface properties.

On the other hand, indium was selected as the acceptor-type cation for this work. Conflicting reports of both improved and diminished photocatalytic performance have been documented in literature for In_2O_3-TiO_2 systems [56-60].

1.4 References

(1) Fujishima, A.; Honda, K. "Electrochemical Photolysis of Water at a Semiconductor Electrode". Nature (1972), 238, 37-38.

(2) Agrios, A. G.; Pichat, P. "State of the art and perspectives on materials and applications of photocatalysis over TiO_2". Journal of Applied Electrochemistry (2005), 35 [7-8], 655-663.

(3) Aroutiounian, V. M.; Arakelyan, V. M.; Shahnazaryan. "Metal oxide photoelectrodes for hydrogen generation using solar radiation-driven water splitting". Sol. Energy (2005), 78, 581-592.

(4) Babu, K. S. C.; Singh, D.; Srivastava, O. N. "Investigations on the mixed-oxide material TiO_2-In_2O_3 in regard to photoelectrolytic hydrogen-production". Semicond. Sci. Technol. (1990), 5 [4], 364-368.

(5) Bak, T.; Nowotny, J.; Rekas, M.; Sorrell, C. C. "Photo-electrochemical hydrogen generation from water using solar energy. Materials-related aspects". International Journal of Hydrogen Energy (2002), 27 [10], 991-1022.

(6) Hashimoto, K.; Irie, H.; Fujishima, A. "TiO_2 Photocatalysis: A Historical Overview and Future Prospects". Jpn. J. Appl. Phys. (2005), 44 [12], 8269-8285.

(7) Hu, C. C.; Lee, Y. L.; Teng, H. S. "Influence of Indium Doping on the Activity of Gallium Oxynitride for Water Splitting under Visible Light Irradiation". Journal of Physical Chemistry C (2011), 115 [6], 2805-2811.

(8) Kelly, N. A.; Gibson, T. L. "Design and characterisation of a robust photoelectrochemical device to generate hydrogen using solar water splitting". International Journal of Hydrogen Energy (2006), 31, 1658-1673.

(9) Khan, S. U. M.; Al-Shahry, M.; Ingler Jr, W. B. "Efficient photochemical water splitting by a chemically modified n-TiO_2". Science (2002), 297, 2243-2245.

(10) Khaselev, O.; Turner, J. A. "A monolithic photovoltaic-photoelectrochemical device for hydrogen production via water splitting". Science (1998), 280 [5362], 425-427.

(11) Kudo, A. "Development of photocatalyst materials for water splitting". International Journal of Hydrogen Energy (2006), 31, 197-202.

(12) Licht, S. "Solar water splitting to generate hydrogen fuel - a photothermal electrochemical analysis". International Journal of Hydrogen Energy (2005), 30, 459-470.

(13) Ni, M.; Leung, M. K. H.; Leung, D. Y. C.; Sumathy, K. "A review and recent developments in photocatalytic water-splitting using TiO_2 for hydrogen production". Renew. Sust. Energ. Rev. (2007), 11 [3], 401-425.

(14) Nowotny, J.; Bak, T.; Nowotny, M. K.; Sheppard, L. R. "TiO_2 surface active sites for water splitting". Journal of Physical Chemistry B (2006), 110 [37], 18492-18495.

(15) Nowotny, J.; Bak, T.; Nowotny, M. K.; Sheppard, L. R. "Titanium dioxide for solar-hydrogen I. Functional properties". International Journal of Hydrogen Energy (2007), 32 [14], 2609-2629.

(16) Nowotny, J.; Bak, T.; Nowotny, M. K.; Sheppard, L. R. "Titanium dioxide for solar-hydrogen IV. Collective and local factors in photoreactivity". International Journal of Hydrogen Energy (2007), 32 [14], 2651-2659.

(17) Park, J. H.; Bard, A. J. "Unassisted water splitting from bipolar Pt/dye-sensitised TiO_2 photoelectrode arrays". Electrochemical and Solid-State Letters (2005), 8 [12], G371-G375.

(18) Zou, Z. G.; Ye, J. H.; Sayama, K.; Arakawa, H. "Direct splitting of water under visible light irradiation with an oxide semiconductor photocatalyst". Nature (2001), 414 [6864], 625-627.
(19) Kajihara, K.; Yao, T. "Oxygen detection in sol-gel derived titania thin films doped with tantalum". Phys. Chem. Chem. Phys. (1999), 1 [8], 1979-1983.
(20) Rothschild, A.; Edelman, F.; Komen, Y.; Cosandey, F. "Sensing behaviour of TiO_2 thin films exposed to air at low temperatures". Sensors and Actuators B (2000), 67.
(21) Ruiz, A. M.; Sakai, G.; Cornet, A.; Shimanoe, K.; Morante, J. R.; Yamazoe, N. "Cr-doped TiO_2 gas sensor for exhaust NO2 monitoring". Sens. Actuator B-Chem. (2003), 93 [1-3], 509-518.
(22) Zakrzewska, K.; Radecka, M.; Rekas, M. "Effect of Nb, Cr, Sn additions on gas sensing properties of TiO_2 thin films". Thin Solid Films (1997), 310 [1–2], 161-166.
(23) Tryk, D. A.; Fujishima, A.; Honda, K. "Recent topics in photoelectrochemistry: achievements and future prospects". Electrochimica Acta (2000), 45 [15-16], 2363-2376.
(24) Bak, T.; Nowotny, J.; Sucher, N. J.; Wachsman, E. "Effect of Crystal Imperfections on Reactivity and Photoreactivity of TiO_2 (Rutile) with Oxygen, Water, and Bacteria". The Journal of Physical Chemistry C (2011), 115 [32], 15711-15738.
(25) Crisan, M.; Braileanu, A.; Raileanu, M.; Zaharescu, M.; Crisan, D.; Dragan, N.; Anastasescu, M.; Ianculescu, A.; Nitoi, I.; Marinescu, V. E.; Hodorogea, S. M. "Sol-gel S-doped TiO_2 materials for environmental protection". J. Non-Cryst. Solids (2008), 354 [2-9], 705-711.
(26) Robert, D.; Malato, S. "Solar photocatalysis: a clean process for water detoxification". Sci. Total Environ. (2002), 291 [1-3], 85-97.
(27) Vidal, A.; Diaz, A. I.; El Hraiki, A.; Romero, M.; Muguruza, I.; Senhaji, F.; Gonzalez, J. "Solar photocatalysis for detoxification and disinfection of contaminated water: pilot plant studies". Catalysis Today (1999), 283-290.
(28) Bak, T.; Burg, T.; Kang, S. J. L.; Nowotny, J.; Rekas, M.; Sheppard, L.; Sorrell, C. C.; Vance, E. R.; Yoshida, Y.; Yamawaki, M. "Charge transport in polycrystalline titanium dioxide". J. Phys. Chem. Solids (2003), 64 [7], 1089-1095.
(29) Bak, T.; Nowotny, J.; Nowotny, M. K. "Defect disorder of titanium dioxide". Journal of Physical Chemistry B (2006), 110 [43], 21560-21567.
(30) Bak, T.; Nowotny, J.; Rekas, M.; Sorrell, C. C. "Defect chemistry and semiconducting properties of titanium dioxide: I. Intrinsic electronic equilibrium". J. Phys. Chem. Solids (2003), 64 [7], 1043-1056.
(31) Bak, T.; Nowotny, J.; Rekas, M.; Sorrell, C. C. "Defect chemistry and semiconducting properties of titanium dioxide: II. Defect diagrams". J. Phys. Chem. Solids (2003), 64 [7], 1057-1067.
(32) Bak, T.; Nowotny, J.; Rekas, M.; Sorrell, C. C. "Defect chemistry and semiconducting properties of titanium dioxide: III. Mobility of electronic charge carriers". J. Phys. Chem. Solids (2003), 64 [7], 1069-1087.
(33) Bak, T.; Nowotny, M. K.; Sheppard, L. R.; Nowotny, J. "Effect of prolonged oxidation on semiconducting properties of titanium dioxide". Journal of Physical Chemistry C (2008), 112 [34], 13248-13257.
(34) Nowotny, J.; Bak, T.; Nowotny, M. K.; Sheppard, L. R. "Titanium dioxide for solar-hydrogen II. Defect chemistry". International Journal of Hydrogen Energy (2007), 32 [14], 2630-2643.
(35) Nowotny, J.; Bak, T.; Nowotny, M. K.; Sheppard, L. R. "Defect Chemistry and Electrical Properties of Titanium Dioxide. 2. Effect of Aliovalent Ions". Journal of Physical Chemistry C (2008), 112, 602-610.

(36) Nowotny, M. K.; Bak, T.; Nowotny, J. "Electrical properties and defect chemistry of TiO_2 single crystal. I. Electrical conductivity". Journal of Physical Chemistry B (2006), 110 [33], 16270-16282.
(37) Nowotny, M. K.; Bak, T.; Nowotny, J. "Electrical properties and defect chemistry of TiO_2 single crystal. II. Thermoelectric power". Journal of Physical Chemistry B (2006), 110 [33], 16283-16291.
(38) Nowotny, M. K.; Bak, T.; Nowotny, J. "Electrical properties and defect chemistry of TiO_2 single crystal. III. Equilibration kinetics and chemical diffusion". Journal of Physical Chemistry B (2006), 110 [33], 16292-16301.
(39) Nowotny, M. K.; Bak, T.; Nowotny, J. "Electrical properties and defect chemistry of TiO_2 single crystal. IV. Prolonged oxidation kinetics and chemical diffusion". Journal of Physical Chemistry B (2006), 110 [33], 16302-16308.
(40) Nowotny, M. K.; Sheppard, L. R.; Bak, T.; Nowotny, J. "Defect chemistry of titanium dioxide. application of defect engineering in processing of TiO_2-based photocatalysts". Journal of Physical Chemistry C (2008), 112 [14], 5275-5300.
(41) Burggraaf, A. J.; Winnubst, A. J. A. Segregation in Oxide Surfaces, Solid Electrolytes and mixed Conductors. In Surface and Near-Surface Chemistry of Oxide Materials; Elsevier: Amsterdam, (1988); pp 448-477.
(42) Cabane, J.; Cabane, F. Equilibrium segregation in interfaces. In Interface segregation and related processes in materials; Nowotny, J., Ed.; Trans Tech Publications Ltd.: Zurich, (1991); pp 1-150.
(43) Nowotny, J. Inteface defect chemistry and its impact on properties of oxide ceramic materials. In Science of Ceramic Interfaces; Nowotny, J., Ed.; Elsevier Science Publishers B.V., (1991); pp 79-204.
(44) Wynblatt, P.; McCune, R. C. Surface Segregation in Metal Oxides. In Surface and Near-Surface Chemistry of Oxide Materials; Elsevier Science Publishers, (1988); pp 247-279.
(45) Yoshitake, M. "Prediction of Influence of Oxygen in Annealing Atmosphere on Surface Segregation Behavior in Layered Materials". Jpn. J. Appl. Phys. (2012), 51 [8].
(46) Bernasik, A.; Radecka, M.; Rekas, M.; Sloma, M. "Electrical properties of Cr-doped and Nb-doped TiO_2 Thin-films". Applied Surface Science (1993), 65-6, 240-245.
(47) Bouchet, R.; Weibel, A.; Knauth, P.; Mountjoy, G.; Chadwick, A. V. "EXAFS study of dopant segregation (Zn, Nb) in nanocrystalline anatase (TiO_2)". Chemistry of Materials (2003), 15 [26], 4996-5002.
(48) Ruiz, A.; Dezanneau, G.; Arbiol, J.; Cornet, A.; Morante, J. R. "Study of the influence of Nb content and sintering temperature on TiO_2 sensing films". Thin Solid Films (2003), 436 [1], 90-94.
(49) Pang, Y.; Wynblatt, P. "Correlation between grain-boundary segregation and grain-boundary plane orientation in Nb-doped TiO_2". Journal of the American Ceramic Society (2005), 88 [8], 2286-2291.
(50) Wang, M. H.; Guo, R. J.; Tso, T. L.; Perng, T. P. "Effects of sintering on the photoelectrochemical properties of Nb-doped TiO_2 electrodes". International Journal of Hydrogen Energy (1995), 20 [7], 555-560.
(51) Nakajima, T.; Sheppard, L. R.; Prince, K. E.; Nowotny, J.; Ogawa, T. "Niobium segregation in TiO_2". Adv. Appl. Ceram. (2007), 106 [1], 1-7.
(52) Sheppard, L. R.; Bak, T.; Nowotny, J.; Nowotny, M. K. "Titanium dioxide for solar-hydrogen V. Metallic-type conduction of Nb-doped TiO_2". International Journal of Hydrogen Energy (2007), 32 [14], 2660-2663.
(53) Baumard, J. F.; Tani, E. "Electrical-conductivity and charge compensation in Nb doped TiO_2 rutile ". J. Chem. Phys. (1977), 67 [3], 857-860.

(54) Choi, W. Y.; Termin, A.; Hoffmann, M. R. "The role of metal-ion dopants in quantam-sized TiO_2 - Correlation between photoreactivity and charge-carrier recombination dynamics". Journal of Physical Chemistry (1994), 98 [51], 13669-13679.

(55) Lee, S.-M.; Guo, R.-J.; Tso, T.-L.; Perng, T.-P. "Photoelectrochemical response and surface variation of TiO_2 electrodes irradiated with laser light". International Journal of Hydrogen Energy (1996), 21 [4], 253-257.

(56) Karn, R. K.; Srivastava, O. N. "On the structural and photochemical studies of In_2O_3 admixed nanostructured TiO_2 with regard to hydrogen production through photoelectrolysis". International Journal of Hydrogen Energy (1998), 23 [6], 439-444.

(57) Shchukin, D.; Poznyak, S.; Kulak, A.; Pichat, P. "TiO_2-In_2O_3 photocatalysts: preparation, characterisations and activity for 2-chlorophenol degradation in water". Journal of Photochemistry and Photobiology A - Chemistry (2004), 162 [2-3], 423-430.

(58) Skorb, E. V.; Ustinovich, E. A.; Kulak, A. I.; Sviridov, D. V. "Photocatalytic activity of TiO_2 : ln2O3 nanocomposite films towards the degradation of arylmethane and azo dyes". J. Photochem. Photobiol. A-Chem. (2008), 193 [2-3], 97-102.

(59) Wang, E. J.; Yang, W. S.; Cao, Y. A. "Unique Surface Chemical Species on Indium Doped TiO_2 and Their Effect on the Visible Light Photocatalytic Activity". Journal of Physical Chemistry C (2009), 113 [49], 20912-20917.

(60) Yang, X.; Wang, Y. H.; Xu, L. L.; Yu, X. D.; Guo, Y. H. "Silver and indium oxide codoped TiO_2 nanocomposites with enhanced photocatalytic activity". Journal of Physical Chemistry C (2008), 112 [30], 11481-11489.

CHAPTER 2

Definition of Terms

2.1 Band Model

Electrons which surround an atom occupy orbitals (or shells) that form a defined set of energy levels. When a large number of these atoms are involved in a periodic lattice, the large number of related orbitals (i.e. energy states) can be considered as continuous bands. Of particular significance for the photoelectrochemical properties of semiconductors is the highest occupied energy band, known as the valance band, and the lowest unoccupied energy band, known as the conduction band. The "space" between these bands is referred to as the band gap. Therefore, the band gap can be described as the smallest energy difference between the top of the valence band and the bottom of the conduction band. The band gap determines the extent of electron interaction between bands and consequently the resulting electrical properties of the solid.

2.1.1. Fermi Level

An important parameter related to the band model is the Fermi Level. This can be defined as the energy level at which the occupation probability of an electron is 0.5. According to the Fermi-Dirac statistics, the probability of an electron occupying an energy state with respect to the Fermi level can be defined by [1]:

$$f(E) = \frac{1}{1 + \exp\frac{E - E_F}{kT}} \qquad \textbf{(2-1)}$$

Where f(E) is the probability that an the energy state E is occupied, E_F is the Fermil Level an T is absolute temperature.

The effect of electronic structure on the band model and Fermi level position are shown schematically in **Figure 2-1** and **Figure 2-2.**

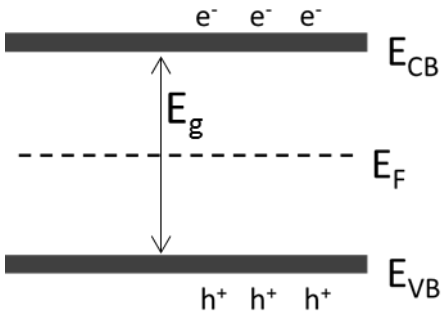

Figure 2-1. Schematic illustration of the semiconductor band model including valence band (E_{VB}), conduction band (E_{CB}), band gap (E_g), Fermi energy level (E_F), electons (e^-) and holes (h^+).

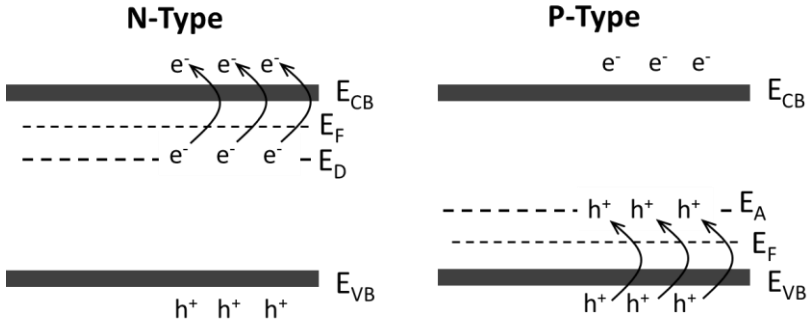

Figure 2-2. Illustration of the Fermi energy level modification associated with the presence of a donor energy level (E_D) or acceptor energy level (E_A) for N- and P-type semiconductors, respectively.

2.1.2. Photocatalytic Water Splitting

An schematic illustration of the light-induced ionisation mechanism and associated charge transfer is shown in **Figure 2-3.**

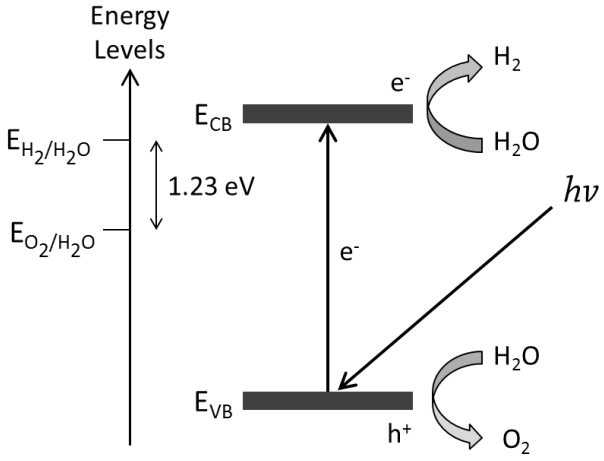

Figure 2-3. Mechanism for photocatalytic water splitting for hydrogen generation with TiO_2 [2]

2.2 Diffusion

Diffusion can be described as the transport of ions within a crystal lattice via periodic "jumping" of ions from one crystal lattice site to another. The segregation induced transport of lattice species occurs via diffusion. Diffusion in ionic crystals can be categorised into three main mechanisms: vacancy, interstitital and interstitialcy. The theory of diffusion in solids is both extensive and complex and cannot be addressed in detail here. Consequently, only the specific diffusion theories and equations directly relevant to this work will be provided. Comprehensive textbooks on diffusion are available elsewhere [3,4].

2.2.1. Thin Film Diffusion

The thin film diffusion scenario refers to a condition where a thin layer of solute is deposited on the sample surface that is initially free of solute. If annealing conditions are appropriate and there is reactivity between the surface solute and the solid, the solute will diffuse into the substrate. The key point in this scenario is the thin initial concentration of solute deposited on the surface (c_o) will decrease as a function of increasing diffusion time. Under these conditions the resulting diffusion concentration profile can be described by [4-6]:

$$c(x,t) = \frac{c_O}{2\sqrt{\pi Dt}} \exp\left(-\frac{x^2}{4Dt}\right) \qquad \textbf{(2-2)}$$

where c(x,t) is the concentration as a function of depth x and/or time t, and c_o is the initial deposited surface solute concentration. The resulting concentration profile can then be plotted as ln c(x,t) versus x^2 which should produce a straight line. The diffusion coefficient, D can then be determined from the gradient, m, of that line based on the following equation [6]:

$$D = -\frac{1}{m \times 4t} \qquad \textbf{(2-3)}$$

Note: **Equation (2-4)** can be used instead of **Equation (2-3)** if Log c vs. x^2 is plotted instead of the natural log, ln c vs x^2:

$$D = -\frac{1}{2.303 \times m \times 4t} \qquad \textbf{(2-4)}$$

2.2.2. Thick Film Diffusion

This diffusion scenario is similar to thin film diffusion (**Section 2.2.1**) except the high solute concentration in the thickly deposited surface layer remains constant over the entire diffusion time. The concentration profile in this case is described by [4,6]:

$$\frac{c(x,t)-c_1}{c_O-c_1} = \mathrm{erfc}\left(\frac{x}{2\sqrt{Dt}}\right) \qquad \textbf{(2-5)}$$

Where c_1 is the background concentration and erfc is the error function compliment. The resulting concentration profile can be used to plot $\mathrm{erfc}^{-1}\left(\frac{c(x,t)-c_1}{c_O-c_1}\right)$ versus x which will result in a linear relationship if the thick diffusion scenario is correct. D can then be determined from the gradient, m, of that linear region based on the following equation [6]:

$$D = \frac{1}{m^2 \times 4t} \qquad \textbf{(2-6)}$$

As diffusion is a thermally activated process, it can also be described with the following Arrhenius relationship [5,6]:

$$D = D_O \exp\left(-\frac{E_a}{RT}\right) \qquad \textbf{(2-7)}$$

where D_o is a pre-exponential factor, R is the ideal gas constant, T is the temperature.

Combining this Arrhenius relationship, **Equation (2-7)**, and the concentration c(x,t) determined at different temperatures from **Equations (2-2)** or **(2-5)** (depending on the applicable scenario), it becomes possible to calculate the activation energy , E_a.

Activation energy is the minimum energy required for ionic and electronic defects to migrate from one lattice position to another. It can be used to determine and compare how energetically favourable the diffusion of specific solute ions are in a particular lattice. Therefore, determining the activation energy for a solute in a given lattice system is critical for the correct interpretation of that same solute lattice system in relation to segregation.

2.3 Defect Chemistry

Point defects in metal oxides can be basically divided into two groups, intrinsic and extrinsic defects. Intrinsic defects refer to defects related to the native lattice components and include:

1. **Metal vacancy.** This is the case when the native lattice cation is missing from its usual lattice position, leaving an empty lattice site.
2. **Oxygen vacancy.** This is the case when the lattice oxygen is missing from its usual lattice position, leaving an empty lattice site.
3. **Interstitial cations.** This defect is formed when native lattice cation is transferred from its lattice position to an interstitial site (between regular lattice positions).

Kröger-Vink [7] notation of point defects (provided in **Table 2-1**) will be used in the present work to represent the reactions between defects.

Table 2-1. Kröger-Vink [7] notation of point defects in MO_2-type oxides

Valency Notation	Description	Kröger-Vink Notation
$\mathbf{M_M^{4+}}$	M^{4+} ion in a M^{4+} lattice site with neutral charge	$M_M^{\times}$
$\mathbf{O_O^{2-}}$	O^{2-} ion in a O^{2-} lattice site	$O_O^{\times}$
$\mathbf{M_M^{3+}}$	M^{3+} ion in its lattice site (electron)	e'
$\mathbf{M_M^{5+}}$	Pentavalent foreign (donor) cation on the M^{4+} cation lattice site	$D_M^{\bullet}$
$\mathbf{M_M^{3+}}$	Trivalent foreign (acceptor) cation in the M^{4+} cation lattice site	A_M'
$\mathbf{V_M}$	Cation vacancy	V_M''
$\mathbf{M_i^{3+}}$	Trivalent foreign cation in an interstitial lattice site	$D_i^{\bullet\bullet\bullet}$
$\mathbf{M_i^{4+}}$	M^{4+} ion in an interstitial lattice site	$D_i^{\bullet\bullet\bullet\bullet}$
$\mathbf{M_i^{5+}}$	Pentavalent foreign cation in an interstitial lattice site	$D_i^{\bullet\bullet\bullet\bullet\bullet}$
$\mathbf{V_O}$	Oxygen vacancy	$V_O^{\bullet\bullet}$
$\mathbf{O_O^{-}}$	Single-valent oxygen on its lattice site (electron hole)	$h^{\bullet}$

2.3.1. Defect Chemistry of TiO_2

TiO_2 is a nonstoichiometric oxide which is generally considered to be oxygen deficient as it contains predominantly oxygen vacancies and titanium interstitials in its defect disorder [1,8-11]. The presence of either oxygen vacancies or titanium interstitials both result in an apparent deficit in the oxygen lattice, consequently TiO_2 is often written as TiO_{2-x} or $Ti_{1+x}O_2$ which makes it an n-type semiconductor. However it was recently shown that Ti vacancies can also be formed after the imposition of prolonged oxidation [12]. These Ti vacancies are form acceptor-type centres that may result in p-type semiconducting properties if their concentration and degree of ionisation is

sufficiently high [12]. Consequently, this scenario may be written as TiO_{2+x} or $T_{1-x}O_2$ which denotes p-type semiconductivity.

The formation of defects in TiO_2 can be therefore be represented by the following defect equilibria (using the Kröger-Vink notation, defined in

Table 2-1) [9]:

$$O_O^X \leftrightarrow V_O^{\bullet\bullet} + 2e' + \frac{1}{2}O_{2(gas)\uparrow} \quad \textbf{(2-8)}$$

$$Ti_{Ti}^X + 2O_O^X \leftrightarrow Ti_i^{\bullet\bullet\bullet} + 3e' + O_{2(gas)\uparrow} \quad \textbf{(2-9)}$$

$$Ti_{Ti}^X + 2O_O^X \leftrightarrow Ti_i^{\bullet\bullet\bullet\bullet} + 4e' + O_{2(gas)\uparrow} \quad \textbf{(2-10)}$$

$$O_{2(gas)\uparrow} \leftrightarrow V_{Ti}^{''''} + 4h^{\bullet} + 2O_O^X \quad \textbf{(2-11)}$$

$$nil \leftrightarrow e' + h^{\bullet} \quad \textbf{(2-12)}$$

The equilibrium constants for the reactions described in **Equations (2-8) - (2-12)** can be expressed as follows [8,9]:

$$K_1 = [V_O^{\bullet\bullet}]n^2 p(O_2)^{1/2} \quad \textbf{(2-13)}$$

$$K_2 = [Ti_i^{\bullet\bullet}]n^3 p(O_2) \quad \textbf{(2-14)}$$

$$K_3 = \left[Ti_i^{\bullet\bullet\bullet\bullet}\right]n^4 p(O_2) \quad \textbf{(2-15)}$$

$$K_4 = \left[V_{Ti}^{''''}\right]p^4 p(O_2)^{-1} \quad \textbf{(2-16)}$$

$$K_i = np \quad \textbf{(2-17)}$$

Where the equilibrium constant is represented by K, the electron and hole charge carrier concentrations are represented by n and p, respectively, and the oxygen activity is represented by $p(O_2)$.

2.3.2. Extrinsic Defects in TiO_2

Extrinsic defects refer to the presence of either unintentional impurity cations or intentionally added dopant cations which are different to those of the host crystal lattice. Their presence can

contribute various effects to the host lattice including, ionic size difference causing localised lattice strain energy, differences in impurity polarisation compared to the host cations and a difference in valence affecting the electroneutrality condition of the lattice, and the generation of charge carriers (electrons or holes). Furthermore, extrinsic defects have also been shown to affect semiconducting properties such as the band gap and Fermi level.

If the extrinsic defects present in the lattice have a valence either greater (donor) or less (acceptor) than the host cation, the excess or deficit in valence electrons caused by the extrinsic defect cations must be compensated within the lattice either ionically or electronically to maintain electroneutrality.

2.4 Adsorption and Segregation

It has been reported that on a very basic level, the same laws and concepts derived for adsorption also can also be applied for segregation [13]. Adsorption occurs when a solid is placed in contact with a gas phase containing atoms that have a tendency to adhere to the solid surface. This leads to the formation of the adsorption layer on the surface, which is enriched with the species present in the gas phase [14]. In a similar fashion, segregation also results in surface enrichment; however, the species originate from the bulk solid phase rather than the gas phase as shown in **Figure 2-4**. For this reason segregation is sometimes referred to as adsorption from the solid phase.

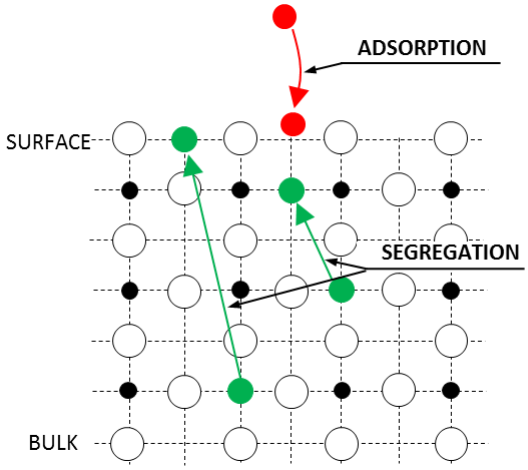

Figure 2-4. Schematic illustration of segregation and gaseous adsorption.

Despite this similarity, there are several significant differences between adsorption and segregation:

- The temperature at which thermodynamic equilibrium is established for adsorption and segregation is different. It has been shown that equilibrium for gaseous adsorption can be established at relatively low temperatures [13,15]. Segregation on the other hand is rate

controlled by lattice diffusion. Lattice diffusion requires sufficiently high temperatures for species in the crystal lattice to become mobile. At the elevated temperatures required for segregation, the contribution to surface enrichment from adsorption can be considered negligible making segregation induced enrichment the dominant effect [15].

- The energy changes driving the adsorption and segregation phenomena also seem to be different due to the difference in their resulting enrichment layers [14,16]. Surface layer enrichment via adsorption is typically limited to the topmost surface (typically a monolayer or so in thickness), while segregation induced enrichment gradients affect both the surface and near surface region and can be anywhere from one monolayer in metals, to several hundred lattice layers for non-stoichiometric oxides [13,15].

Based on the above points, the contribution of adsorption to surface and near surface enrichment can be assumed to be negligible when assessing segregation induced enrichment as is the case in the present work.

2.5 Analysis Techniques

2.5.1. Surface analysis

2.5.1.1. Secondary ion mass spectrometry (SIMS)

The SIMS technique is able to probe the surface region of samples with high resolution and high sensitivity. It is a destructive technique in which a low energy (keV) primary ion beam (typically O or Cs) is used to continuously sputter secondary ions from the surface of the specimen. During analysis, the rastered primary beam sputters progressively deeper in the sample. The simultaneous detection of the secondary ions during the sputtering process generates a surface-to-bulk profile, referred to as a depth profile, for the species of interest in terms of intensity (counts) as a function of analysis time.

2.5.1.1.1. SIMS Matrix Effects

It is well known that SIMS suffers from strong matrix effects which can produce secondary ion yield variations up to several orders of magnitude caused by differences in sample matrix composition, rather than reflecting true differences in concentration [17,18]. This makes the interpretation and quantification of SIMS data in samples of different matrix compositions complicated. The influence of matrix effects on SIMS depth profiles has been demonstrated by Gao et al. [18] who analysed a multilayered sample grown by molecular beam epitaxy (MBE). The sample

consisted of 5 layers of $Al_xGa_{1-x}As$ (0.2 µm thick each) with decreasing x values: 0, 0.4, 0.3, 0.2 and 0.1 but all doped with the same concentration of Be (1 $x10^{19}$ atoms/cm^3). Each $Al_xGa_{1-x}As$ layer was also separated by a 0.1 µm thick layer of undoped GaAs. The SIMS depth profile, shown in **Figure 2-5**, shows that the obtained Be secondary ion intensity for each layer, despite having the same Be concentration, is significantly affected by the change in matrix composition.

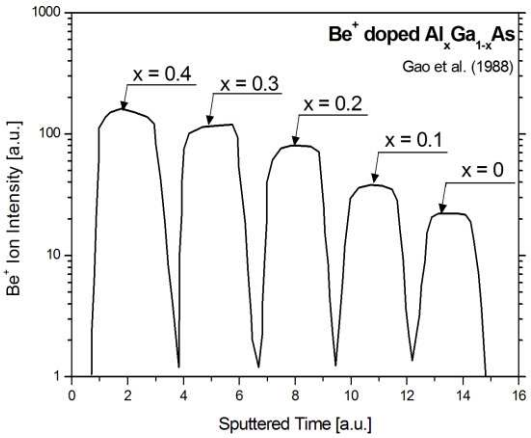

Figure 2-5. SIMS depth profile of Be^+ secondary ions in a multilayered sample consisting of five layers of $Al_xGa_{1-x}As$ (x = 0.4, 0.3, 0.2, 0.1 and 0) equally doped with 1x10^{19} atoms/cm^3 Be and separated by undoped GaAs. SIMS analysis was performed with 12.5 keV O_2^+ primary ions, 130 eV energy window and Be ion intensities normalised to the undoped GaAs region [18].

Although there is no way to completely eliminate matrix effects, it has been previously reported that it can be reduced by utilising the MCs^+ technique [19,20] which has been utilised in the present work.

2.5.1.2. X-ray Photoelectron Spectroscopy (XPS)

XPS is a surface specific analysis technique which involves irradiating a sample with monoenergetic X-rays. The interaction of these X-rays with atoms in the surface causes photoelectrons to be emitted with a measured kinetic energy of [21,22]:

$$KE = hv - BE - \phi_s \qquad \textbf{(2-18)}$$

Where hv is the energy of the X-ray photon, BE is the binding energy of the electrons originating atomic orbital, and ϕ_s is the spectrometer work function.

The binding energy can be described as the difference in energy between the initial and final states after ejection of the photoelectron. As each element has a unique set of characteristic binding energies, XPS can identify and determine the concentration of elements present in the sample surface. Although the path length of the incident photons into the samples is on the order of micrometers, the

probability of electron interaction with matter is so high that only photoelectrons located at a maximum of ~10 nm below the sample surface can escape without energy loss. The electrons which leave the surface without energy loss are detected by an electron spectrometer according to their kinetic energy, KE and produce the peaks in the XPS spectrum. The concentration, N of an element can be determined from the XPS spectra peak intensity as follows [21,22]:

$$N = \frac{I}{\sigma DJL\lambda AT} \quad \textbf{(2-19)}$$

where N is the atomic concentration of the element, I is the photoelectron peak area, σ is the photoelectron cross-section, D is the detector efficiency, J is the X-ray flux, L is the orbital symmetry factor, λ is the inelastic mean free path, A is the analysis area and T is the analyser transmission efficiency.

2.5.1.3. Rutherford Backscattering (RBS)

RBS is a technique capable of non-destructively quantifying the atomic mass of elements and their depth distribution in the near surface region of a target sample. When a particle of mass, M_1 is accelerated at an energy, $E_{incident}$ which ensures an elastic collision regime and collides with a stationary atom of mass, M_2 in the target sample, the momentum and energy is conserved and a transfer of energy occurs between the projectile particle and the target atom. If $M_1 < M_2$ the incident particle is backscattered with precisely this energy which can be calculated from [21,23]:

$$E_{backscattered} = E_{incident}.k \quad \textbf{(2-20)}$$

where the kinematic factor, k is given by [21,23]:

$$k = \frac{M_1^2}{(M_1 + M_2)^2}\left(cos\theta + \left[\left(\frac{M_2}{M_1}\right)^2 - sin^2\theta\right]^{1/2}\right)^2 \quad \textbf{(2-21)}$$

where M_1 is the atomic mass of the incident ion, and M_2 is the atomic mass of the atom it collides with in the target and θ is the scattering angle.

Based on **Eq. (2-20)**, the energy at which the incident particle is backscattered is dependent on the initial particle energy, the scattering geometry (i.e. angle of both the incident beam and the detector) and the atomic mass of the target atom involved in the collision process. Therefore, the energy of the incident particles backscattered from atoms present at the surface and near surface region of the target sample can used to directly determine the type of atoms present, M_2 as illustrated in **Figure 2-6 (a) and (b)**.

An advantage of RBS is that it can also provide some elemental information related to depth in the near surface region. This is due to an additional energy loss, ΔE, that the incident projectile particle experiences as it travels both into and out of the sample, shown as ΔE_{in} and ΔE_{out} in **Figure 2-6 (a)**. For a thick target, this increasing loss in energy results in a characteristic step-like shape extending to lower energies in relation to the leading edge energy for that element **Figure 2-6 (b)**. The width of the step, ΔE is proportional to the thickness of a thin layer or depth, d from the surface [21,23]:

$$\Delta E = [S]d \qquad \textbf{(2-22)}$$

where [S] is the energy loss factor which depends on the kinematic factor and on the energy loss per unit length for a given material [21,23].

[S] is also dependent on the target material density.The error related to RBS thickness measurement is determined by the energy resolution of the detector.

In backscattered experiments, the detector subtends a solid angle, Ω, so the yield, Y, of detected backscattered particles from a thin layer of target atoms in the sample is given by [21,23]:

$$Y = \sigma(\theta)\Omega Q N \Delta x \qquad \textbf{(2-23)}$$

where $\sigma(\theta)$ is the differential scattering cross section, Q is the total number of incident projectiles, N is the number of target atoms per unit volume in the layer and , Δx is the thickness in the target from which backscattering took place.

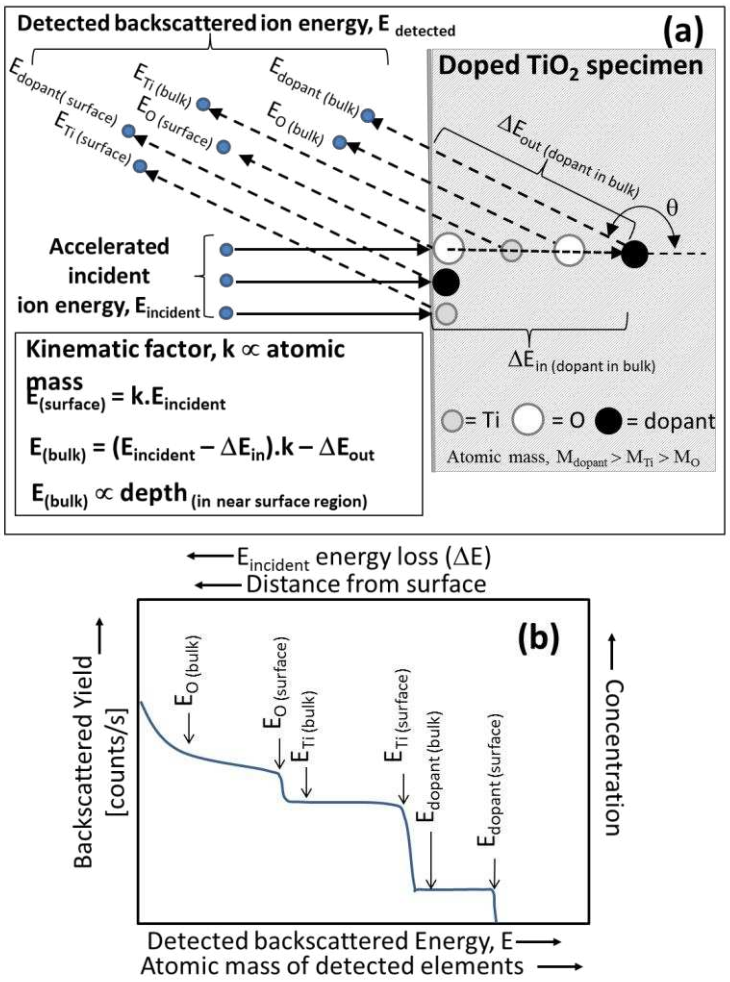

Figure 2-6. Schematic illustration of RBS analysis interaction of (a) ion beam with a TiO_2 sample, and (b) the resulting backscattered ion spectrum.

2.5.2. Bulk Analysis

2.5.2.1. Thermogravimetric Analysis (TGA)

Thermogravimetric analysis is a technique that monitors the mass of a material as a function of a controlled temperature ramp (either heating or cooling). TGA essentially consists of a sample pan supported by a high precision balance, inside a furnace. As the temperature of the sample is ramped up or down, the corresponding mass of the sample is recorded. The results of TGA are used to determine specific temperatures at which regimes such as water vaporisation, melting or phase changes occur.

2.5.2.2. Differential Scanning Calorimetry (DSC)

Differential scanning calorimetry is a thermoanalytical technique that is complimentary to TGA. DSC measures the difference in amount of heat that is required to increase the temperature of a sample

and reference (with well-defined heat capacity) as a function of linearly increasing temperature. The basic principle of DSC consists of trying to keep both the sample and reference maintained at nearly the same temperature throughout the analysis. In other words, if the sample undergoes a temperature induced transformation, such as a phase transition, more or less heat will be required to be input to it compared with the reference to maintain both at the same temperature. Depending on whether the heat input to the sample is more or less than the reference specimen will determine whether the process is endothermic or exothermic, respectively.

2.5.2.3. X-ray Diffraction (XRD)

X-ray diffraction (XRD), sometimes referred to as X-ray powder diffraction, is a non-destructive technique mainly used for identifying crystalline phases in solid materials. Typically, the solid material is homogenised by grinding to a fine powder prior to analysis. Consequently, XRD results in averaged bulk composition and crystallographic structure analysis. XRD is based on the constructive interference of monochromatic X-rays interacting with a crystalline sample. The constructive interference is produced when the interaction conditions satisfy Bragg's Law [24]:

$$n\lambda = 2d\sin\theta \qquad \textbf{(2-24)}$$

where n is the order of reflection, λ is the wavelength of the incident X-rays, d is the interplanar spacing of the crystal and θ is the angle of incidence.

By scanning the sample through a range of 2θ angles while detecting the diffracted X-rays, all of the possible diffraction directions related to the various crystalline lattices present in the sample should be obtained due to the powdered samples random lattice orientation. As every crystalline material has a unique set of d-spacings, the resulting XRD spectrum can be used to identify the crystalline phases present in the material by comparing the d-spacings with a database of standard reference patterns [24].

2.5.2.4. Proton Induced X-ray Emission (PIXE)

Particle (or proton) induced X-ray emission is a non-destructive analytical method based on X-ray spectrometry. As shown in **Figure 2-7**, the accelerated particle beam ejects an inner-shell electron from the atoms present in the target sample which produces a vacancy. When that vacancy is filled by an outer-shell electron, an X-ray of characteristic energy related to that particular atom is emitted and detected. A typical PIXE spectrum consists of a number of X-ray peaks superimposed over a broad background peak observed in the low energy region of the spectrum as shown in **Figure 2-8**. This broad background is caused by Bremsstrahlung processes and gamma rays from nuclear

interactions which are well-defined and can be accurately modelled to perform the necessary background subtraction. The energy (or position) of the X-ray peaks in the PIXE spectrum are characteristic of atomic number (Z) of the elements in the sample from which they originated, and the yield (counts) of these peaks are directly proportional to the concentration of that element. This can be expressed as [25]:

$$C_Z = \frac{I_Z(E_{K\alpha})}{M.Q.J(E_{K\alpha})} \quad \textbf{(2-25)}$$

Where C_Z is the concentration of Z-element, $I_z(E_{K\alpha})$ is the number of counts in the principal Kα peak of Z-element, M [g/cm^2] is the total mass density of the target, Q [C] is the charge collected during the analysis and $J(E_{K\alpha})$ [g^{-1}cm^{2}C^{-1}] is the value of the sensitivity function at the peak energy determined from experimental data.

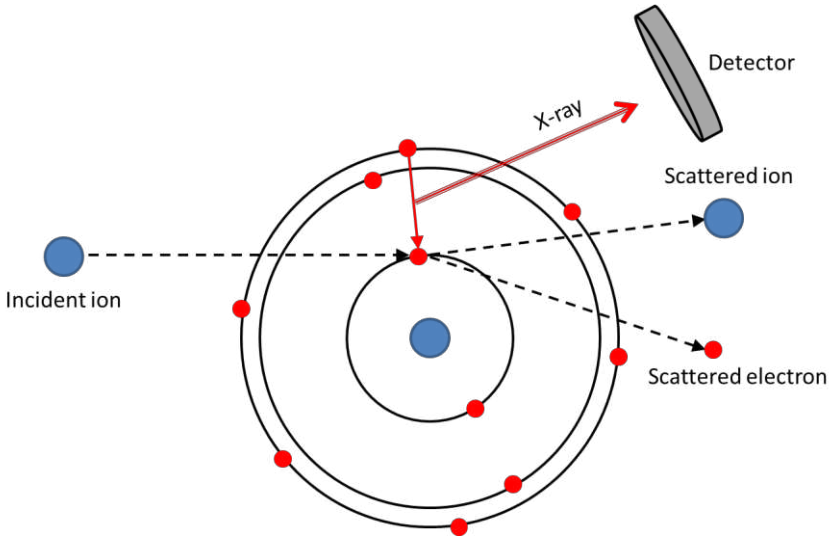

Figure 2-7. Schematic illustration of inner-shell vacancy creation and subsequent X-ray emission due to high energy particle interaction.

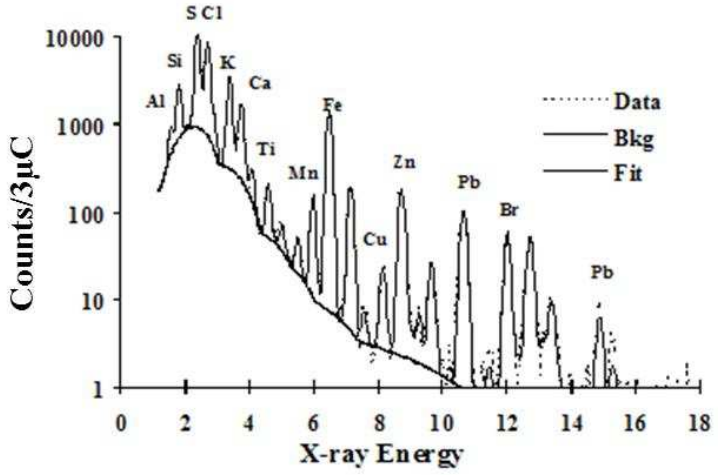

Figure 2-8. Example of a typical PIXE spectrum.

2.7 References

(1) Kofstad, P. Nonstoichiometry, diffusion and electrical conductivity in binary metal oxides; Wiley: New York, 1972.

(2) Ni, M.; Leung, M. K. H.; Leung, D. Y. C.; Sumathy, K. "A review and recent developments in photocatalytic water-splitting using TiO_2 for hydrogen production". Renew. Sust. Energ. Rev. (2007), 11 [3], 401-425.

(3) Shewmon, P. G. Diffusion in Solids; McGraw-Hill Book Company, Inc., 1963.

(4) Crank, J. The Mathematics of Diffusion, 2nd ed.; Oxford Science Publications, 1997.

(5) Sheppard, L. R.; Atanacio, A. J.; Bak, T.; Nowotny, J.; Prince, K. E. "Bulk diffusion of niobium in single-crystal titanium dioxide". Journal of Physical Chemistry B (2007), 111 [28], 8126-8130.

(6) Sheppard, L. Defect Chemistry and Charge Transport in Niobium-Doped Titanium Dioxide. PhD, PhD Thesis, University of New South Wales, 2007.

(7) Solid State Physics; Kröger, F. A.; Vink, H. J., Eds.; Academic Press: New York, (1956); Vol. 3, pp 307.

(8) Bak, T.; Nowotny, J.; Nowotny, M. K. "Defect disorder of titanium dioxide". Journal of Physical Chemistry B (2006), 110 [43], 21560-21567.

(9) Nowotny, J.; Bak, T.; Nowotny, M. K.; Sheppard, L. R. "Titanium dioxide for solar-hydrogen II. Defect chemistry". International Journal of Hydrogen Energy (2007), 32 [14], 2630-2643.

(10) Khan, S. U. M.; Al-Shahry, M.; Ingler Jr, W. B. "Efficient photochemical water splitting by a chemically modified n-TiO_2". Science (2002), 297, 2243-2245.

(11) Neumann, B.; Bogdanoff, P.; Tributsch, H.; Sakthivel, S.; Kisch, H. "Electrochemical mass spectroscopic and surface photovoltage studies of catalytic water photooxidation by undoped and carbon-doped titania". Journal of Physical Chemistry B (2005), 109 [35], 16579-16586.

(12) Nowotny, M. K.; Bak, T.; Nowotny, J.; Sorrell, C. C. "Titanium vacancies in nonstoichiometric TiO_2 single crystal". Phys. Status Solidi B-Basic Solid State Phys. (2005), 242 [11], R88-R90.

(13) Nowotny, J.; Bak, T.; Nowotny, M. K.; Sorrell, C. C. "Charge transfer at oxygen/zirconia interface at elevated temperatures - Part 3: Segregation induced interface properties". Adv. Appl. Ceram. (2005), 104 [4], 165-173.

(14) Wynblatt, P.; Chatain, D. "Anisotropy of segregation at grain boundaries and surfaces". Metall. Mater. Trans. A-Phys. Metall. Mater. Sci. (2006), 37A [9], 2595-2620.

(15) Nowotny, J. Inteface defect chemistry and its impact on properties of oxide ceramic materials. In Science of Ceramic Interfaces; Nowotny, J., Ed.; Elsevier Science Publishers B.V., (1991); pp 79-204.

(16) Nowotny, J. "Interface defect chemistry of oxide ceramic materials - Unresolved problems ". Solid State Ion. (1991), 49, 119-128.

(17) Deline, V. R.; Katz, W.; Evans, C. A. "Mechanism of SIMS matrix effect". Appl. Phys. Lett. (1978), 33 [9], 832-835.

(18) Gao, Y. "Influence of experimental conditions on matrix effects in SIMS". Applied Surface Science (1988), 32 [4], 420-430.

(19) Gao, Y.; Marie, Y.; Saldi, F.; Migeon, H. N. "On the SIMS depth profiling analysis - Reduction of matrix effect". International Journal of Mass Spectrometry and Ion Processes (1995), 143, 11-18.

(20) Gnaser, H. "Improved quantification in Secondary Ion Mass Spectrometry detecting MCs^+ molecular ions ". J. Vac. Sci. Technol. A-Vac. Surf. Films (1994), 12 [2], 452-456.

(21) Methods of Surface Analysis: Techniques and Applications; Walls, J. M., Ed.; Cambridge university Press: Cambridge, (1990).

(22) Handbook of X-ray Photoelectron Spectroscopy 2nd Ed.; Moulder, J. F.; Stickle, W. F.; Sobel, P. E.; Bomben, K.; Chastain, J., Eds.; Perkin-Elmer Corporation (Physical Electronics), (1992).
(23) Chu, W.; Mayer, J.; Nicolet, M. Backscattering Spectrometry; Academic Press: New York, 1978.
(24) Klug, H. P.; Alexander, L. E. X-ray Diffraction Procedures for Polycrystalline and Amorphous Materials. 2nd Ed.; Wiley: New York, 1974.
(25) Bertin, E. P. Introduction to X-Ray Spectrometric Analysis; Plenum Press: New York, 1980.

CHAPTER 3

Literature Overview

It should be noted that the included papers of this thesis (comprising Chapters 6 to 10) each contain their own section in which literature specifically related to the work of that chapter is assessed. Consequently, some repetition of the literature findings presented in the present overarching chapter with that of sections in subsequent chapters will occur.

3.1 Diffusion in TiO_2

To date, the most comprehensive report on cation self-diffusion in single crystal TiO_2 has been given by Sasaki et al. [1]. Sasaki utilized the radiotracer-sectioning technique to investigate Sc, Cr, Mn, Fe, Co, Ni and Zr as a function of temperature, oxygen activity and crystal orientation. Sasaki proposed the following conclusions from his results [1]:

- Trivalent (Sc and Cr) and tetravalent (Zr) cations dissolved substitutionally and diffused via the interstitialcy mechanism.
- Mixed valence (Fe and Mn) cations diffused both as divalent ions along the open channels and as trivalent ions via the interstitialcy mechanism.
- The charge of the impurity was more significant than size in determining both diffusion rate and whether a cation diffused along the open channels parallel to the c-axis.

Peterson and Sasaki [2] went on to generalise that divalent cations diffused interstitially, while tri- and tetravalent cations diffused according to the interstitialcy mechanism.

The diffusion of Zr and Hf in rutile was investigated by Cherniak et al. [3] over the temperature range 1023 K - 1373 K (in air) using RBS. They determined that Hf and Zr are likely to dissolve substitutionally for Ti cations in the rutile structure which supports with the findings of Sasaki et al. [1]. However Cherniak's results also suggested that the oxygen activity

had very little influence on Zr and Hf diffusion which is inconsistent with the findings of Sasaki [1] and Hoshino [4].

Sheppard and Atanacio et al. [5] studied Nb diffusion in single crystal TiO_2 over the temperature range of 1073 K – 1573 K in air and determined 244 kJ/mol activation energy and pre-exponent factor of ~$5x10^{-7}$ m^2s^{-1}. They also proposed that Nb bulk diffusion in TiO_2 proceeded via the interstitialcy diffusion mechanism due to the similarity of the data with the Ti self diffusion results reported by Lundy and Coghlan [6] and Hoshino et al. [4], **Figure 3-1**.

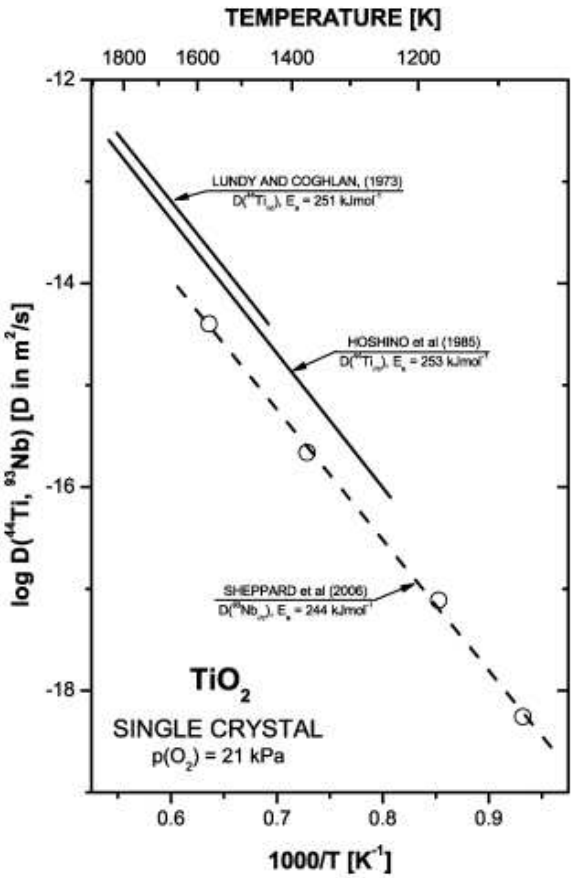

Figure 3-1. Comparison of Nb diffusion reported by Sheppard et al. [5] with Ti self-diffusion results from Lundy and Coghlan [6] and Hoshino et al. [4].

A summary of the activation energy results from literature for cation diffusion in TiO_2 parallel to the c-axis are presented in **Figure 3-2** below.

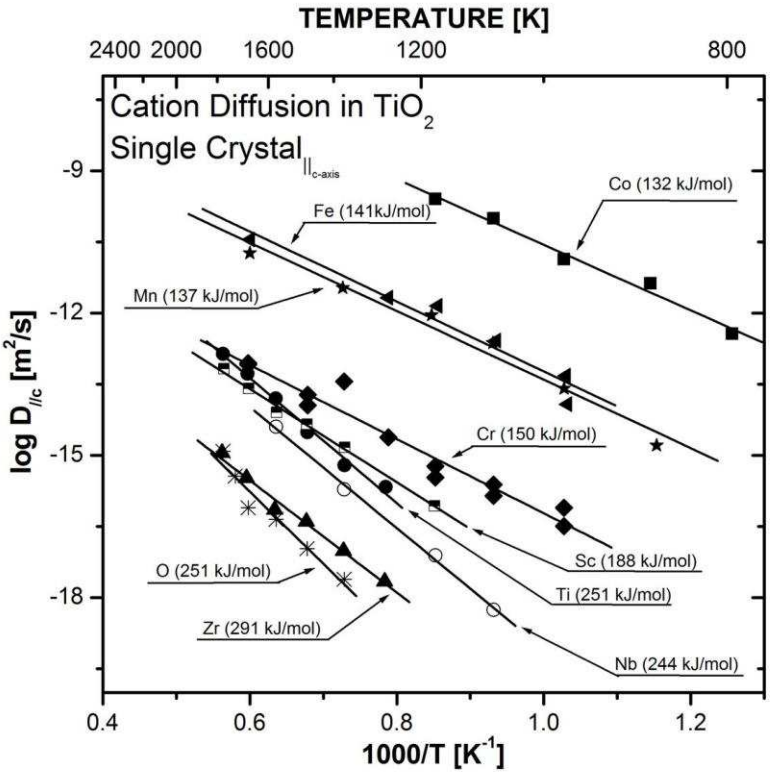

Figure 3-2. Summary of reported activation energies for aliovalent cation diffusion in single crystal TiO_2 [1,5].

3.1.1. Bulk Diffusion Coefficient

The formation of well-defined solid solutions is a key condition for correctly examining segregation. This requires knowledge of the processing conditions (temperature, time, and $p(O_2)$) to achieve specimens in which the dopant is incorporated and distributed homogeneously throughout the lattice. Consequently, knowledge of the bulk diffusion coefficient is essential to correctly study segregation.

The present author and colleagues [5] have recently assessed Nb bulk diffusion in single crystal TiO_2 at $p(O_2)$ = 21 kPa over the temperature range 1073 K – 1573 K using SIMS. The results suggested that Nb bulk diffusion proceeded via an interstitialcy-type mechanism, similar to the self-diffusion of ^{44}Ti [5]. Moreover, the temperature dependence of Nb bulk diffusion in single crystal TiO_2 was determined to be:

$$D_{Nb-TiO_2} = (4.7 m^2 s^{-1}) \times 10^{-7 \pm 0.4} \exp\left(\frac{-244 \pm 9 kJ mol^{-1}}{RT}\right) \quad \textbf{(3-1)}$$

To the best of my knowledge, no data for In diffusion in TiO_2 has been reported in literature. Consequently, determination of In bulk diffusion in single crystal TiO_2 will be addressed in the present work.

3.1.2. The Effect of TiO_2 Doping

A large variety of aliovalent cation doped-TiO_2 systems and resulting properties have been reported in literature. These include C [7,8],Ca [9], N [10], Al [11,12], S [13], Ca [9], V [14,15], Cr [16-19], Mn [14], Fe [12,20], Ni [18], Zn [12,18,21], Cu [14], Y[22], Zr [12], Nb [12,16,21,23-29], Mo[19,30], Sb [12,31], Ta [12,32], W [33], Ir [34], and rare earths (La, Ce, Er, Pr, Gd, Nd, Sm) [35]. However, much of the reported results relating to doped TiO_2 are inconsistent and display wide variability. For example, Choi [12] carried out an extensive study of 21 metal ion dopants and their effect on the photo-reactivity of TiO_2. Of the 21 dopants studied, Fe, Mo, Os, Ru, V, Re and Rh ion were shown to increase the photocatalytic activity to varying degrees. Most interestingly Choi also reported that so-called "closed-shell" electronic configuration dopants Li, Mg, Al, Zn, Ga, Zr, Nb, Sn, Sb, and Ta had little effect on photoreactivity due to unfavourable electron (or hole) trapping. This contradicts the results of Trenczek-Zajac et al. [36] who observed that Nb doping in TiO_2 considerable improved the measured photocurrent and resulting energy conversion efficiency. Similarly, the observations for carbon doped TiO_2 reported by Khan et al. [7] and Neumann et al. [8] also contradict each other as seen in **Figure 3-3**. Khan [7] reported that carbon substitutionally incorporated into the TiO_2 lattice was able to reduce the band-gap significantly from 3 eV to 2.32 eV which in-turn resulted in a substantial increase in photocatalytic performance. While Neumann [8], studying seemingly the same carbon-TiO_2 system with a range of doping concentrations, reported that in all cases the photocatalytic response actually decreased markedly compared with the undoped TiO_2. These examples clearly highlight the discrepancies in literature regarding the effect of doped-TiO_2 on resulting functional properties. Furthermore, it emphasises the important need to have well-defined sample processing methods and subsequent surface vs. bulk characterisation techniques in order to correctly identify the relationship between the dopant and observed functional properties. Without well-defined and characterised samples it becomes almost impossible to compare published results even for seemingly the same oxide systems [37].

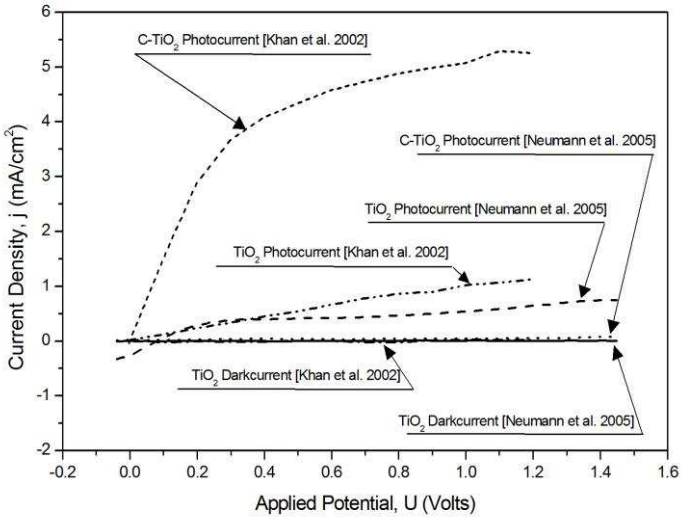

Figure 3-3. Comparison of photoreactivity results reported for C-doped TiO_2 in literature [7,8].

Consequently, the aim of the present work is to study dopant segregation within well–defined processing conditions using an appropriate combination of surface and bulk analysis techniques. To facilitate this, indium (In^{3+}) was selected as the acceptor dopant and niobium (Nb^{5+}) as the donor dopant in our TiO_2 systems.

3.1.2.1. Indium Doped TiO_2

In_2O_3 has excellent electrical and optical properties and has been shown to improve the performance of dye sensitised photovoltaic devices [38], optoelectronic devices [39], and gas sensors [40]. Consequently, it is reasonable to anticipate a similar performance enhancement in TiO_2.

Karn and Srivastava [41] reported a significantly higher photocurrent of 14 $mA.cm^{-2}$ for their In_2O_3-admixed TiO_2 photo-electrodes compared with 4 $mA.cm^{-2}$ for TiO_2. However, their sample preparation method and subsequent XRD results clearly showed that indium ions did not incorporate into the TiO_2 lattice as a solid solution but instead only formed islands on the surface of the TiO_2 [41]. Shchukin et al. [42] studied nanocrystalline TiO_2-In_2O_3 powders prepared by the sol-gel technique as a function of Ti/In ratios. They observed that modifying TiO_2 with In_2O_3 resulted in significantly improved photo-reactivity. However, similar to the work of Karn and Srivastava [41], XRD analysis determined a binary phase material consisting of two crystalline phases: TiO_2 (anatase) and In_2O_3 (cubic) with no Ti-In mixed phase detected. Several other studies on binary phase In_2O_3: TiO_2 have been reported [43-45] with similarly

positive photo-response results, however, these data cannot be interpreted and compared with the present work in terms of defect disorder due to lack of incorporation of indium ions into the TiO_2 lattice as a solid solution. At the very least, they do, however, provide preliminary evidence that In_2O_3 doped TiO_2 systems may possess improved photoreactivity properties.

The work of Cerrato et al. [46] demonstrated that doping of TiO_2 (anatase) with In_2O_3 enhanced its hydrophilic properties and increased its adsorption capacity for water which one would anticipate as a beneficial property for water splitting.

In summary, the general lack of literature related to well-defined In-doped TiO_2 solid solutions, combined with the promising reports of improved photoreactivity and water adsorption in In_2O_3:TiO_2 systems [41-45] warrants the need for further research into In-doped TiO_2.

3.1.2.2. Niobium Doped TiO_2

Nb-doped TiO_2 systems have been studied for use as gas sensors [47,48], as a photocatalyst for water splitting [29,36,49,50] or as a photocatalyst for water purification [51].

Atashbar and co-workers [47] prepared Nb_2O_5 doped TiO_2 thin films using sol-gel with a concentration of 0.62 at% Nb to examine for gas sensor applications. They observed that their Nb-doped TiO_2 film resulted in a 40% increase in sensitivity to oxygen gas as well as decreasing the required operating temperature compared with an undoped film.

Ruiz et al. [23] examined Nb-doped TiO_2 nanopowders over a range of Nb concentrations (0 – 10%) and calcining temperatures (873 – 1173 K) with X-ray diffraction (XRD), Raman spectroscopy and transmission electron microscopy (TEM). They determined that increased doping with Nb diminished the materials response to ethanol gas but improved its sensitivity to CO detection due to a different reaction mechanism but were unable to specify the specific influence of niobium.

Kikkawa and collegues [50] examined the photochemical properties of Nb-doped TiO_2 thin films in terms of firing temperature (673 – 973 K), film thickness (0.1 – 1.1 µm) and Nb doping concentration (0 – 10 mol%). They observed that the measured conductivity and photocurrent increased as a function of Nb dopant concentration, firing temperature and membrane thickness.

The effect of Nb doping on the photoelectrochemical water splitting properties of TiO_2 has been studied by Trenczek-Zajac et al. [36]. They reported that the addition of Nb resulted in increased solar energy conversion efficiency (ECE), with 1 at% Nb doping concentration providing the maximum ECE. Unfortunately, no attempt was made to characterise the surface

composition in order for correlation with the observed surface reactivity. While the results are certainly promising, it is unclear how the surface chemistry, in terms of composition or structure, differs from that of the bulk.

Wang and co-workers [25] studied the photoelectrochemical properties of TiO_2 pellets doped with 0.05 – 0.9 mol% of Nb_2O_5. Their samples were prepared by mixing TiO_2 and Nb_2O_5 powders in a mortar and pestle, followed by pressing and sintering in air at temperatures ranging from 1473 K to 1623 K. They observed that the measured photo-currents were greater for specimens with lower doping concentration than the specimens with higher doping concentrations. They postulated that this was caused by the "segregation" of excess Nb cations in specimens with higher doping concentrations to form recombination centres [25]. The use of the term "segregation" by Wang et al. [25] seems to suggest an effect related to solubility limit of Nb in the TiO_2 lattice. While this explanation is plausible, the following alternative explanation is suggested based on the definition of "segregation" used in the present work. During high temperature sintering, Nb segregation from the bulk to the surface occurs, an effect that has been confirmed previously in Nb-doped TiO_2 by Sheppard et al. [52]. This segregation-induced transport effect is driven not by an exceeding of the solubility limit, but by a need to reduce the excess energy at the surface. Sheppard et al. [52] also observed that segregation induced enrichment of Nb at the surface was significantly greater for specimens with lower dopant concentrations. Moreover, surface segregation results in an associated electric field at the enriched surface that may inhibit charge recombination and result in the improved photo-current measurements observed by Wang et al. Consequently, the effect of surface segregation is certainly another plausible explanation, not considered by Wang et al. [25],that could explain the higher photo-currents observed in their specimens of lower Nb concentration.

The potential of Nb-doped TiO_2 systems for improved performance in applications such photocatalytic water splitting is clearly evident in literature. Although the theoretical influence of Nb in Nb-doped TiO_2 in terms of bulk defect chemistry is relatively well understood, the same cannot be said for the surface and near-surface region. Consequently, further studies are required to characterise the surface vs. bulk properties of Nb-doped TiO_2, particularly, the phenomenon of segregation.

3.2 Segregation

The surface properties of solids can be substantially different, in terms of chemical composition, structure and the related semiconducting properties; from those of the bulk phase as a result of segregation. [53-55].

To date, segregation has mainly been determined for metals and alloys [56-58]. However, the understanding of segregation in metal oxides is much more complex than in metals. Unlike metal alloys, metal-oxides are not constrained by local charge compensation but charge compensation can occur over much larger ranges resulting in ionic space charge formation [59,60]. Furthermore, segregation in metal-oxides have been shown to be substantially influenced by the oxygen activity in the ambient gas phase surrounding the specimen [61].

The main driving forces for segregation in oxides have been postulated by Kingery [62], Wynblatt and McCune [55] and Yan et al.[63] which include:

(1) A difference in vacancy-formation energies resulting in localised non-stoichiometry
(2) Electrostatic potential difference caused by the localised non-stoichiometric charged species
(3) Elastic strain energy induced by defect lattice distortion
(4) Effect of the gas phase (oxygen activity)
(5) Effect of surface energy

An extensive series of segregation studies by Hirschwald et al. confirmed the effect of Cr segregation in the relatively simple metal oxides NiO [64,65] and CoO [66,67]. It has also been documented that the segregation-induced enrichment of the surface layer of oxides, such as Cr-doped NiO, is strongly affected by the oxygen activity in the gas phase [65]. It has also been shown that the segregation-induced surface enrichment may substantially surpass the bulk solubility limit, and in some cases, induce the formation of a new low-dimensional surface structure [54,68,69].

In general, the studies of segregation in oxides indicate that both intrinsic defects, such as oxygen and cation vacancies, and extrinsic defects segregate to the surface [61]. Consequently, potential interaction between intrinsic and extrinsic defects must be taken into account when assessing segregation and its effect on surface properties. This adds additional complexity for metal oxides, such as TiO_2, which can display such a wide range of nonstoichiometry and defect chemistry.

3.2.1. Indium segregation in TiO_2

Nakamura et al. [70] studied the defect location of TiO_2 single crystal ion implanted with In using RBS channelling. They performed two annealing steps on the implanted sample, one at 650 K and the other at 1000 K. At 1000 K, they observed that the In atoms diffused toward the surface. This was not the case at 650 K. Moreover, further annealing at 1173 K resulted in the diffusion of up to 15% of the implanted In ions to the surface. Unfortunately, no information was provided about the gas phase oxygen activity during annealing and no explanation is offered for the observed indium diffusion towards the surface as a result of annealing. Nakamura et al. [70] further reported that while the majority (72-88%) of In atoms occupied substitutional sites as one might expect, 11-24% occupied interstitial sites depending on the implantation dose. Furthermore, the percentage of interstitial site occupancy increased with increasing In implantation dose. Interestingly, they reported that at high doses (up to 5×10^5 In/cm^2) the implanted In atoms formed clusters or some other type of unidentified second phase in which interstitial site occupancy was still observed [70].

Although reports specifically studying the segregation of In in In-doped TiO_2 are absent in literature, it is clear from the observations of Nakamura et al. [70], that In surface enrichment, most likely due to segregation, has been observed and justifies the need for further study.

3.2.2. Niobium segregation in TiO_2

A recent review by Nakajima et al. [26] comparing experimental data previously reported for Nb segregation in Nb-doped TiO_2, reproduced in **Figure 3-4**, shows a large degree of variability between surface compositions and related enrichment factors. While they essentially show agreement, in terms of confirming segregation induced Nb surface enrichment, they differ regarding the initial bulk concentration vs. resulting enrichment factor and temperature dependence.

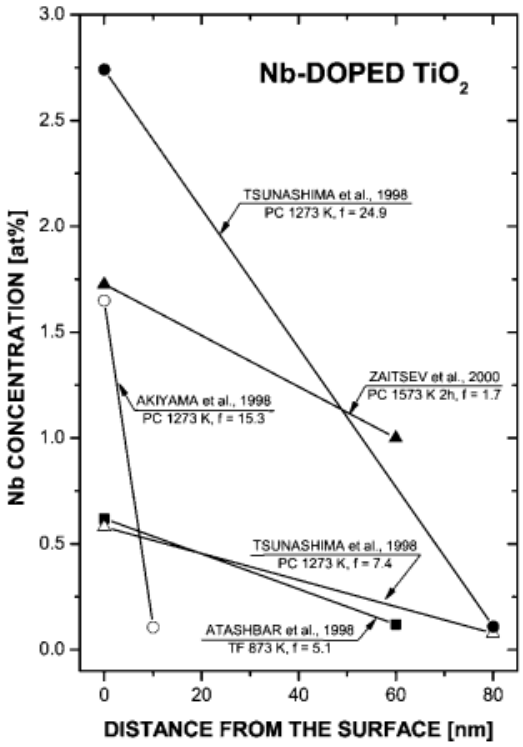

Figure 3-4. Comparison of Nb concentrations as a function of distance from the surface according to several reports [47,71-73]. Reproduced from Nakajima et al. [26]

A similar variability can be seen when comparing more recently reported experimental data for polycrystalline Nb-doped TiO_2 reported by Nakajima et al. [26] Sheppard et al. [52,74], shown in **Figure 3-5**. The solid lines in **Figure 3-5** relate to specimens annealed in an oxygen gas phase and the dashed line represents annealing in the gas phase of argon. In addition to the similar bulk concentration vs. enrichment variability seen in **Figure 3-4**, there is also a conflict between the observed effect of oxygen activity on Nb surface enrichment. The data of Sheppard et al. [74] shows an inverse relationship between surface enrichment and oxygen activity, with the Nb surface concentration from 4.3 at% to 7.3 at% as the $p(O_2)$ decreased from 21 kPa to 10 Pa, respectively. On the other hand, Nakajima et al. [26] reported the opposite effect where enrichment increased from 9.0 at% in $p(O_2)$ = 10 Pa to 21.2 at% in $p(O_2)$ = 21 kPa.

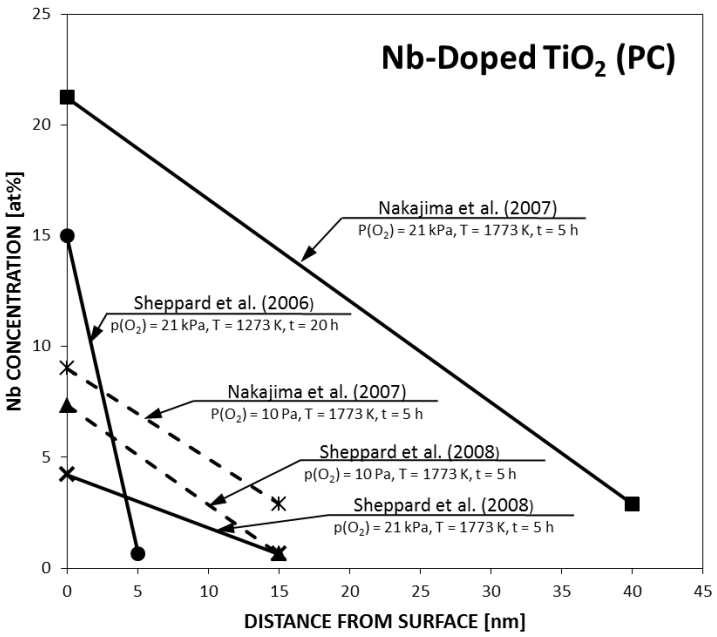

Figure 3-5. Comparison of Nb concentrations as a function of distance from the surface according to several recent studies [26,52,74].

It is clear from **Figure 3-4** and **Figure 3-5** that despite the accumulation of reports for Nb confirming that solutes present as dopants in TiO_2 bulk phase segregate to the surface, the variability and conflict in the data indicates that the understanding of segregation in Nb-doped TiO_2 is still not clear.

3.2.3. Effect of Time on Segregation

For nonstoichiometric oxides, equilibrium segregation is completely determined by the equilibrium parameters of temperature and oxygen activity and is independent of experimental parameters such as heating/cooling rates or previous thermal history [26,75]. The comprehensive series of studies by Nowotny et al. [76] using electrical conductivity and thermoelectric power measurements have shown that when either the oxygen activity or temperature is altered for an oxide in equilibrium, the system assumes a new equilibrium state that is related to a modified stoichiometry. Furthermore, they demonstrated that equilibrium at the surface is established rapidly in the order of hours, resulting in a so-called operational equilibrium, while it takes significantly longer (hundreds of hours) to establish the so-called effective equilibrium in the bulk [76] .

It is therefore critical when assessing the properties of doped oxides that the time required to achieve equilibrium is determined and established in the sample. Without this knowledge, it becomes unclear if the resulting properties are related to a well-defined thermodynamic property

or is instead representative of kinetic condition in which the observed properties are at some point within a greater process. Properties related to the latter are extremely difficult, if not impossible, to reproduce reliably.

3.2.4. Effect of Temperature on Segregation

A strong effect of specimen processing temperature on Nb- and Cr doped TiO_2 surface enrichment has been documented by Ruiz et al. [17,77] as shown in **Figure 3-6** and **Figure 3-7**. However, based on the provided experimental details it is not clear whether equilibrium segregation had been acheived in the specimens at both low and high temperatures. Consequently, it is difficult to draw any thermodynamic conclusions as the data may simply confirm the faster diffusion kinetics that occur at the higher sintering temperature resulting in comparatively greater surface enrichment during the calcining time of 3h.

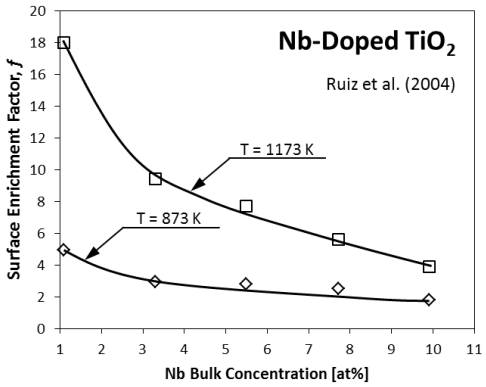

Figure 3-6. Surface enrichment factor of Nb (determined from XPS) vs. nominal bulk Nb concentration for specimens calcined at 873 K and 1173 K reported by Ruiz et al. [77].

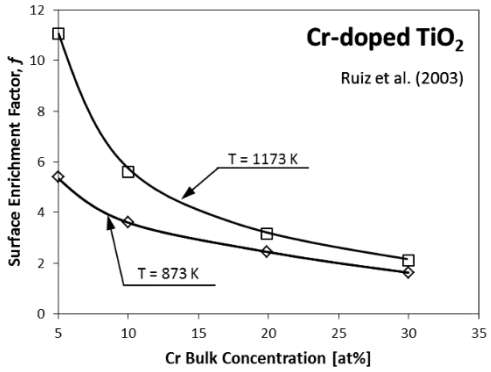

Figure 3-7. Surface enrichment factor of Cr as a function of bulk Cr concentration in for specimens calcined at 873 K and 1173 K, reported by Ruiz et al. [17]**.**

3.2.5. Effect of Oxygen Activity on Segregation

The effect of oxygen activity on the segregation-induced enrichment in oxides was first reported by Black and Kingery [78] for Cr-doped MgO and Fe-doped MgO and Sikora et al. [79] for Cr-doped CoO.

The observed data of Black and Kingery [78], shown in **Figure 3-8** revealed that the segregation of Fe favoured high $p(O_2)$ conditions, while no surface enrichment was observed at low $p(O_2)$. They explained the effect of $p(O_2)$ on Fe segregation in terms of the interaction of the space charge with the valency of Fe (Fe^{2+} and Fe^{3+}).

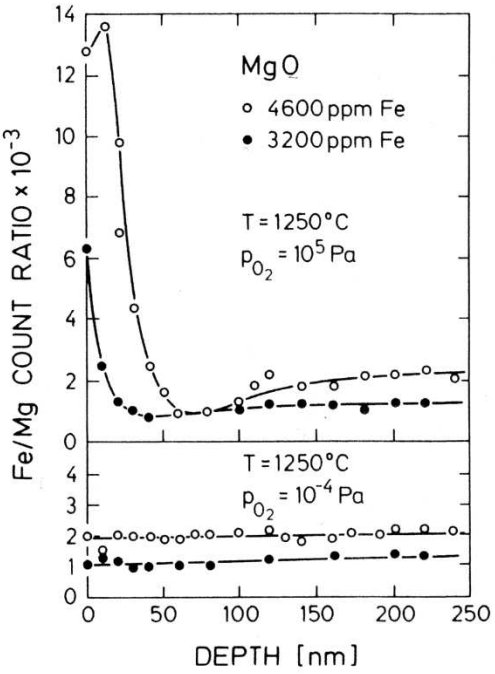

Figure 3-8. Fe depth profile showing the effect of oxygen activity, $p(O_2)$ on segregation in Fe-doped MgO [78]

In contrast, Black and Kingery [78] observed the opposite effect for Cr segregation in the same MgO system. **Figure 3-9** shows a significant decrease in Cr surface enrichment at high $p(O_2)$. They postulated that this effect was due to Cr loss through volatilisation of CrO_3 at high $p(O_2)$ [78].

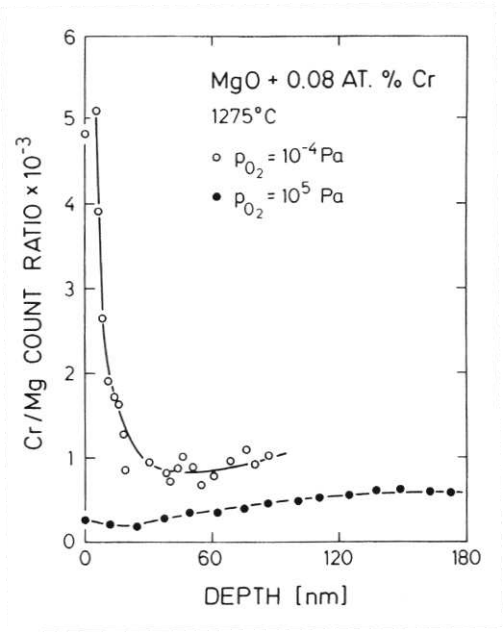

Figure 3-9. Cr depth profile showing the effect of oxygen activity, $p(O_2)$ on segregation in Cr-doped MgO [78]

Additionally, Bernasik et al. [20] studying Fe-doped TiO_2 observed an increase in Fe surface segregation when the $p(O_2)$ was decreased.

The work of Sheppard and co-workers [80], using SIMS analysis, indicated that increasing the oxygen activity results in increased segregation of Nb to the surface in Nb-doped TiO_2.

The reported results of Hirschwald et al. [65] for Cr doped NiO shown in **Figure 3-10** suggest Cr segregation favours the reducing argon gas environment compared with air. However, as the annealing times of 48h and 1 week differed significantly, it is unclear if the result is indicative of a kinetic condition rather than thermodynamic equilibrium.

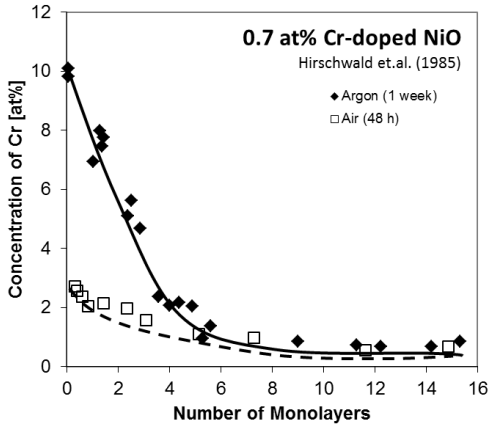

Figure 3-10. Depth profile of Cr in Cr-doped NiO showing the effect of annealing in argon or air gas phase on segregation [65]

Nakajima et al. [26] studying Nb segregation in TiO_2, observed that oxygen activity during high temperature annealing resulted in increased Nb segregation. The Nb/Ti ratio determined at the surface of the specimen annealed in the oxidising air gas phase (Nb/Ti = 5) was close to double that of samples annealed in the reducing argon gas phase (Nb/Ti = 2.6), **Figure 3-11**. Nakajima et al. [26] postulated from this result that a critical $p(O_2)$ capable of suppressing segregation entirely may theoretically be possible.

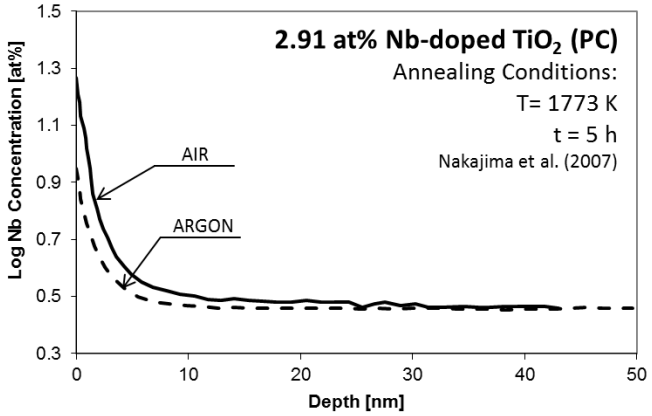

Figure 3-11. Depth profiles showing Nb/Ti versus depth in Nb doped TiO_2 for samples annealed in argon and air [26].

This trend is supported by the findings of Bernasik et al.[20] who observed increased segregation under increased oxygen activity in the investigation of Fe segregation in TiO_2, **Figure 3-12**.

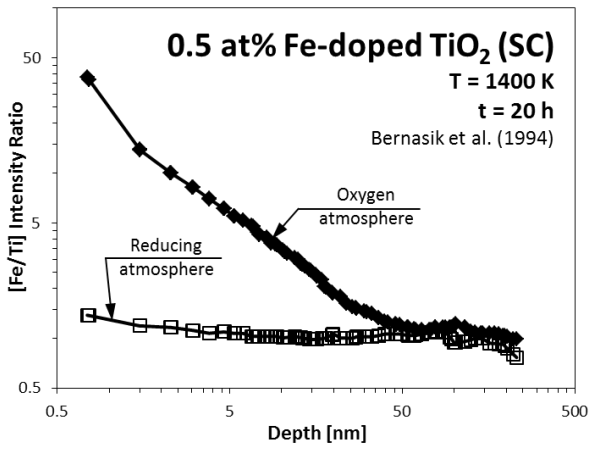

Figure 3-12. SIMS depth profile of Fe-doped TiO_2 single crystal annealed in an oxidising and reducing atmosphere reported by Bernasik et al. [20].

However, a conflicting effect was reported by Hughes [81] who observed a significant increase in Y at the surface of ZrO_2 under reducing conditions, $p(O_2)$ = 10Pa, compared with oxidising conditions, $p(O_2)$ = 21kPa, **Figure 3-13**.

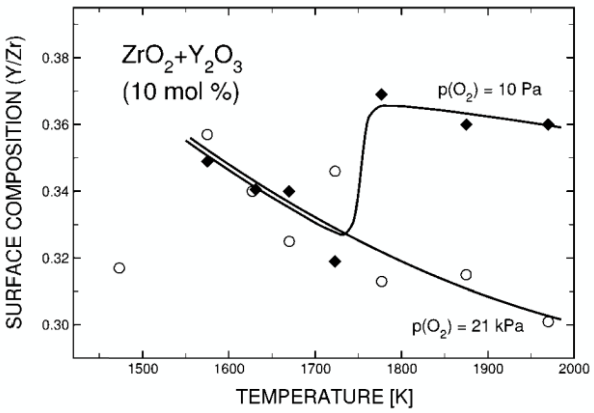

Figure 3-13. Effect of oxygen partial pressure on surface Y/Zr ratio as a function of temperature [81].

A similar effect was also reported by Sheppard et al.[74] for Nb-doped TiO_2 showing an inverse relationship between Nb enrichment and oxygen activity, **Figure 3-14**, with an enrichment factor of f = 11.3 and f = 6.5 in $p(O_2)$ = 10 Pa and 21 kPa, respectively.

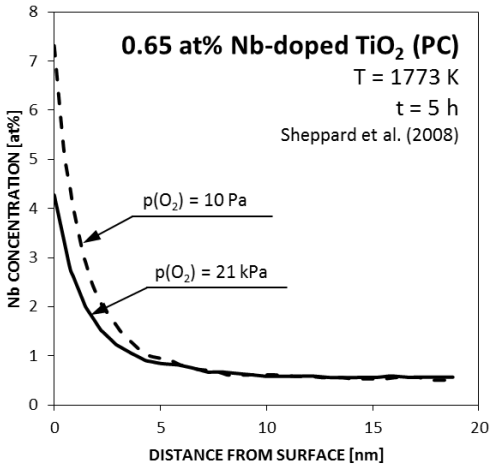

Figure 3-14. Effect of oxygen activity, $p(O_2)$ on Nb surface segregation in polycrystalline 0.65at% Nb-doped TiO_2, as reported by Sheppard et al. [74].

3.2.6. Effect of Dopant Concentration on Segregation

The results reported by Haber et al. [68] for Cr-doped CoO, shown in **Figure 3-15**, determined that the Cr surface enrichment factor increased as bulk concentration decreased.

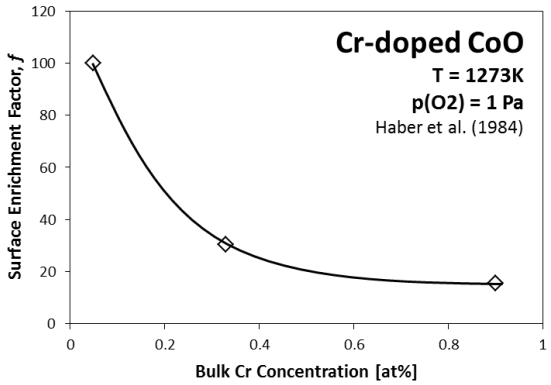

Figure 3-15. Enrichment factor as a function of bulk concentration for Cr-doped CoO, as reported by Haber et al. [68]

A similar effect was also observed by Ruiz and colleagues [17,77] who reported an increase in surface enrichment with lower bulk concentration, as shown previously in **Figure 3-6** for Nb-doped TiO_2 and **Figure 3-7** for Cr-doped TiO_2.

In general, the reported experimental data seem to agree that specimens with lower bulk dopant concentration result in greater segregation induced surface enrichment than those with higher bulk concentrations.

3.3 Summary

The literature review identified several key issues that have been summarised in the following points:

- To date, the literature examining segregation in oxides in general, and TiO_2 in particular, are limited and the reported data are not compatible.
- The reported effects on segregation induced surface properties are not reproducible even for the same systems. Most likely, the inconsistencies result from:
    - The applied experimental processing, such as surface cleaning procedures and sample cooling rates, on surface properties. Therefore, data obtained on surface properties are often governed by the experimental procedures used rather than the materials properties themselves.
    - The reported studies on surface segregation in oxides failed to recognise that the segregation induced enrichment depends on oxygen activity.
    - It has been documented that segregation can result in significant surface modification which can extend long distances from the surface toward the bulk

in metal-oxides, approximately 50 nm – 100 nm, compared to approximately 1 nm in metallic solids. Consequently, the analysis techniques used must be capable of characterising not only the topmost surface layer of the metal-oxide (~1 - 2 nm), but the near-surface layer (2 - 100 nm) and also the bulk phase (~100 nm – 10 um). Only when all three regions have been well-defined can correct assessment be made regarding the effects of surface segregation on functional properties, such as reactivity. The majority of segregation reports to date fail to appropriately characterise all three critical regions.

- Most of the reported segregation enrichment data do not correspond to segregation equilibrium. Knowledge of diffusion data is needed to properly assess the time and temperature required to reach segregation equilibrium.

It is evident that much of the reported segregation data on TiO_2 and oxide systems in general cannot be quantitatively assessed with any accuracy due to a general failure to achieve well-defined test conditions or specimens. This makes the interpretation and correlation of these results extremely difficult. Consequently, considerable discrepancies continue to be prevalent in literature; consequently, the development of any consistent theory for segregation in nonstoichiometric oxide systems such as TiO_2 still lags far behind that of metallic systems.

3.4 Research Objectives

The present work aims to address the following general questions:

1. What is the effect of acceptor-type (In^{3+}) cation segregation on the surface layer, near-surface layer and bulk composition of In-doped TiO_2?
2. What is the effect of donor-type (Nb^{5+}) cation segregation on the surface layer, near-surface layer and bulk composition of Nb-doped TiO_2?
3. What is the effect of oxygen activity on segregation-induced enrichment, in the surface, near-surface and bulk, of acceptor (In^{3+}) and donor (Nb^{5+}) cations in In-doped TiO_2 and Nb-doped TiO_2, respectively?
4. Based on the results, what theoretical models can be utilised or developed which explains the effect of In^{3+} and Nb^{5+} segregation in terms of the surface and near surface chemistry, including their predominant driving force in In-doped TiO_2 and Nb-doped TiO_2, respectively?

In addition, the following specific questions should be addressed:

1. What are the optimal processing conditions (time, temperature and oxygen activity, diffusion coefficient) required to form well-defined In^{3+} and Nb^{5+} doped TiO_2 solid solutions?
2. What surface analysis techniques are available and appropriate for determining segregation-induced surface and near-surface enrichment in TiO_2?
3. What is the segregation-induced enrichment of the outermost surface layer of TiO_2 in indium, In^{3+} (acceptor) and niobium, Nb^{5+} (donor) cations?
4. What is the segregation-induced enrichment of indium, In^{3+} (acceptor) and niobium, Nb^{5+} (donor) cations in the near–surface region beneath the topmost surface, i.e. the region which exhibits a surface-to-bulk concentration gradient?
5. What is the effect of bulk dopant concentration on the segregation-induced enrichment?
6. What is the effect of annealing time on the segregation-induced enrichment?
7. What is the effect of oxygen activity $p(O_2)$ on segregation-induced enrichment?

3.5 References

(1) Sasaki, J.; Peterson, N. L.; Hoshino, K. "Tracer impurity diffusion in single-crystal rutile (TiO_{2-x})". J. Phys. Chem. Solids (1985), 46 [11], 1267-1283.

(2) Peterson, N. L.; Sasaki, J. Mechanisms of impurity diffusion in rutile. In Transport in Nonstoichiometric Compounds; Simkovich, G., Stubican, V. S., Eds.; Plenum Press: New York, (1985); pp 269-284.

(3) Cherniak, D. J.; Manchester, J.; Watson, E. B. "Zr and Hf diffusion in rutile". Earth and Planetary Science Letters (2007), 261 [1-2], 267-279.

(4) Hoshino, K.; Peterson, N. L.; Wiley, C. L. "Diffusion and point defects in TiO_{2-x}". J. Phys. Chem. Solids (1985), 46 [12], 1397-1411.

(5) Sheppard, L. R.; Atanacio, A. J.; Bak, T.; Nowotny, J.; Prince, K. E. "Bulk diffusion of niobium in single-crystal titanium dioxide". Journal of Physical Chemistry B (2007), 111 [28], 8126-8130.

(6) Lundy, T. S.; Coghlan, W. A. "Cation self diffusion in rutile". Journal de Physique Colloques (1973), C9, 299-302.

(7) Khan, S. U. M.; Al-Shahry, M.; Ingler Jr, W. B. "Efficient photochemical water splitting by a chemically modified n-TiO_2". Science (2002), 297, 2243-2245.

(8) Neumann, B.; Bogdanoff, P.; Tributsch, H.; Sakthivel, S.; Kisch, H. "Electrochemical mass spectroscopic and surface photovoltage studies of catalytic water photooxidation by undoped and carbon-doped titania". Journal of Physical Chemistry B (2005), 109 [35], 16579-16586.

(9) Zhang, L. P.; Li, M.; Diebold, U. "Characterization of Ca impurity segregation on the TiO_2(110) surface". Surf. Sci. (1998), 412-413, 242-251.

(10) Asahi, R.; Morikawa, T.; Ohwaki, T.; Aoki, K.; Taga, Y. "Visible-light photocatalysis in nitrogen-doped titanium oxides". Science (2001), 293 [5528], 269-271.

(11) Yahia, J. "Dependence of electrical conductivity and thermoelectric power of pure and aluminium-doped rutile on equilibrium oxygen pressure and temperature. ". Phys. Rev. (1963), 1 [5], 1711-1719.

(12) Choi, W. Y.; Termin, A.; Hoffmann, M. R. "The role of metal-ion dopants in quantam-sized TiO_2 - Correlation between photoreactivity and charge-carrier recombination dynamics". Journal of Physical Chemistry (1994), 98 [51], 13669-13679.

(13) Crisan, M.; Braileanu, A.; Raileanu, M.; Zaharescu, M.; Crisan, D.; Dragan, N.; Anastasescu, M.; Ianculescu, A.; Nitoi, I.; Marinescu, V. E.; Hodorogea, S. M. "Sol-gel S-doped TiO_2 materials for environmental protection". J. Non-Cryst. Solids (2008), 354 [2-9], 705-711.

(14) Matsumoto, Y.; Kurimoto, J.; Shimizu, T.; Sato, E. "Photoelectrochemical properties of polycrystalline TiO_2 doped with 3d transition-metals". J. Electrochem. Soc. (1981), 128 [5], 1040-1044.

(15) Martin, S. T.; Morrison, C. L.; Hoffmann, M. R. "Photochemical Mechanism of Size-Quantized Vanadium-Doped TiO_2 Particles". Journal of Physical Chemistry (1994), 98 [51], 13695.

(16) Bernasik, A.; Radecka, M.; Rekas, M.; Sloma, M. "Electrical properties of Cr-doped and Nb-doped TiO_2 Thin-films". Applied Surface Science (1993), 65-6, 240-245.

(17) Ruiz, A. M.; Sakai, G.; Cornet, A.; Shimanoe, K.; Morante, J. R.; Yamazoe, N. "Cr-doped TiO_2 gas sensor for exhaust NO_2 monitoring". Sens. Actuator B-Chem. (2003), 93 [1-3], 509-518.

(18) Monnier, A.; Augustynski, J. "Photoelectrolysis of water - Photoresponses of Nickel, Chromium and Zinc-doped polycrystalline TiO_2 electrodes". J. Electrochem. Soc. (1980), 127 [7], 1576-1579.
(19) Wilke, K.; Breuer, H. D. "The influence of transition metal doping on the physical and photocatalytic properties of titania". J. Photochem. Photobiol. A-Chem. (1999), 121 [1], 49-53.
(20) Bernasik, A.; Rekas, M.; Sloma, M.; Weppner, W. "Electrical surface versus bulk properties of Fe-doped TiO_2 single crystals". Solid State Ion. (1994), 72 [Part 2], 12-18.
(21) Bouchet, R.; Weibel, A.; Knauth, P.; Mountjoy, G.; Chadwick, A. V. "EXAFS study of dopant segregation (Zn, Nb) in nanocrystalline anatase (TiO_2)". Chemistry of Materials (2003), 15 [26], 4996-5002.
(22) Wang, Q. L.; Lian, G.; Dickey, E. C. "Grain boundary segregation in yttrium-doped polycrystalline TiO_2". Acta Materialia (2004), 52 [4], 809-820.
(23) Ruiz, A.; Dezanneau, G.; Arbiol, J.; Cornet, A.; Morante, J. R. "Study of the influence of Nb content and sintering temperature on TiO_2 sensing films". Thin Solid Films (2003), 436 [1], 90-94.
(24) Pang, Y.; Wynblatt, P. "Correlation between grain-boundary segregation and grain-boundary plane orientation in Nb-doped TiO_2". Journal of the American Ceramic Society (2005), 88 [8], 2286-2291.
(25) Wang, M. H.; Guo, R. J.; Tso, T. L.; Perng, T. P. "Effects of sintering on the photoelectrochemical properties of Nb-doped TiO_2 electrodes". International Journal of Hydrogen Energy (1995), 20 [7], 555-560.
(26) Nakajima, T.; Sheppard, L. R.; Prince, K. E.; Nowotny, J.; Ogawa, T. "Niobium segregation in TiO_2". Adv. Appl. Ceram. (2007), 106 [1], 1-7.
(27) Sheppard, L. R.; Bak, T.; Nowotny, J.; Nowotny, M. K. "Titanium dioxide for solar-hydrogen V. Metallic-type conduction of Nb-doped TiO_2". International Journal of Hydrogen Energy (2007), 32 [14], 2660-2663.
(28) Baumard, J. F.; Tani, E. "Electrical-conductivity and charge compensation in Nb doped TiO_2 rutile ". J. Chem. Phys. (1977), 67 [3], 857-860.
(29) Lee, S.-M.; Guo, R.-J.; Tso, T.-L.; Perng, T.-P. "Photoelectrochemical response and surface variation of TiO_2 electrodes irradiated with laser light". International Journal of Hydrogen Energy (1996), 21 [4], 253-257.
(30) Lee, W.; Do, Y. R.; Dwight, K.; Wold, A. "Enhancement of Photocatalytic Activity of Titanium(IV) Oxide with Molybdenum(VI) Oxide". Mater. Res. Bull. (1993), 28 [11], 1127-1134.
(31) Gulino, A.; Condorelli, G. G.; Fragalà, I.; Egdell, R. G. "Surface segregation of Sb in doped TiO_2 rutile". Applied Surface Science (1995), 90 [3], 289-295.
(32) Tani, E.; Baumard, J. F. "Electrical properties and defect structure of rutile slightly doped with Cr and Ta". Journal of Solid State Chemistry (1980), 32 [1], 105-113.
(33) Do, Y. R.; Lee, W.; Dwight, K.; Wold, A. "The Effect of WO_3 on the Photocatalytic Activity of TiO_2". Journal of Solid State Chemistry (1994), 108 [1], 198-201.
(34) Matsumoto, Y.; Shimizu, T.; Toyoda, A.; Sato, E. "New preparation method for doped polycrystalline TiO_2 and Nb2O5 and their photo-electrochemical properties". Journal of Physical Chemistry (1982), 86 [18], 3581-3585.
(35) Xu, A.-W.; Gao, Y.; Liu, H.-Q. "The Preparation, Characterization, and their Photocatalytic Activities of Rare-Earth-Doped TiO_2 Nanoparticles". Journal of Catalysis (2002), 207 [2], 151-157.
(36) Trenczek-Zajac, A.; Radecka, M.; Rekas, M. "Photoelectrochemical properties of Nb-doped titanium dioxide". Physica B-Condensed Matter (2007), 399 [1], 55-59.

(37) Nowotny, M. K.; Sheppard, L. R.; Bak, T.; Nowotny, J. "Defect chemistry of titanium dioxide. application of defect engineering in processing of TiO_2-based photocatalysts". Journal of Physical Chemistry C (2008), 112 [14], 5275-5300.

(38) Menzies, D. B.; Dai, Q.; Bourgeois, L.; Caruso, R. A.; Cheng, Y. B.; Simon, G. P.; Spiccia, L. "Modification of mesoporous TiO_2 electrodes by surface treatment with titanium(IV), indium(III) and zirconium(IV) oxide precursors: preparation, characterization and photovoltaic performance in dye-sensitized nanocrystalline solar cells". Nanotechnology (2007), 18 [12], 11.

(39) Brehm, J. U.; Winterer, M.; Hahn, H. "Indium Tin Oxide Nanoparticles Prepared by Chemical Vapor Synthesis". Materials Research Society Symposium Proceedings (2002), 704, W5.3.1 - W5.3.6.

(40) Guoa, L. J.; Shen, X. P.; Zhu, G. X.; Chen, K. M. "Preparation and gas-sensing performance of In(2)O(3) porous nanoplatelets". Sens. Actuator B-Chem., 155 [2], 752-758.

(41) Karn, R. K.; Srivastava, O. N. "On the structural and photochemical studies of In_2O_3 admixed nanostructured TiO_2 with regard to hydrogen production through photoelectrolysis". International Journal of Hydrogen Energy (1998), 23 [6], 439-444.

(42) Shchukin, D.; Poznyak, S.; Kulak, A.; Pichat, P. "TiO_2-In_2O_3 photocatalysts: preparation, characterisations and activity for 2-chlorophenol degradation in water". Journal of Photochemistry and Photobiology A - Chemistry (2004), 162 [2-3], 423-430.

(43) Skorb, E. V.; Ustinovich, E. A.; Kulak, A. I.; Sviridov, D. V. "Photocatalytic activity of TiO_2 : ln2O3 nanocomposite films towards the degradation of arylmethane and azo dyes". J. Photochem. Photobiol. A-Chem. (2008), 193 [2-3], 97-102.

(44) Poznyak, S. K.; Talapin, D. V.; Kulak, A. I. "Structural, optical and photoelectrochemical properties of nanocrystalline TiO_2-In_2O_3 composite solids and films prepared by sol-gel method.". Journal of Physical Chemistry B (2001), 105, 4816-4823.

(45) Poznyak, S. K.; Talapin, D. V.; Kulak, A. I. "Optical properties and charge transport in nanocrystalline TiO_2-In_2O_3 composite films.". Thin Solid Films (2002), 405, 35-41.

(46) Cerrato, G.; Magnacca, G.; Morterra, C.; Montero, J.; Anderson, J. A. "Modification to the Surface Properties of Titania by Addition of India". Journal of Physical Chemistry C (2009), 113 [47], 20401-20410.

(47) Atashbar, M. Z.; Sun, H. T.; Gong, B.; Wlodarski, W.; Lamb, R. "XPS study of Nb-doped oxygen sensing TiO_2 thin films prepared by sol-gel method". Thin Solid Films (1998), 326 [1], 238-244.

(48) Kokusen, H.; Matsuhara, S.; Nishino, Y.; Hasegawa, S.; Kubono, K. "Effects of loading niobium compounds on sensing factor and function of TiO_2". Catalysis Today (1996), 28, 191-197.

(49) Karakitsou, K. E.; Verykios, X. E. "Effects of altervalent cation doping of titania on its performance as a photocatalyst for water cleavage". The Journal of Physical Chemistry (1993), 97 [6], 1184-1189.

(50) Kikkawa, H.; O'Regan, B.; Anderson, M. A. "The photoelectrochemical properties of Nb-doped TiO_2 semiconducting ceramic membrane". Journal of Electroanalytical Chemistry and Interfacial Electrochemistry (1991), 309 [1–2], 91-101.

(51) Kesselman, J. M.; Weres, O.; Lewis, N. S.; Hoffmann, M. R. "Electrochemical Production of Hydroxyl Radical at Polycrystalline Nb-Doped TiO_2 Electrodes and Estimation of the Partitioning between Hydroxyl Radical and Direct Hole Oxidation Pathways". Journal of Physical Chemistry B (1997), 101, 2637-2643.

(52) Sheppard, L. R.; Atanacio, A.; Bak, T.; Nowotny, J.; Prince, K. E. Effect of niobium segregation on the surface properties of titanium dioxide. In Solar Hydrogen and

Nanotechnology; Vayssieres, L., Ed.; Spie-Int Soc Optical Engineering: Bellingham, (2006); Vol. 6340; pp U298-U306.

(53) Burggraaf, A. J.; Winnubst, A. J. A. Segregation in Oxide Surfaces, Solid Electrolytes and mixed Conductors. In Surface and Near-Surface Chemistry of Oxide Materials; Elsevier: Amsterdam, (1988); pp 448-477.

(54) Cabane, J.; Cabane, F. Equilibrium segregation in interfaces. In Interface segregation and related processes in materials; Nowotny, J., Ed.; Trans Tech Publications Ltd.: Zurich, (1991); pp 1-150.

(55) Wynblatt, P.; McCune, R. C. Surface Segregation in Metal Oxides. In Surface and Near-Surface Chemistry of Oxide Materials; Elsevier Science Publishers, (1988); pp 247-279.

(56) Kuivers, F. J.; Ponec, V. Surf. Sci. (1977), 68.

(57) Leygraf, C.; Hultquis, G.; Ekelund, S.; Eriksson, J. C. "Surface composition studies of (100) and (110) faces of monocrystalline $Fe_{84}Cr_{16}$". Surf. Sci. (1974), 46, 157-176.

(58) Rolland, A.; Aufray, B. "Superficial composition in binary solid solutions A(B): Drastic effect of pure element surface tensions". Surf. Sci. (1985), 162 [1-3], 530-537.

(59) Ikeda, J. A. S.; Chiang, Y. M. "Space-charge segregation at grain-boundaries in titanium-dioxide. 1. Relationship between lattice deffect chemistry and space-charge potential ". Journal of the American Ceramic Society (1993), 76 [10], 2437-2446.

(60) Ikeda, J. A. S.; Chiang, Y. M.; Garrattreed, A. J.; Vandersande, J. B. "Space-charge segregation at grain-boundaries in titanium-dioxide. 2. Model experiments". Journal of the American Ceramic Society (1993), 76 [10], 2447-2459.

(61) Nowotny, J. Inteface defect chemistry and its impact on properties of oxide ceramic materials. In Science of Ceramic Interfaces; Nowotny, J., Ed.; Elsevier Science Publishers B.V., (1991); pp 79-204.

(62) Kingery, W. D. "Plausible concepts necessary and sufficient for interpretation of ceramic grain-boundary phenomena .1. Grain-boundary characteristics, structure, and electrostatic potential". Journal of the American Ceramic Society (1974), 57 [1], 1-8.

(63) Yan, M. F.; Cannon, R. M.; Bowen, H. K. "Space charge, elastic field, and dipole contributions to equilibrium solute segregation at interfaces". Journal of Applied Physics (1983), 54 [2], 764-768.

(64) Hirschwald, W.; Loechel, B.; Nowotny, J.; Oblakowski, J.; Sikora, I.; Stolze, F. "SIMS studies of segregation for NiO-Cr_2O_3 solid-solution". Bulletin De L Academie Polonaise Des Sciences-Serie Des Sciences Chimiques (1981), 29 [7-8], 369-375.

(65) Hirschwald, W.; Sikora, I.; Stolze, F. "Effect of gas-phase composition on chromium segregation in NiO-Cr_2O_3 solid-solutions". Surface and Interface Analysis (1985), 7 [3], 155-157.

(66) Hirschwald, W.; Sikora, I.; Stolze, F.; Oblakowski, J. "Effect of temperature on chromuim segregation to CoO (100) and NiO (100) surfaces ". Surface and Interface Analysis (1989), 14 [8], 477-481.

(67) Hirschwald, W.; Sikora, I.; Stolze, F.; Oblakowski, J. "Effect of Temperature on Chromium Segregation to CoO(100) and NiO(100) Surfaces". Surface and Interface Analysis (1989), 14 [8], 477-481.

(68) Haber, J.; Nowotny, J.; Sikora, I.; Stoch, J. "Electron-Spectroscopy in Studies of Surface Segregation of Cr in Cr-Doped CoO". Applied Surface Science (1984), 17 [3], 324-330.

(69) Nowotny, J. "Interface defect chemistry of oxide ceramic materials - Unresolved problems ". Solid State Ion. (1991), 49, 119-128.

(70) Nakamura, S.; Yagi, E.; Osaka, T.; Iwaki, M. "Lattice disorder and behavior of implanted atoms in In-implanted TiO_2 (rutile)". Nuclear Instruments and Methods in Physics Research Section B: Beam Interactions with Materials and Atoms (1988), 33 [1-4], 729-733.

(71) Akiyama, K.; Toyama, N.; Muraoka, K.; Tsunashima, M. "Configurational observation of titanium oxide pigment particles". Journal of the American Ceramic Society (1998), 81 [4], 1071-1073.
(72) Tsunashima, M.; Muraoka, K.; Akiyama, K.; Toyama, N. "Relationships between particle properties and pigment characteristics of nb containing TiO_2". Shikizai kyokaishi (In Japanese) (1998)[71], 297-304.
(73) Zaitsev, S. V.; Moon, J.; Takagi, H.; Awano, M. "Preparation and characterization of nanocrystalline doped TiO_2". Advanced Powder Technology (2000), 11 [2], 211-220.
(74) Sheppard, L. R.; Bak, T.; Nowotny, J.; Nowotny, M. K. "Effect of Oxygen Activity on Niobium Segregation in Niobium-Doped Titanium Dioxide". Journal of the Australian Ceramic Society (2008), 44 [2], 42-46.
(75) Nowotny, J.; Bak, T.; Nowotny, M. K.; Sheppard, L. R. "Chemical diffusion in metal oxides. Example of TiO_2". Ionics (2006), 12 [3], 227-243.
(76) Nowotny, M. K.; Bak, T.; Nowotny, J. "Electrical properties and defect chemistry of TiO_2 single crystal. IV. Prolonged oxidation kinetics and chemical diffusion". Journal of Physical Chemistry B (2006), 110 [33], 16302-16308.
(77) Ruiz, A. M.; Dezanneau, G.; Arbiol, J.; Cornet, A.; Morante, J. R. "Insights into the structural and chemical modifications of Nb additive on TiO_2 nanoparticles". Chemistry of Materials (2004), 16 [5], 862-871.
(78) Black, J. R.; Kingery, D. W. "Segregation of Aliovalent Solutes Adjacent Surfaces in MgO". Journal of the American Ceramic Society (1979), 62, 176-178.
(79) Sikora, I.; Stolze, F.; Hirschwald, W. "Segregation of chromium in CoO-Cr_2O_3 solid-solutions and $CoCr_2O_4$ spinel phases studied by SIMS and ESCA". Surface and Interface Analysis (1987), 10 [8], 424-429.
(80) Sheppard, L. R.; Atanacio, A. J.; Bak, T.; Nowotny, J.; Prince, K. E. "Application of secondary ion mass spectrometry in studies of niobium segregation in Nb-doped TiO_2". Journal of the Australian Ceramic Society (2008), 44, 42-46.
(81) Nowotny, J.; Bak, T.; Nowotny, M. K.; Sorrell, C. C. "Charge transfer at oxygen/zirconia interface at elevated temperatures - Part 3: Segregation induced interface properties". Adv. Appl. Ceram. (2005), 104 [4], 165-173.

CHAPTER 4

Experimental Procedure

It should be noted that each of the included papers (Chapters 6 to 10) also contain experimental sections outlining the specific experimental details related to that work. Therefore, this chapter will provide only an overview of the experimental procedure adopted for this work, including any additional experimental details not provided in the individual papers due to length restriction imposed by journals.

The flow diagram, provided in **Figure 4-1**, summarises the sample preparation and analysis methodology used in the present work.

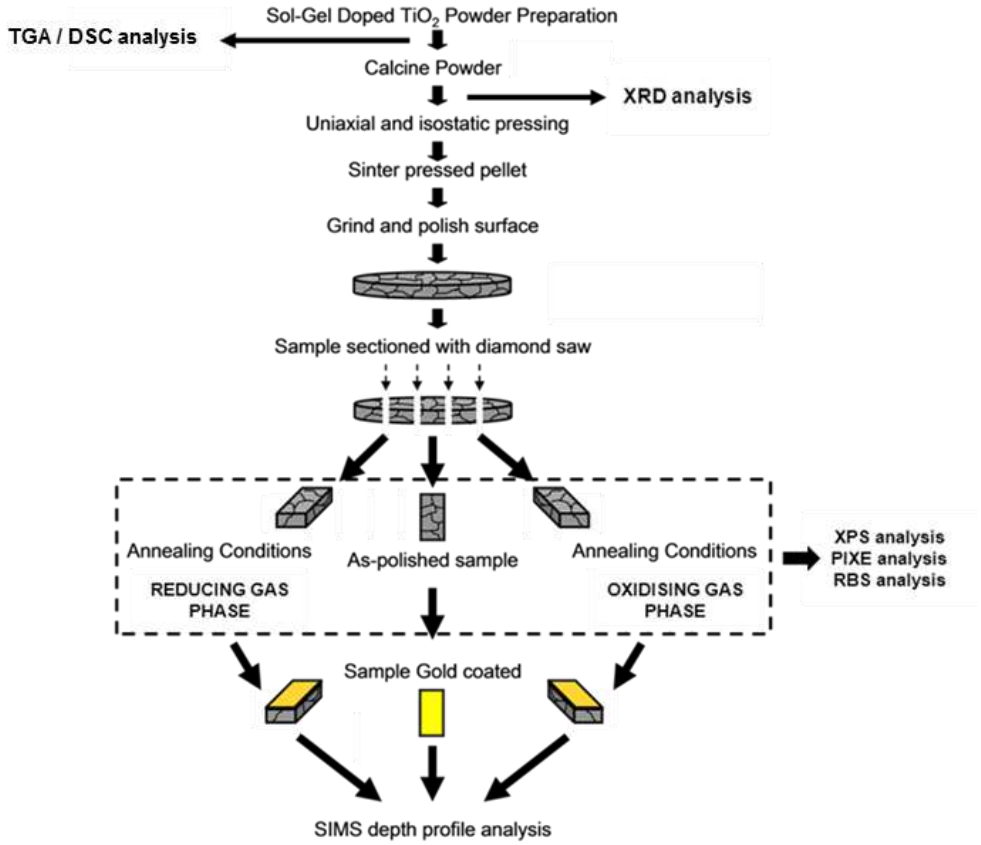

Figure 4-1. Flow diagram of the experimental methodology used for sample preparation and analysis.

4.1 Specimen Preparation

4.1.1. Sol Gel

Indium and niobium doped TiO_2 powders were prepared using the sol-gel technique. The precursors used included titanium isopropoxide (97%-Aldrich), glacial acetic acid, anhydrous ethanol, deionised water and either indium (III) chloride (99.999%-Aldrich) or niobium (V) chloride (99%-Aldrich). Specific details on the sol-gel methodology used are provided in Chapter 8 and 9 (sections 8.3 and 9.3) for indium-doped TiO_2 and Chapter 10 (section 10.3) for niobium-doped TiO_2.

4.1.2. Powder Calcination

4.1.2.1. Thermogravimetric Analysis (TGA) and Differential Scanning Calorimetry (DSC)

Simultaneous thermogravimetric analysis (TGA) and differential scanning calorimetry (DSC) was used to characterise the thermal properties of the bulk amorphous TiO_2 powder synthesised by the sol-gel method.

The TGA and DSC sample analysis was performed in air from ambient temperature to 1073 K (800˚C) with a heating rate of 10˚C/min. The TGA results, **Figure 4-2**, show the most significant weight loss of ~12.5% occurred between 0˚C and 350˚C.

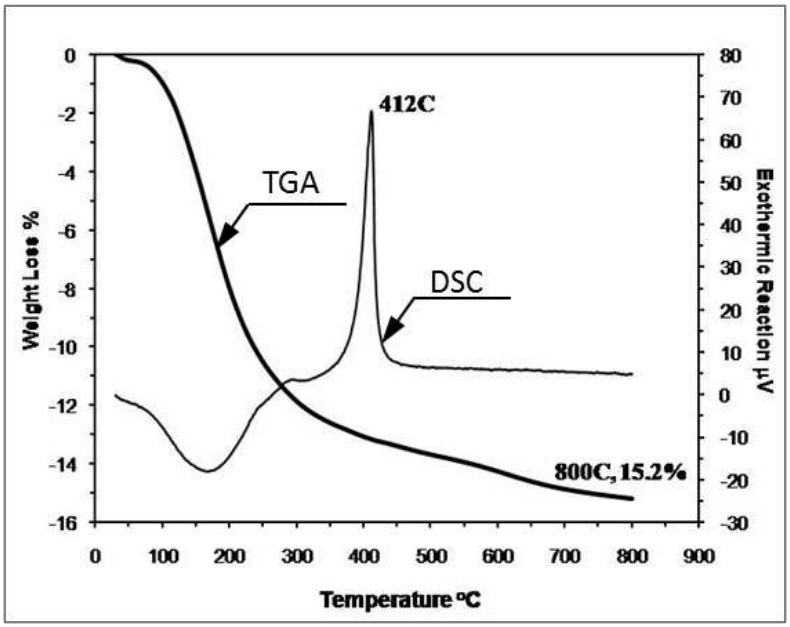

Figure 4-2. Combined TGA and DSC analysis of sol-gel synthesised amorphous TiO_2 powder.

From 350˚C to 800˚C the loss of weight was significantly less with a total weight loss of 15.2% measured at 800˚C. It appears the trend is tending toward achieving a minimum at a temperature above 800˚C. The complimentary DSC results, **Figure 4-2**, shows as a broad endothermic peak at 150-200˚C, which corresponds to the large weight loss seen in TGA and is associated with water vaporisation. A broad exothermic increase seen between 200˚C and 390˚C is related to organic impurity elimination, followed by and a sharp exothermic peak at 412˚C corresponding to the anatase-rutile phase transformation. A stable flat DSC response is observed from 450 to 800˚C. Based on the TGA-DSC results, a maximum calcining temperature of 1173 K (900˚C) and intermediate temperature dwell points, shown in **Figure**

4-3, were selected to achieve water and organic decomposition, as well as complete anatase-rutile phase transformation.Powder calcination was performed in platinum foil lined alumina boats in a tube furnace open to atmosphere.

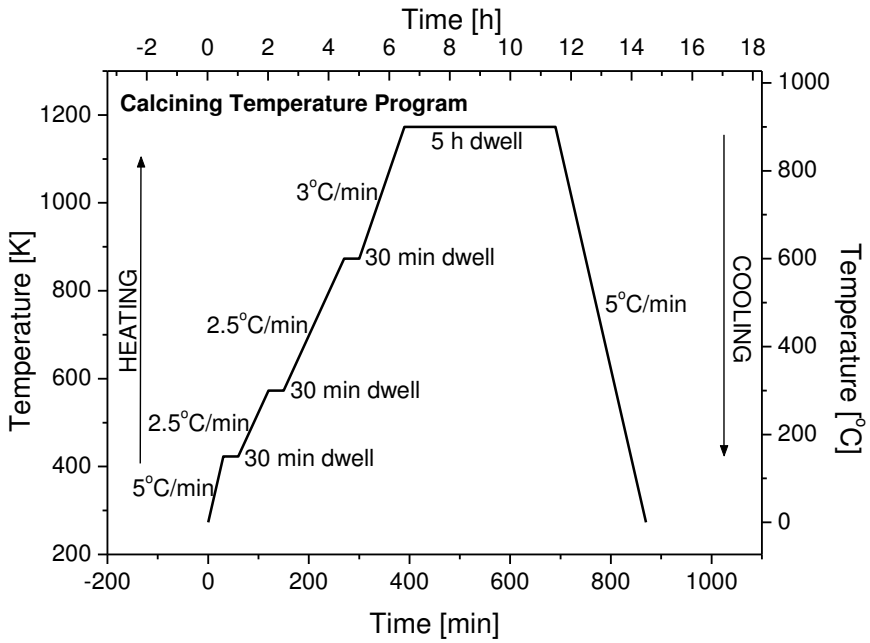

Figure 4-3. Heating and cooling conditions used for specimen calcining

4.1.2.2. X-Ray Diffraction (XRD)

XRD analysis was subsequently performed to confirm the phase of the powders after calcination. Details on the applied XRD analysis parameters are provided in Chapter 9 (section 9.3). The obtained X-ray diffraction patterns for undoped and In-doped TiO_2 powders are shown in **Figure 4-4.**

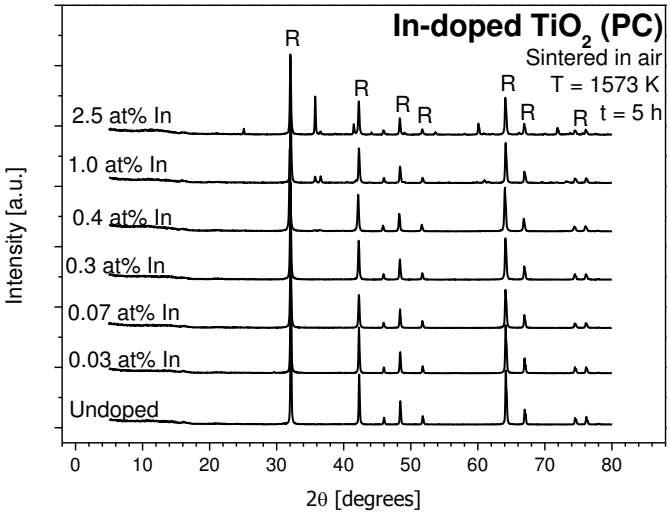

Figure 4-4. XRD patterns of undoped and indium-doped TiO_2 powder calcined at 1573 K for 5 h in air. Peaks corresponding to the rutile phase are marked with an R.

4.1.3. Sample Consolidation

The calcined powder was pressed into cylindrical pellets (approximately 3mm thick and 10mm in diameter) using a uniaxial press (40-50 MPa) and stainless steel die without the addition of any binding agents. The resulting pellets were vacuum sealed into thin latex tubes and subsequently pressed isostatically using a cold isostatic press (CIP) to 400 MPa with a full pressure dwell time of 2 minutes. The pellets were then sintered in air at 1773 K for 5 hours to achieve densification. An example of the resulting pellet and typical grain structure obtained with an optical microscope are shown in **Figure 4-5**.

The final stage of specimen preparation involved removing a surface layer (~30-50 µm) by grinding and polishing to ~ 1µm finish using a series of diamond pads and diamond suspension liquids (Struers LaboSystem). This was done for two reasons, (i) to remove of any surface segregation imposed during sintering, so the resulting polished surface is reflective of the bulk dopant composition, (ii) the depth resolution of surface sensitive techniques such as SIMS are diminished by surface roughness. The resulting as polished specimens are considered in the present work as reference specimens.

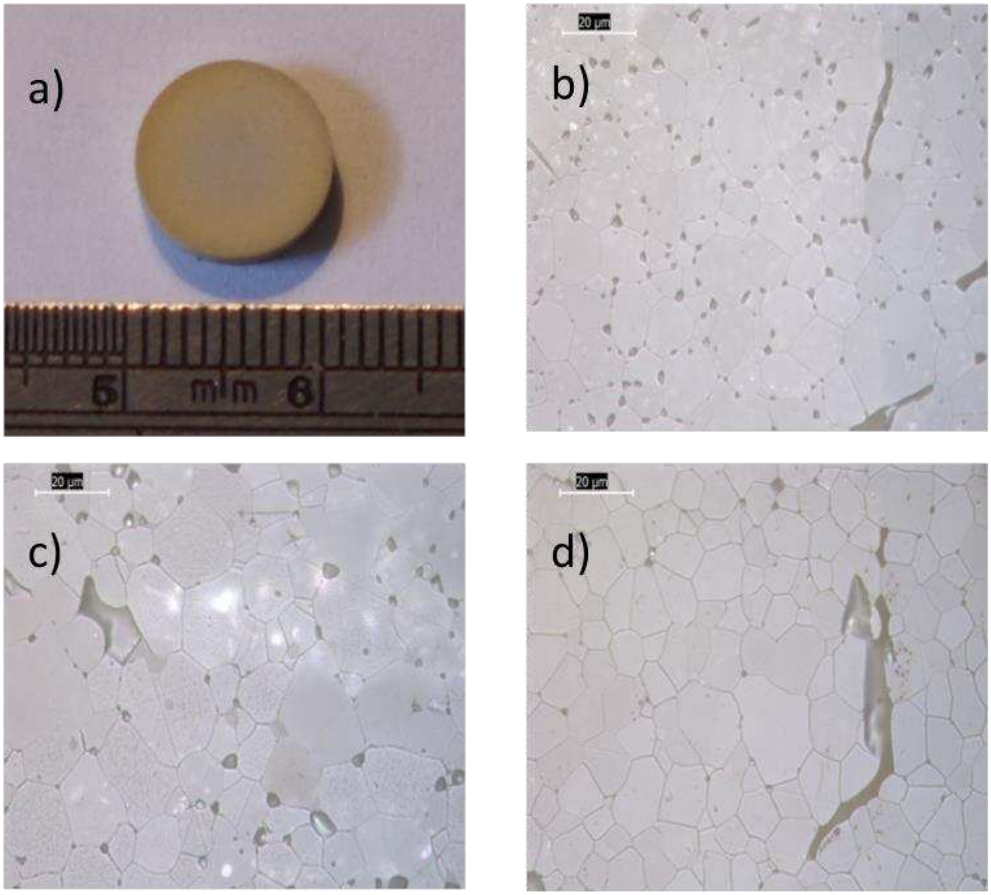

Figure 4-5. a) Example of pressed and sintered TiO_2 pellet, b) undoped TiO_2 microstructure c) 0.03 at% In-doped TiO_2 microstructure d) 0.4 at% In-doped TiO_2 microstructure.

4.2 Specimen Processing

The schematic illustration shown in **Figure 4-6** summarises the basic experimental set-up used in the present work for sample annealing in the gas phase of controlled oxygen activity. It can be seen that a water filled bubbler is located at the end of the experimental set-up to allow the input gas to be released whilst stopping the backflow of any ambient air into the system.

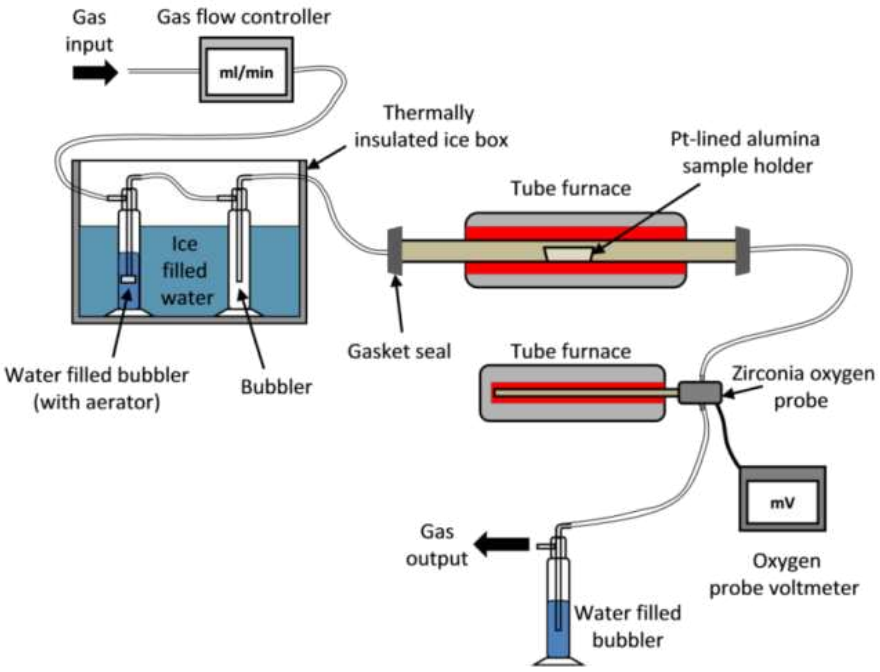

Figure 4-6. Schematic illustration of the experimental set-up used to control oxygen activity during annealing.

4.2.1. Oxygen Activity

It is essential that the gas phase oxygen activity during annealing is well-defined. For this work a zirconia-based oxygen probe was used to monitor oxygen activity electrochemically. As shown schematically in **Figure 4-7**, the oxygen probe is made of an alumina (Al_2O_3) tube closed on one end with a zirconia disc that has platinum contacts attached to both sides and artificial air (21% of oxygen and 79% of nitrogen) used as the reference gas. The oxygen activity was determined using the Nerst equation:

$$E = \frac{kT}{4} \ln \frac{p(O_2)_x}{p(O_2)_{air}} \qquad \textbf{(4-1)}$$

where E is the voltage (mV) measured on the oxygen sensor voltmeter, k is Boltzman constant, T absolute temperature, and $p(O_2)_x$ and $p(O_2)_{air}$ denote the oxygen activity in the studied gas flowing through the reactor and the reference gas (air), respectively. The zirconia based oxygen probe was positioned on the downstream side of the reaction furnace and held at a separate operating temperature of 1023 K.

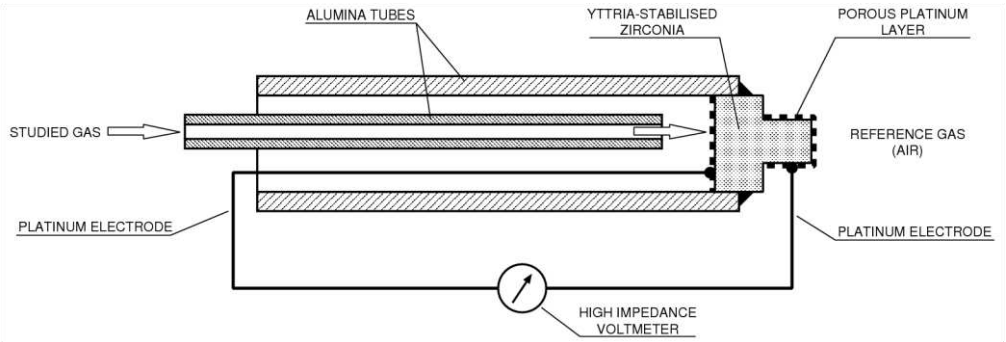

Figure 4-7. Schematic illustration of a yttria-stabilised zirconia electrochemical oxygen sensor.

The flow rate of input gas for all processed specimens was controlled at a rate of 100 ml/min using a mass flow controller (Mass-trak, Sierra instruments Inc.).

4.2.1.1. Reducing Gas Phase Conditions

Reducing gas phase conditions were established during annealing using a hydrogen-argon gas mixture (1% of hydrogen and 99% of argon). As the oxygen activity in gas mixtures involving H_2/H_2O are influenced by temperature, this gas mixture prior to entering the reaction furnace was bubbled through deionised water held at close to ~273 K using an ice bath, as illustrated in **Figure 4-6**. This minimises variations in $p(O_2)$ caused by changes in ambient lab temperatures, and allows the same 273 K temperature condition for the input gas to be established reproducibly. The oxygen activity for the H_2/Ar mixture is approximately $p(O_2) = 10^{-10}$ Pa at T =1273 K.

4.2.1.2. Oxidising Gas Phase Conditions

Oxidising gas phase conditions were established during annealing using pure oxygen gas (99.9%) or pure argon gas (99.999%). The resulting oxygen activity of these pure gases are not affected by temperature, therefore, use of the ice bath, shown in **Figure 4-6**, was not required and was by-passed during annealing. The oxygen activity for pure argon and pure oxygen gas is $p(O_2) = 10$ Pa, and $p(O_2) = 75$ kPa, respectively.

4.3 Specimen Analysis

4.3.1. Bulk Analysis

Determination of both the dopant and impurity concentration is crucial for having well-defined reference specimens. PIXE analysis was used to determine the bulk elemental concentrations.

An advantage of PIXE is that it does not require any specific sample preparation, unlike the sample digestion step required for the commonly used inductively coupled plasma mass spectrometry (ICP-MS) technique, which often requires the use of hydrofluoric acid due to the chemical resistance of TiO_2. As PIXE is non-destructive, it can therefore be performed directly on the actual pre- and post-annealed polished pellets. Specific details on the PIXE analysis conditions are provided in Chapter 8 (sections 8.3), Chapter 9 (section 9.3) and chapter 10 (section 10.3).

4.3.2. Surface Analysis

The surface layer of each sample was characterised using a range of analysis techniques. XPS was the first technique applied on each sample as it is non-destructive; uses low energy X-rays (1486.6 eV) and requires no additional sample preparation. The samples were then analysed with RBS which uses significantly higher incident beam energies (~2 MeV) compared with XPS. The RBS technique is also non-destructive and can be performed directly on the annealed specimens without any additional sample preparation. SIMS was the final analysis technique performed on each sample because of its destructive nature and the fact that it required deposition of a thin gold surface layer to eliminate sample charging during analysis.

CHAPTER 5

Overarching Statement

The outcomes of the present work are presented as a series of five papers, three of which have been published in refereed journals while the other two are presently in submission for publication. These papers, which report integral stages of the present PhD research, have been included directly as individual chapters of this thesis. Each of the following chapters, therefore, contain a separate, Introduction, Definition of Terms, Experimental, Results, Discussion and Conclusions section related to that specific stage of the research. The following five papers are included:

Paper 1 (Chapter 6)

Reactivity Between In_2O_3 and TiO_2 (Rutile) Studied Using Secondary Ion Mass Spectrometry, SIMS. AJ Atanacio, J Nowotny, KE Prince. Separation and Purification Technology, 91 (2012) 96-102.

This paper assessed the reactivity between TiO_2 single crystal and a thin layer of In_2O_3 deposited on its surface. It considers the reaction progress in terms of thermal diffusion of indium in the rutile phase at one temperature and oxygen activity.

Paper 2 (Chapter 7)

Diffusion Kinetics of Indium in TiO_2 (Rutile). AJ Atanacio, T Bak, J Nowotny, KE Prince. Journal of the American Ceramic Society, DOI: 10.1111/jace.12244.

The work in this paper determined the self-diffusion coefficients of indium in TiO_2 single crystal over a range of temperatures. The determination of this data was essential for selecting

the optimal processing conditions necessary to form of well-defined In-doped TiO_2 solid solutions.

Paper 3 (Chapter 8)

Effect of Oxygen Activity on Surface Composition of In-doped TiO_2 at Elevated Temperatures. AJ Atanacio, J Nowotny, KE Prince. Journal of Physical Chemistry C, 116 (2012) 19246-19251.

This paper determined the effect of oxygen activity on the segregation of indium in In-doped TiO_2 solid solutions as a function of annealing time. The reported data was used to determining the optimal processing conditions in terms of temperature, time and oxygen activity, required to reach segregation equilibrium in In-doped TiO_2.

Paper 4 (Chapter 9)

Effect of Indium Segregation on the Surface versus Bulk Chemistry for Indium-doped TiO_2. AJ Atanacio, T Bak, J Nowotny. ACS Applied Materials and Interfaces. DOI: 10.1021/am301729z.

This paper assessed the enrichment of In in In-doped TiO_2 induced by segregation based on the processing conditions, temperature, time and $p(O_2)$, established in papers (2) and (3). The reported segregation data and derived model may be used for the determination of optimal surface processing conditions.

Paper 5 (Chapter 10)

Effect of Niobium Segregation on Surface Chemistry and the Related Electric Field Light-Induced Charge Carrier Separation in Nb-Doped TiO_2. AJ Atanacio, T Bak, J Nowotny. In submission.

This paper examined the segregation-induced concentration gradients of niobium in Nb-doped TiO_2 in oxidising and reducing gas phase conditions. The obtained data for Nb^{5+} was also assessed in relation to the effects observed for In^{3+} in chapter 9 (paper 4). The reported segregation data and derived model may be used for the determination of optimal surface processing conditions in both oxidising and reducing conditions.

CHAPTER 6

Reactivity between In_2O_3 and TiO_2 (rutile) studied using secondary ion mass spectrometry (SIMS)

6.1 Abstract

The present work considers the reaction kinetics between titanium dioxide, TiO_2 (rutile) single crystal and a thin layer of indium oxide, In_2O_3 deposited on its surface. The reported experimental data are reflective of a chemical reaction involving the diffusive transport of In^{3+} in the rutile phase. The reaction progress at 1173 K is monitored using the secondary ion mass spectrometry (SIMS) technique. It is shown that the SIMS depth profiles may be considered in terms of two distinctly different components, i) related to the surface layer of In_2O_3, and ii) the rutile single crystal phase beneath. The depth profile of the rutile phase includes regions related to bulk diffusion of indium as well as the background composition. The bulk diffusion coefficient of indium, In^{3+} in single crystal TiO_2 (rutile) at 1173K and $p(O_2)$ = 21 kPa was determined to be $4.4(\pm0.2) \times 10^{-18}$ m^2s^{-1}.

6.2 Introduction

Since the pioneering work of Fujishima and Honda in 1972 [1], titanium dioxide TiO_2 has received particular research attention due to its potential application for generating hydrogen gas from water using sunlight. This has the potential to provide a sustainable, clean and environmentally friendly fuel alternative to fossil fuels. So far, however, the energy conversion efficiency (ECE) of commercially available TiO_2 is too low for this technology to be

commercially viable. It is well known that the functional properties of TiO_2; such as photocatalytic activity and electrical conductivity, are related to the materials defect chemistry which includes the presence of aliovalent dopants or impurities in the lattice [2-5]. Consequently, there has been significant research effort aimed at improving the functional performance of TiO_2 via a number of methods including the intentional introduction of foreign dopant species as shown in a recent review [6]. However, often the reported results show significant variability and contradiction regarding a dopants effect on functional performance [4]. A failure to correctly address the reactivity of these solid solutions under well-defined processing conditions is likely to have contributed to these discrepancies. Without well-defined specimens it becomes extremely difficult, if not impossible, to correctly assess and compare results even for seemingly the same dopants. Knowledge of the diffusion coefficient under specific processing conditions allows prediction of the time required to achieve either a homogenous distribution of the chosen dopants throughout the specimen; or alternatively to impose controlled concentration gradients within the surface layer under specific and reproducible processing conditions. The diffusion data may be determined from the diffusion-induced concentration profiles using secondary ion mass spectrometry, SIMS. The correct interpretation of depth profiles determined by SIMS is a critical issue in the interpretation of diffusion data.

The intention of the study was to assess the diffusion of a trivalent ion, in this case In^{3+}, in single crystal TiO_2. In_2O_3 exhibits high electrical properties and has been shown to be a promising material for dye sensitised photovoltaic devices [7], optoelectronic devices [8], and gas sensors [9]. Furthermore, the large ionic radius of In^{3+} (80Å) compared to Ti^{4+} (61Å) may also have a strong influence on the diffusion (and segregation) driving forces due to an energy strain contribution. In order to correctly assess the effect of In^{3+} on the functional properties of In-TiO_2 solid solutions, knowledge of its diffusion rate is essential.

Karakitsou et al.[10] reported on the effect of a number of aliovalent dopants in TiO_2, including In^{3+}, toward photocatalytic water splitting performance. They determined that higher valence dopants (W^{6+}, Ta^{5+}, Nb^{5+}) enhanced water cleavage while dopants of lower valence (In^{3+}, Zn^{2+}, Li^{+}) reduced the rate of H_2 production [10]. This contradicts the findings of Shchukin et al.[11] who studied TiO_2-In_2O_3 powders with various Ti/In ratios against their photocatalytic activity to degrade 2-chlorophenol in water. They observed greatly enhanced performance of TiO_2-In_2O_3 compared to pure TiO_2 which was explained on the basis of better charge carrier separation, improved oxygen reduction and increased surface acidity [11]. Wang et al. [12] also

observed enhanced photocatalytic activity of In^{3+} doped TiO_2 compared to pure TiO_2 which was attributed to the formation of a unique O-In-Cl_x chemical species on the surface. These conflicting reports highlight the need for further investigation of In-doped TiO_2.

It is important to note that diffusion requires sufficiently elevated temperatures for lattice mobility to occur. Therefore, the rutile phase was selected as it is stable in the temperature ranges for which both oxygen and dopant diffusion can take place under control oxygen activity conditions. For the same reason, it is difficult to control oxygen activity in the anatase phase.

The aim of this paper is to identify the physical meaning of diffusion depth profiles obtained with SIMS in terms of two distinctively different components, one related to the deposited surface layer of In_2O_3, and the other being the rutile single crystal phase beneath. The present work also demonstrates how the quantitative diffusion coefficient of indium in TiO_2 can be determined from the depth profile component related to the rutile single crystal. To the best of our knowledge, the determination of indium diffusion in TiO_2 has not been previously reported in literature. It therefore constitutes new materials data which may be used for engineering well-defined indium-doped TiO_2 specimens with controlled composition and functional properties.

6.2.1. Determination of Diffusion Profiles

The determination of diffusion coefficients requires accurate measurement of the diffusing species concentration into the host lattice as a function of depth from the surface. The radiotracer technique, commonly used in literature, requires use of a radioactive diffusion species. After diffusion has occurred, the sample is sectioned sequentially from the surface and chemical analysis performed on each sectioned piece to determine the concentration of the radiotracer. The resulting concentrations and sectioning depths are correlated to generate a surface-to-bulk concentration profile. Even with the improved sectioning methods currently available, diffusion depths of several microns are often necessary to achieve accurate results using this method [13]. On the other hand, the secondary ion mass spectrometry (SIMS) technique utilises a focused low energy (keV) primary ion beam to continuously sputter ions from the surface of the specimen. The liberated secondary ions are simultaneously analysed in a mass spectrometer to provide a concentration profile as a function of depth. The advantage of the SIMS technique for diffusion determination is that it provides high chemical sensitivity without the need for radioactive tracers, has high depth resolution (2 - 5 nm) and minimal sample damage. However, a critical and often challenging issue with SIMS is the correct interpretation of depth profiles in

order to separate intrinsic sputtering artefacts (such as pre-equilibrium sputtering and matrix effects) from the data related to actual composition changes in the sample.

6.2.2. Basic Diffusion Model and Equations

Diffusion can occur in solids via a number of potential pathways, including lattice diffusion, grain boundary diffusion and dislocation planes. Often several diffusion pathways contribute to the overall concentration profile of a diffusion species, which consequently reflects the sum of the individual concentration profiles related to each different pathway [13]:

$$C(x) = C_1(x) + C_2(x) + C_3(x) \qquad \textbf{(6-1)}$$

where C(x) is the overall concentration profile and $C_1(x)$, $C_2(x)$ and $C_3(x)$ represents the concentration profile for each contributing diffusion pathway. As only the overall concentration profile can be measured experimentally, it is necessary to correctly identify the individual concentration profile regions corresponding to the various contributing pathways. This is schematically represented in **Figure 6-1** for a system in which overall diffusion occurs by a combination of lattice and grain boundary pathways [13].

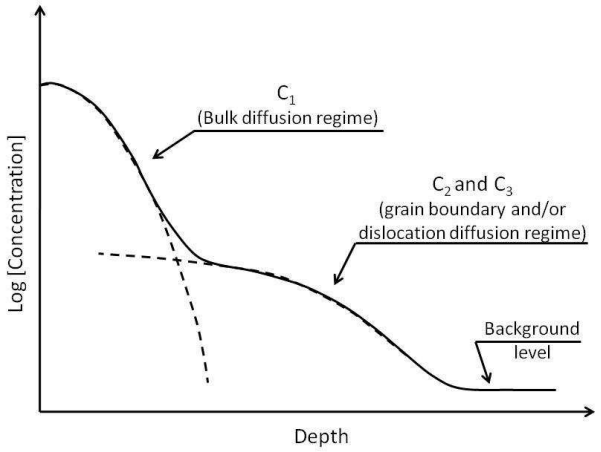

Figure 6-1. Schematic illustration of the concentration profile of for a species diffusing into a solid via bulk and grain boundary diffusion pathways [13].

It is important to note that the SIMS technique provides depth profiles in terms of ion yield (i.e. counts) rather than absolute concentration. However, as the SIMS ion yield is proportional to absolute elemental concentration, a reasonable estimation of relative concentration can be made by normalising the intensity of the species of interest against a species whose intensity

throughout the sample remains relatively stable such as the host (matrix) lattice species [13-15]. In the present work, the diffusion species is indium and the matrix species chosen was titanium. Therefore, the concentration of indium can be estimated using:

$$C_{In} = \frac{I_{In}}{I_{Ti}} \qquad \textbf{(6-2)}$$

where C_{In} is the estimated concentration of indium, and I_{In} and I_{Ti} are the SIMS measured intensity of In and Ti respectively. It is important to note that estimated concentration determined in this method represents only a relative value not an absolute value. This however is sufficient for the determination of diffusion coefficients as calculations are based upon relative changes in concentration only, hence knowledge of absolute concentration is not necessary [13].

According to Crank [16], an "instantaneous source" or "thin film source" diffusion condition occurs when the diffusion species is deposited as a thin layer on the surface of a solid and annealed at constant temperature for a known time. Under these conditions the diffusion coefficient can be related to the concentration profile described by [16]:

$$C(x,t) = \frac{M}{(\pi Dt)^{1/2}} \exp\left(-\frac{x^2}{4Dt}\right) \qquad \textbf{(6-3)}$$

where C(x,t) is the solute concentration at a specific distance and time, M is the surface concentration of solute at $t = 0$, x is the diffusion distance, t is the annealing time and D is the diffusion coefficient of the species of interest. Based on this relationship, a plot of ln(C) vs. x^2 (where ln is natural Log) of the diffusion data relating to the lattice (bulk) diffusion pathway will be linear, and the diffusion coefficient of indium, D_{In} can then be determined from the gradient, m of this linear plot using the equation:

$$D_{In} = -\frac{1}{m \times 4 \times t} \qquad \textbf{(6-4)}$$

6.3 Experimental

6.3.1. Sample Preparation and Processing

In^{3+} bulk diffusion experiments were performed on undoped high purity polished single crystal rutile TiO_2 (Surface Net GmbH). The single crystal was first cut into a small brick-like specimen approximately 3mm x 3mm x 10mm in size using a diamond saw**.** The brick was then pre-annealed for 72 hours under the same diffusion conditions (1173K and $p(O_2)$ = 21kPa) to remove any pre-existing surface effects that may have been introduced during grinding/polishing, and also to ensure the starting samples were in thermodynamic equilibrium at the given temperature and $p(O_2)$ prior to diffusion [17]. A 6.8 x 10^{-2} mol/L indium salt solution of was prepared by dissolving $InCl_3$ powder (99.999%-Aldrich) in ethanol. The undoped pre-annealed brick was then heated to approximately 40-50°C on a hot plate and several drops of the indium salt solution deposited carefully on to only the polished [001] surface. This procedure was adapted from the method reported by Sasaki et al. [17] who have used the similar deposition procedure in their comprehensive study of cation diffusion in TiO_2 (SC). Furthermore, this deposition method is less destructive than other methods such as ion implantation which may contribute additional effects to the composition (nonstoichiometry) of the In_2O_3 layer or impart surface damage such as ion tracks to the near surface layers of the TiO_2 which could influence the diffusion results. The ethanol in the salt solution quickly evaporated from the heated crystal leaving a visible indium chloride film on the surface perpendicular to the c-axis. It is important to note that any indium solution that dripped down the sides of the crystal during deposition was quickly wiped off using an ethanol soaked tissue before it could dry to avoid formation of additional layers that could contribute as additional indium diffusion sources. After complete drying of the deposited indium surface layer the sample was ready for the diffusion anneal.

For annealing, an electric horizontal tube furnace was first preheated to the desired temperature of 1173K. The sample was placed in a platinum lined alumina boat and inserted into the furnace hot zone as quickly as possible. After an annealing time of 5 hours at 1173K in air ($p(O_2)$ = 21 kPa, the sample was quenched by quickly pushing the sample boat to a pre-determined position outside of the furnaces central hot zone for 1 minute, before being moved to the end of the furnace at a steady rate. The aim of this cooling procedure was to quench the sample temperature from 1173K to room temperature as quickly as possible without introducing thermal shock.

6.3.2. Determination of Diffusion Concentration Profiles

Secondary Ion Mass Spectrometry, SIMS (Cameca ims 5f) depth profiles were used to analyse the resulting diffusion gradients. Prior to SIMS analysis it was necessary for the surface of the samples to be coated in a thin layer (~5 nm) of gold to overcome surface charging effects. The gold coating also helps to locate the crater for subsequently performed profilometry measurements. A Cs^+ primary ion beam of 40 nA beam current and 3 keV net impact energy was used to sputter the sample surface with a raster size of 250 x 250µm. Lens and aperture settings were used to restrict the analysis of secondary ions to a 55 µm diameter circular region in the centre of the rastered area to minimize potential crater edge effects. ^{16}O, ^{48}Ti, ^{113}In, ^{133}Cs and ^{197}Au elements were monitored using the MCs^+ technique which has been shown to minimize matrix effects [18-22]. Profilometry (Alpha step 2000, KLA Tencor) was used to measure the resulting total crater depth as shown in **Figure 6-2.** The average SIMS sputter rate was then calculated by dividing the total crater depth by the total time of analysis.

6.4 Results and Discussion

6.4.1. SIMS Depth Profile Conversion

The raw SIMS depth profile is shown in **Figure 6-3** as intensity (counts) vs time (s). The relative indium concentration C_{In} can be calculated from these raw elemental intensities using **Equation (6-2)**. A sputter rate of 0.25 nm/s was determined by dividing the measured crater depth (**Figure 6-2**) by the total analysis time. It is important to note that this method determines an average sputter rate which does not account for the different sputter rates in the In_2O_3 oxide layer and TiO_2 substrate. The average sputter rate can then be used to convert the SIMS analysis time to a related analysis depth from the surface. Consequently, the uncertainty related to depth conversion using this average sputter rate is the assumption of constant sputter rate through each layer. The resulting converted depth profile is shown in **Figure 6-4** as a plot of the natural Log of In relative concentration against depth which can be used for quantitative diffusion calculations.

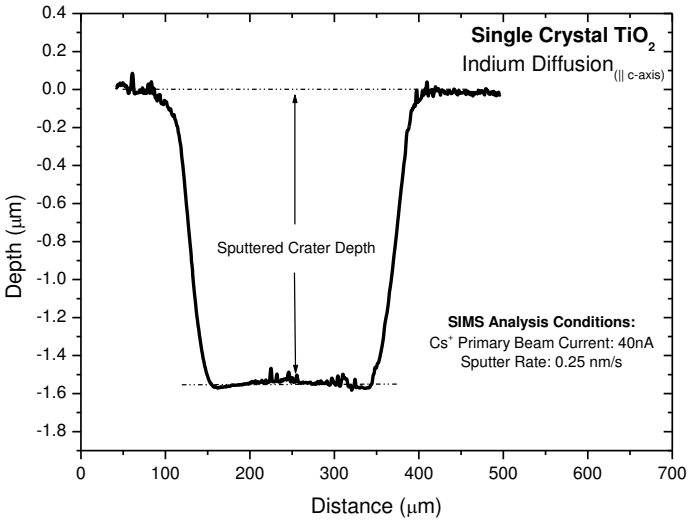

Figure 6-2. Example of a profilometry sputtered crater profile resulting from SIMS analysis of indium doped TiO_2 specimen.

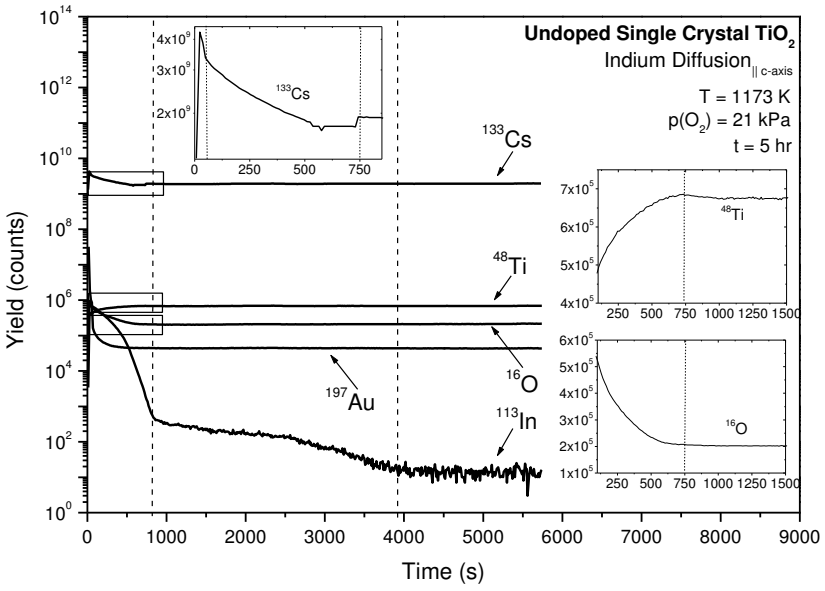

Figure 6-3. Raw SIMS intensity vs. time depth profile for indium diffusion in undoped TiO_2 annealed at 1173K in $p(O_2)$ = 21kPa. The insert plots show enlargements of the depth profile in the near surface region for Cs, Ti and O.

6.4.2. SIMS Depth Profile Interpretation

Although SIMS is a relatively simple but powerful surface analysis technique, it can also present the user with significant data interpretation challenges such as non-equilibrium sputtering and matrix effects. It is therefore essential understand the influence of these effects on the resulting SIMS depth profile to avoid incorrect data analysis. A schematic model showing the key regions identified in a typical SIMS intensity vs. time diffusion depth profile for indium in single crystal TiO_2 is provided in **Figure 6-4.**

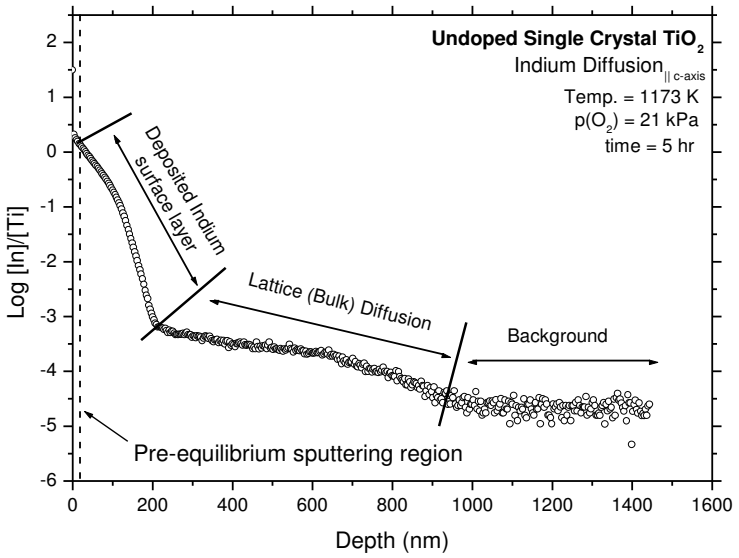

Figure 6-4. SIMS Concentration vs. depth plot showing regions corresponding to the surface deposited laer and bulk diffusion pathway.

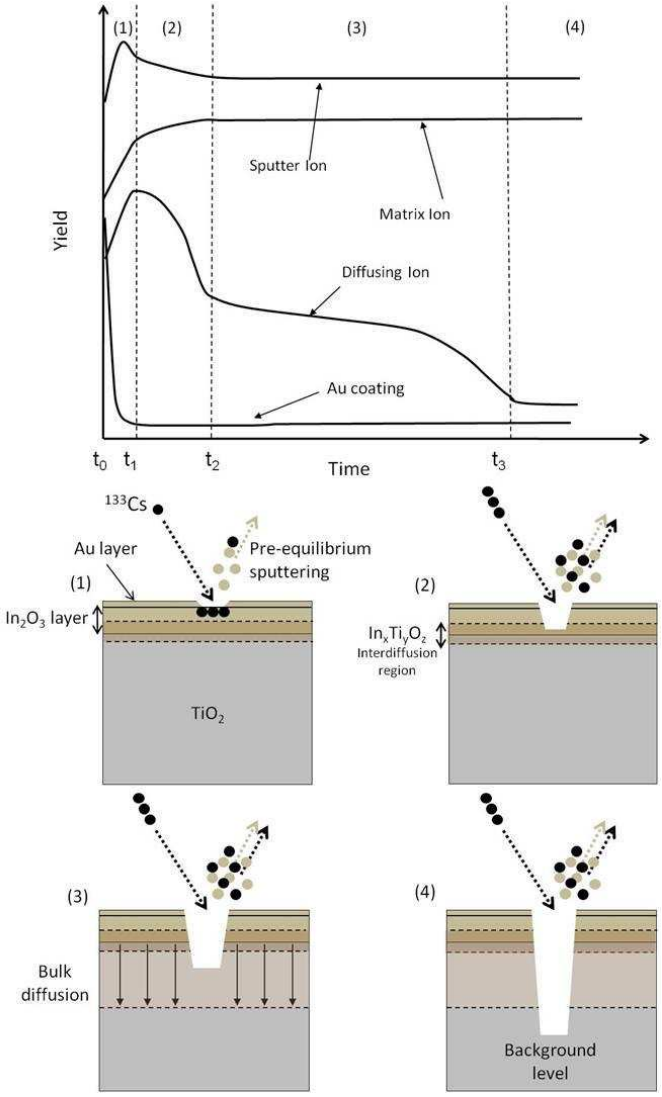

Figure 6-5. (Top figure) Schematic SIMS diffusion depth profile highlighting four significant regions within the depth profile. (Bottom series of figures) Illustration of the related specimen sputter process corresponding to (1) pre-equilibrium sputtering; (2) surface and inter-diffusion layer; (3) bulk diffusion region; (4) background

Region (1): At the onset of SIMS sample sputtering, t_0 (**Figure 6-5**), the incoming Cs^+ ions tend to be implanted into the surface at a greater rate than they are being sputtered from the surface. This sputtering imbalance has two effects; firstly it produces a layer in the sample slightly deeper than the sputter depth that is increasingly being enriched with implanted Cs^+ ions. Secondly, the unstable sputtering characteristic of this region, caused by the imbalance between implanted and sputtered ions, distorts the depth profile causing unreliability in the results. It is therefore imperative that the extent of this transient region be determined so that the first reliable data point of the depth profile can be ascertained [23]. This non-steady state sputtering condition is referred to as pre-equilibrium or non-equilibrium sputtering and introduces significant complications when attempting to analyse and interpret data obtained

from the topmost surface layers of a sample. This preliminary sputter instability can be further compounded by the presence of the gold surface coating necessary to minimise sample charging as well as any adsorbed surface oxygen present on the sample. The pre-equilibrium sputtering condition is typically accompanied by a characteristically unstable and often rapidly increasing Cs^+ yield to a maximum during the initial stages of the depth profile as shown in **Figure 6-5**. As a consequence, all of the secondary ion yields related to the other species in the depth profile between time t_0 - t_1 are questionable. However, as the area of interest in the sample for the determination of diffusion is the TiO_2 single crystal below both the gold and In_2O_3 layers, a precise determination of the topmost pre-equilibrium sputtering region is not necessary in the present work. Equilibrium sputtering is established when the incoming Cs^+ sputter ions become equal to the outgoing Cs^+ sputter ions. This typically occurs after a maximum in the Cs^+ sputter ion yield has been observed as shown between t_0 and t_1 in **Figure 6-5**. It is also important to note that the time (or depth) it takes for SIMS to achieve equilibrium sputtering is not always the same but is influenced by a combination of primary ion parameters (net impact energy, primary ion mass, current density, impact angle) and the nature of the target sample (mass, density, crystallinity, topography and surface binding energy) [23]. Consequently, simply assuming a nominal time or depth value for equilibrium sputtering can result in either overestimation, causing a loss of useful SIMS data; or underestimation, resulting in the incorporation of inaccurate SIMS data. Only when equilibrium sputtering is established can the depth profile data be considered reliable.

Region (2): At t_1, equilibrium sputtering has been achieved. Ideally, once equilibrium has been established, the Cs^+ yield between t_1 and t_2 should remain at a constant stable level; however, we instead see that the Cs^+ yield is actually falling in the region between t_1 and t_2. A corresponding increase in secondary ion yield related to the matrix ion, as well as a large decrease from maximum of the diffusing ion yield is also observed approaching the film-substrate interface at t_2. The combination of these features suggests the presence of an inhomogeneous layer (or interface region) possibly due to inter-diffusion reactivity between the surface oxide layer and the substrate during annealing. There is likely also a contribution from ion beam mixing effects.

Region (3): The depth profile within this region corresponds to sputtering within the TiO_2 single crystal. Data within this region can therefore be used for the determination of diffusion coefficient.

Region (4): Background level where diffusion of the dopant species has not occurred.

6.4.3. Bulk Diffusion Determination

Figure 6-4 clearly shows the 3 distinct regions displayed in the obtained indium depth profile illustrated in **Figure 6-5**. These correspond to the deposited surface layer, bulk (lattice) diffusion pathway and the background level. As the TiO_2 specimens used were single crystals there are no additional contributing diffusion pathways such as grain boundaries.

Using **Equations (6-3)** and **(6-4)**, the In bulk diffusion coefficient can be determined using a plot of ln(In) vs. depth^2 for the region of data corresponding to the bulk diffusion pathway as shown in **Figure 6-6.**

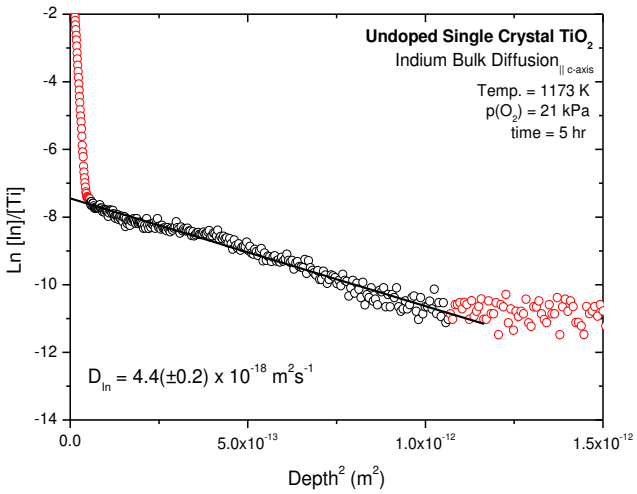

Figure 6-6. Diffusion profile of natural log(In) vs. depth^2 showing linear regression used for calculation of diffusion coefficient.

The presence of a linear region in this plot also confirms the applicability of bulk diffusion model used. The bulk diffusion coefficient for indium in TiO_2 at 1173 K and $p(O_2)$ = 21 kPa has been determined as:

$$D_{In} = 4.4(\pm 0.2) \times 10^{-18} m^2 s^{-1} \qquad \textbf{(6-5)}$$

As far as we are aware, this is the first reported diffusion coefficient for indium in TiO_2, hence we are unable to make any direct literature comparison of this result. However, if we compare the diffusion coefficient of In^{3+} (ionic radii = 80Å) with the diffusion coefficients

reported by Sasaki et al.[17] of 5.90 x 10^{-16} m^2s^{-1} and 8.63 x 10^{-17} m^2s^{-1} for Cr^{3+} (62Å) and Sc^{3+} (75Å) respectively; it tentatively suggests an inverse relationship of decreasing diffusion coefficient with increasing ionic radii. On the other hand, if we extrapolate the diffusion data reported by Sasaki et al.[17] l for tetravalent Zr^{4+} (72) to 1173K, a diffusion coefficient approximately 3 orders of magnitude smaller than D_{In} is obtained even though the ionic radii of Zr and In are very close. This suggests that the charge of the dopant species has a significantly greater influence on the diffusion coefficient than ionic radii which is in agreement with the findings of Sasaki et al. [17].

6.5 Conclusion

This work studied the progress of solid state reaction between TiO_2 single crystal and a thin layer of indium oxide deposited on its surface. It is shown that the depth profile of In^{3+} determined by SIMS allows one to distinguish between the components related to the In_2O_3 surface layer and the diffusion-induced In^{3+} concentration in the TiO_2 phase beneath. The latter profile may be considered in terms the bulk diffusion of In^{3+} in the TiO_2 single crystal. The data obtained in this work may be used in the assessment of the physical meaning of depth profiles corresponding to solid-solid reaction in oxides and the related diffusion data. The determination indium diffusion coefficient constitutes new materials data which may be used to process well-defined TiO_2 with controlled dopant composition and functional properties.

6.6 References

(1) Fujishima, A.; Honda, K. "Electrochemical Photolysis of Water at a Semiconductor Electrode". Nature (1972), 238, 37-38.

(2) Bernasik, A.; Radecka, M.; Rekas, M.; Sloma, M. "Electrical properties of Cr-doped and Nb-doped TiO_2 Thin-films". Applied Surface Science (1993), 65-6, 240-245.

(3) Monnier, A.; Augustynski, J. "Photoelectrolysis of water - Photoresponses of Nickel, Chromium and Zinc-doped polycrystalline TiO_2 electrodes". J. Electrochem. Soc. (1980), 127 [7], 1576-1579.

(4) Nowotny, J.; Bak, T.; Nowotny, M. K.; Sheppard, L. R. "Titanium dioxide for solar-hydrogen I. Functional properties". International Journal of Hydrogen Energy (2007), 32 [14], 2609-2629.

(5) Nowotny, J.; Bak, T.; Nowotny, M. K.; Sheppard, L. R. "Defect Chemistry and Electrical Properties of Titanium Dioxide. 2. Effect of Aliovalent Ions". Journal of Physical Chemistry C (2008), 112, 602-610.

(6) Ni, M.; Leung, M. K. H.; Leung, D. Y. C.; Sumathy, K. "A review and recent developments in photocatalytic water-splitting using TiO_2 for hydrogen production". Renew. Sust. Energ. Rev. (2007), 11 [3], 401-425.

(7) Menzies, D. B.; Dai, Q.; Bourgeois, L.; Caruso, R. A.; Cheng, Y. B.; Simon, G. P.; Spiccia, L. "Modification of mesoporous TiO_2 electrodes by surface treatment with titanium(IV), indium(III) and zirconium(IV) oxide precursors: preparation, characterization and photovoltaic performance in dye-sensitized nanocrystalline solar cells". Nanotechnology (2007), 18 [12], 11.

(8) Brehm, J. U.; Winterer, M.; Hahn, H. "Indium Tin Oxide Nanoparticles Prepared by Chemical Vapor Synthesis". Materials Research Society Symposium Proceedings (2002), 704, W5.3.1 - W5.3.6.

(9) Guoa, L. J.; Shen, X. P.; Zhu, G. X.; Chen, K. M. "Preparation and gas-sensing performance of In(2)O(3) porous nanoplatelets". Sens. Actuator B-Chem., 155 [2], 752-758.

(10) Karakitsou, K. E.; Verykios, X. E. "Effects of altervalent cation doping of titania on its performance as a photocatalyst for water cleavage". The Journal of Physical Chemistry (1993), 97 [6], 1184-1189.

(11) Shchukin, D.; Poznyak, S.; Kulak, A.; Pichat, P. "TiO_2-In_2O_3 photocatalysts: preparation, characterisations and activity for 2-chlorophenol degradation in water". Journal of Photochemistry and Photobiology A - Chemistry (2004), 162 [2-3], 423-430.

(12) Wang, E. J.; Yang, W. S.; Cao, Y. A. "Unique Surface Chemical Species on Indium Doped TiO_2 and Their Effect on the Visible Light Photocatalytic Activity". Journal of Physical Chemistry C (2009), 113 [49], 20912-20917.

(13) Sheppard, L. R.; Zhou, M. F.; Atanacio, A.; Bak, T.; Nowotny, J.; Prince, K. E. "Determination of niobium diffusion in titania and zirconia using secondary ion mass spectrometry". Adv. Appl. Ceram. (2007), 106 [1-2], 89-94.

(14) Bak, T.; Nowotny, J.; Prince, K.; Rekas, M.; Sorrell, C. C. "Grain boundary diffusion of magnesium in zirconia". Journal of the American Ceramic Society (2002), 85 [9], 2244-2250.

(15) Sheppard, L. R.; Atanacio, A. J.; Bak, T.; Nowotny, J.; Prince, K. E. "Bulk diffusion of niobium in single-crystal titanium dioxide". Journal of Physical Chemistry B (2007), 111 [28], 8126-8130.

(16) Crank, J. The Mathematics of Diffusion, 2nd ed.; Oxford Science Publications, 1997.

(17) Sasaki, J.; Peterson, N. L.; Hoshino, K. "Tracer impurity diffusion in single-crystal rutile (TiO_{2-x})". J. Phys. Chem. Solids (1985), 46 [11], 1267-1283.
(18) Gao, Y. "A new secondary ion mass spectrometry technique for III-V semiconductor compounds using the molecular ions CsM[sup +]". Journal of Applied Physics (1988), 64 [7], 3760-3762.
(19) Gao, Y. "Influence of experimental conditions on matrix effects in SIMS". Applied Surface Science (1988), 32 [4], 420-430.
(20) Gao, Y.; Marie, Y.; Saldi, F.; Migeon, H. N. "On the SIMS depth profiling analysis - Reduction of matrix effect". International Journal of Mass Spectrometry and Ion Processes (1995), 143, 11-18.
(21) Gerardi, C.; Massaro, C. "On the improvement of SIMS technique by the use of MCs^+ molecular ions ". Microscopy, Microanalysis, Microstructures (1995), 6, 523-531.
(22) Gnaser, H. "Improved quantification in Secondary Ion Mass Spectrometry detecting MCs^+ molecular ions ". J. Vac. Sci. Technol. A-Vac. Surf. Films (1994), 12 [2], 452-456.
(23) Chanbasha, A. R. A study of the effects of ultralow-energy secondary ion mass spectrometry (SIMS) on surface transient and depth resolution. PhD Thesis, National University of Singapore, 2007.

CHAPTER 7

Diffusion Kinetics of Indium in TiO_2 Single Crystal

7.1 Abstract

The present work determines the self-diffusion coefficients of indium in TiO_2 single crystal (rutile) in the temperature range 1073 - 1573 K. Diffusion concentration profiles of indium were imposed by annealing high purity TiO_2 single crystal in air with a thin covering layer of $InCl_3$. The diffusion-induced concentration profiles of indium as a function of depth were determined using secondary ion mass spectrometry (SIMS). These diffusion profiles were used to calculate the self-diffusion coefficients of indium in both the polycrystalline In_2O_3 surface layer and the TiO_2 single crystal. The temperature dependence of the respective diffusion coefficients, in the range 1073 K – 1573 K, can be expressed by the following formulas:

$$D_{In-In_2TiO_5} = 1.9\times10^{-13}\exp\left(\frac{-142\,kJ/mol}{RT}\right)\left[m^2s^{-1}\right]$$

and

$$D_{In-TiO_2} = 7.4\times10^{-4}\exp\left(\frac{-316\,kJ/mol}{RT}\right)\left[m^2s^{-1}\right]$$

The obtained activation energy for bulk diffusion of indium in rutile (316 kJ/mol) is similar to that of zirconium in rutile (325 kJ/mol). The determined diffusion data can be used in selection of optimal processing of TiO_2-In_2O_3 solid solutions.

7.2 Introduction

The formation of well-defined solid solutions requires diffusion data related to their mass transport kinetics. The formation of solid solutions has been widely applied in TiO_2 to form TiO_2-based systems with enhanced solar energy conversion performance.

The discovery of Fujishima and Honda [1], showing that TiO_2 is a promising candidate for photo-electrochemical water decomposition, generated an interest in this compound. Since then, intensive studies aim at the modification of its properties in order to enhance the performance in solar-to-chemical energy conversion. These studies include investigations on the effect of composition on the performance-related properties [2-8]. The ultimate aim of the research strategy is the formation of TiO_2-based semiconductors with enhanced performance as photoelectrodes for photoelectrochemical water splitting and photocatalysts for water purification. Modification of semiconducting properties can be achieved through a change of chemical composition using (i) oxidation or reduction or (ii) doping:

Oxidation/Reduction. Oxidation or reduction of TiO_2 results in a change of nonstoichiometry and the related Fermi level. However, imposition of well-defined oxygen activity requires knowledge of the chemical diffusion coefficient [9].

Doping. Incorporation of aliovalent ions, forming donors and acceptors, results in a change of Fermi level. However, the formation of well-defined solid solution requires knowledge of the diffusion coefficients of the dopant ions.

Commonly reported processing procedures are often related to arbitrarily selected processing conditions, such as temperatures and time of annealing or sintering which may not necessarily lead to the formation of well-defined systems in terms of dopant distribution within the oxide matrix. For this reason their properties cannot necessarily be readily compared. Consequently, knowledge of the diffusion data for the doping elements is essential in order to select the time and the temperature of the process. In certain cases, doping aims at the imposition of interface concentration gradients. Also in this case, knowledge of the diffusion data is needed.

The aim of the present work is to determine the self-diffusion coefficient of indium in single crystal TiO_2. The diffusion-induced concentration profiles are determined by secondary ion mass spectrometry, SIMS. The experimental part of the study is preceded by a brief overview of the diffusion data reported in the literature for TiO_2 (rutile) and a definition of terms used.

7.2.1. Brief literature overview

The crystal structure of rutile exhibits anisotropy, including mass transport. This structure, which exhibits open channels parallel to the c-axis, is responsible for anisotropy of TiO_2. Therefore, the transport of small cations along these channels is faster than in the direction perpendicular to the c-axis, while oxygen diffusion is faster perpendicular to the c-axis [10-12].

According to Lundy & Coghlan [12], the self-diffusion of ^{44}Ti in rutile in the direction perpendicular and parallel to the c-axis as a function of temperature is given by the following respective expressions:

$$D_{\parallel c} = 4.6\times10^{-6}\exp\left(\frac{-59.9\text{kJ/mol}}{RT}\right)\left[\text{m}^2\text{s}^{-1}\right] \quad \textbf{(7-1)}$$

$$D_{\perp c} = 2.4\times10^{-7}\exp\left(\frac{-48.5\text{kJ/mol}}{RT}\right)\left[\text{m}^2\text{s}^{-1}\right] \quad \textbf{(7-2)}$$

As seen, the activation energy of diffusion in the direction perpendicular to the c-axis, represented by $D_{\perp c}$, is larger than that of diffusion in the direction parallel to the c-axis, represented by $D_{\parallel c}$. According to Hoshino *et al.* [11], the activation energy of diffusion in the direction parallel to the c-axis and also in the direction perpendicular to the c-axis are similar:

$$D_{\parallel c} = 6.5\times10^{-4}\exp\left(\frac{-277\,\text{kJ/mol}}{RT}\right)\left[\text{m}^2\text{s}^{-1}\right] \quad \textbf{(7-3)}$$

$$D_{\perp c} = 4.55\times10^{-4}\exp\left(\frac{-268\,\text{kJ/mol}}{RT}\right)\left[\text{m}^2\text{s}^{-1}\right] \quad \textbf{(7-4)}$$

Diffusion data reported by Lundy and Coghlan [12], Hoshino *et al.* [11], Venkatu and Poteat [13] and Akse and Whitehurst [10], are shown in **Figure 7-1**. In general, there is good agreement between the reported diffusion data in terms of the absolute values of the diffusion coefficients and their temperature dependence.

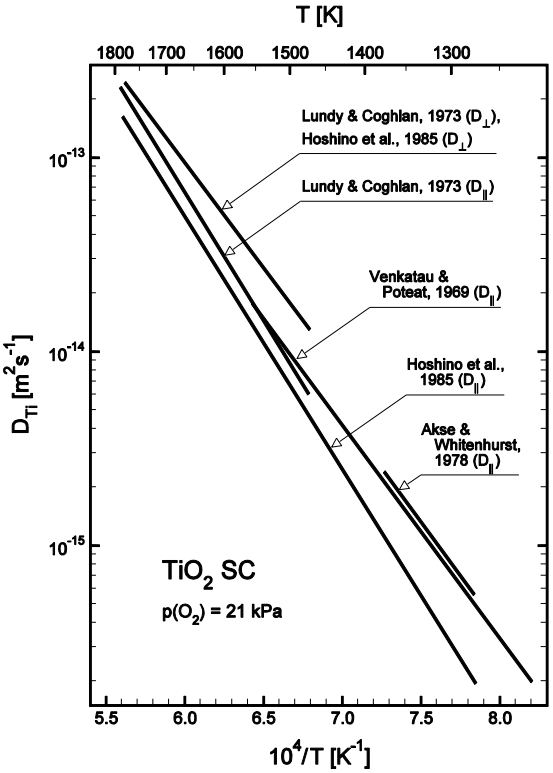

Figure 7-1. Arrhenius plot of the diffusion coefficient of titanium in single crystal of TiO_2 (rutile), according to Lundy and Coghlan [12], Hoshino et al. [11], Venkatu and Poteat [13], and Akse and Whitehurst [10].

All these data indicate that diffusion in the direction perpendicular to the c-axis is faster than parallel to the c-axis. Therefore:

$$D_{\perp c} > D_{\parallel c} \qquad \textbf{(7-5)}$$

According to Sasaki *et al.* [14], the effect of anisotropy is more substantial for the diffusion of cobalt in Al-doped TiO_2. The effect of anisotropy in TiO_2 has also been considered by Millot *et al.* [15].

Sasaki et al. [14] as well as Peterson and Sasaki [16] reported the self-diffusion coefficients for a wide range of cations, including ^{60}Co, ^{63}Ni, ^{59}Fe, ^{54}Mn, ^{51}Cr, ^{46}Sc, ^{95}Zr, $^{1}H^{+}$, in rutile. The related diffusion coefficients in the direction parallel to the c-axis are shown in **Figure 7-2. Figure 7-2** also compares the data for titanium, ^{44}Ti, oxygen, ^{18}O, and the self-diffusion coefficient of ^{93}Nb [17]. Sasaki *et al.* [14] claimed that tri- and tetra-valent ions diffuse via the interstitialcy mechanism. The diffusion coefficients for cations in TiO_2 were also reported by Johnson [18], Johnson *et al.* [19] and Wittke [20]. Extensive studies have also been reported for oxygen tracer diffusion in TiO_2 [21-27].

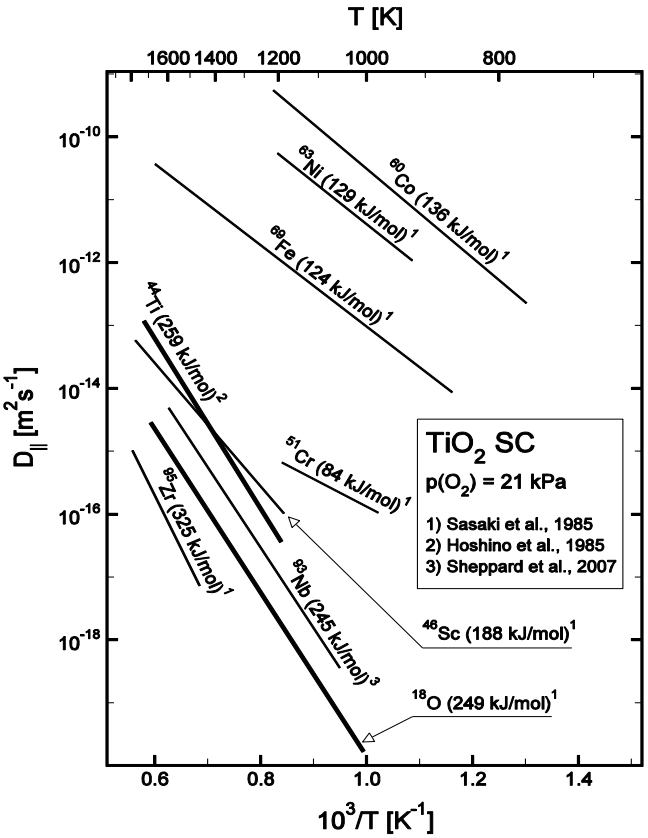

Figure 7-2. Arrhenius plot of the self-diffusion coefficient for several intrinsic and extrinsic ions in TiO_2, according to Sasaki et al. [14], Hoshino and Peterson [11] and Sheppard et al. [17].

The self-diffusion coefficients shown in **Figure 7-2** for ^{44}Ti and ^{18}O indicate that the transport of titanium ions is faster than that of oxygen diffusion. Oxygen ions are transported according to the vacancy mechanism and their diffusion rate is determined by the concentration of oxygen vacancies.

The reported effect of anisotropy for oxygen transport is $D_{\parallel} : D_{\perp} = 0.2$ [25]. However, the interstitial transport of titanium ions is comparatively faster by approximately one order of magnitude. The reported effect of anisotropy for titanium is $D_{\parallel} : D_{\perp} = 2.5$ [12].

In summary, the diffusion rate of cations is dependent on their size, valence state and diffusion mechanism.

7.2.2. Definition of Terms

Diffusion coefficients for oxide crystals depend on oxygen activity when the transport occurs via defects since their concentration is closely related to oxygen activity, p(O_2). The effect of both temperature and oxygen activity on the diffusion coefficient may be expressed by the following:

$$D = D_o\, p(O_2)^{-1/m} \exp\left(\frac{-E_a}{RT}\right) \quad \textbf{(7-6)}$$

where m is the $p(O_2)$ exponent that is related to the valence of the defects involved in the transport and E_a is the activation energy for diffusion.

A commonly applied technique for determination of diffusion kinetics in oxides is based on the deposition of a tracer-containing surface layer and annealing for well-defined time intervals. The resulting diffusion concentration profiles can be determined either by removal of several layers by grinding (sectioning) and subsequent determination of tracer concentrations in each section. Alternatively, the diffusion concentration profile can be determined using surface-sensitive techniques, such as secondary ion mass spectrometry (SIMS). This technique has been applied in the present work.

It is important to note that the SIMS technique provides depth profiles in terms of ion yield (i.e. counts) rather than absolute concentrations. However, as the SIMS ion yield is often proportional to absolute elemental concentration, a reasonable estimation of relative concentration can be made by normalising the intensity of the species of interest against a species whose intensity throughout the sample remains relatively stable, such as the host (matrix) lattice species [17,28,29]. In the present work, the diffusing species is indium and the matrix species chosen for normalisation purposes was titanium. The concentration of indium can be estimated using

$$[C_{In}] = \frac{[I_{In}]}{[I_{Ti}]} F_{In} \quad \textbf{(7-7)}$$

where C_{In} is the concentration of indium, I_{In} and I_{Ti} are the SIMS measured intensity of indium and titanium, respectively, and F_{In} is the relative sensitivity factor. It is important to note that the physical meaning of the sensitivity factor is complex as it depends on both the element of interest and the sputtering conditions. Moreover, the concentration determined in this method represents only relative values, not absolute values, since the relative sensitivity factor is unknown. This, however, is sufficient for the determination of diffusion coefficients as diffusion calculations are based upon relative changes in the concentration only.

According to Crank [30] an “instantaneous source” or “thin film source” diffusion condition occurs when the diffusing species are deposited as a thin layer on the surface of a solid and annealed at constant temperature for a known time. Under these conditions the diffusion coefficient can be related to the concentration profile described by [30]:

$$C(x,t) = \frac{M}{(\pi Dt)^{1/2}} \exp\left(-\frac{x^2}{4Dt}\right) \quad \textbf{(7-8)}$$

where $C(x,t)$ is the solute concentration at a specific distance and time, M is the surface concentration of solute at $t = 0$, x is the diffusion distance, t is the annealing time and D is the diffusion coefficient of the species of interest. Based on this relationship, a plot of $ln(C)$ vs. x^2 (where ln is natural log) of the diffusion data relating to the lattice (bulk) diffusion pathway will be linear, and the diffusion coefficient of indium, D_{In} can then be determined from the gradient, m of this linear plot using the equation:

$$D_{In} = -\frac{1}{m \times 4 \times t} \quad \textbf{(7-9)}$$

7.3 Experimental

7.3.1. Specimen

The specimen used in the present study was a 2 x 3 x 10 mm tablet of high purity TiO_2 single crystal provided by SurfaceNet, Germany. The diffusion concentration profiles of ^{113}In were imposed by deposition of a thin layer of $InCl_3$ on the surface normal to the c-axis so that diffusion proceeds along the c-axis. The deposition procedure involved the preparation of 0.1501 g $InCl_3$ dissolved in 10 ml of ethanol. The resulting solution concentration was 0.0679 mol/L. This solution was then dropped on the polished surface of the TiO_2 specimen. The $InCl_3$ layer was allowed to dry at 50°C. The specimen was subsequently annealed at elevated temperatures in air to allow indium penetration into the lattice and the imposition of a diffusion gradient. Each specimen was used at only one temperature of annealing. Four independent specimens were used to generate diffusion profiles at four temperatures in the range 1073 K - 1573 K. The annealing times were selected in order to impose comparable diffusion-induced concentration gradients. These were: 1440 min, 300 min, 15 min and 10 min at 1073 K, 1173 K, 1373 K and 1573 K, respectively. These conditions were based on preliminary diffusion experiments.

7.3.2. Surface Analysis

The resulting diffusion concentration profiles were determined with secondary ion mass spectrometry, SIMS (Cameca IMS 5f). In order to minimize sample charging, a thin layer of

gold (~20 nm) was first deposited on the sample surface. A Cs^+ primary ion beam of 3 keV net impact energy and 80 nA current, was rastered over an area of approximately 250 x 250 μm. A sputter rate of 0.57 nm/s was calculated using the known total analysis time and the resulting crater depth for a representative analysis. As all subsequent samples have the same matrix, and analyses were performed under the same SIMS conditions, it is reasonable to assume that the same sputter rate applies to each. The crater used for determining the sputter rate is shown in **Figure 7-3**. The area of the square-shaped crater image is slightly larger than 250 x 250 μm. The light spots are likely to be related to the islets of gold introduced prior to SIMS analysis. The total depth of the crater, measured accurately using a high precision profilometer, was applied to calibrate the sputtering time versus depth.

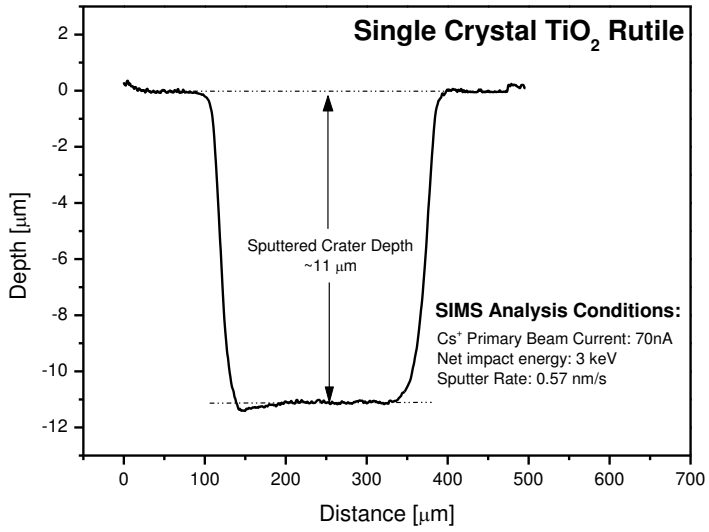

Figure 7-3. Typical crater generated by SIMS primary ions sputtering.

7.4 Results and Discussion

The raw SIMS spectra of indium diffusion in TiO_2 along with the profiles of oxygen, titanium and cesium for the specimen annealed at 1073 K, is shown in **Figure 7-4** in terms of the intensity of secondary ions vs. sputtering time.

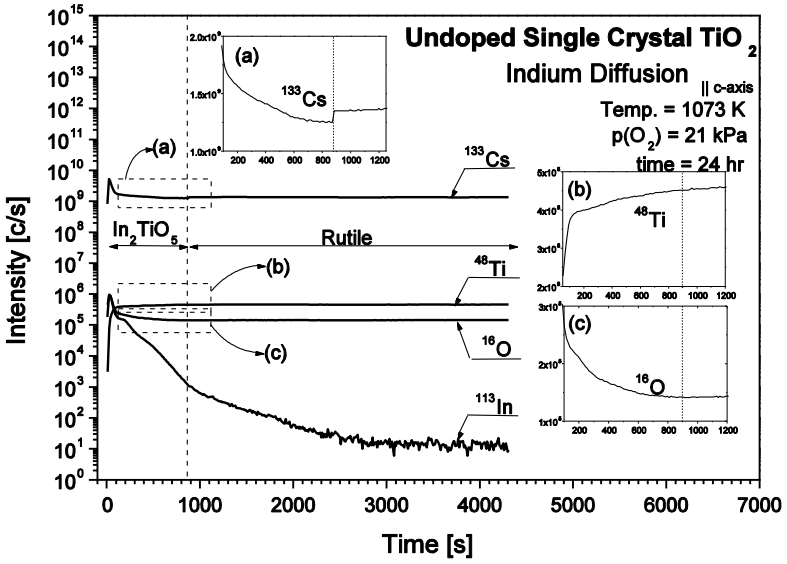

Figure 7-4. The secondary ion intensities for Cs, Ti, O and In (in counts per second) in TiO_2 annealed at 1073 K in air.

It takes some time in the initial stages of SIMS analysis for equilibrium sputtering to be established. For this reason, the data recorded at the commencement of the analysis is not well-defined and cannot be considered reliable enough for calculating concentration gradients in the lattice. Consequently, the initial abrupt changes of ion yield intensities, related to non-equilibrium sputtering, have not been taken into account in the analysis.

Identification of the transition region between non-equilibrium and equilibrium sputtering in the spectra is highly subjective. However, this assessment is essential for determining the diffusion coefficient correctly.

The depth profiles related to ^{133}Cs, ^{48}Ti, ^{16}O and ^{113}In are shown in **Figure 7-4**. As seen, these profiles exhibit the following characteristic features:

- The profiles related to ^{133}Cs exhibit a sharp initial decrease, subsequent step-like change and a stable value following the step.
- The profiles related to ^{48}Ti exhibit a sharp initial rise followed by a stable value. As seen, the stability range corresponds to the time of sputtering larger than the time of the step.

- The profiles related to ^{16}O exhibit a sharp initial decrease followed by a stable value. In analogy to the profile of ^{48}Ti, the stability range corresponds to the time of sputtering larger than the time of the step.

The shape of the profile of ^{113}In depends on the annealing temperature and time. However, the character of the changes in ^{113}In vs. time, which is schematically represented in **Figure 7-5** may be considered in terms of the following four regimes:

Regime I. This regime is related to non-equilibrium sputtering. The intensity profile in this regime shows a rapid initial rise, reaching maximum, and subsequent rapid decrease.

Regime II. This regime, which corresponds to the flat part of the ^{133}Cs (before the step-like change) is related to the surface layer that is formed by the reaction between the deposited $InCl_3$ layer and the TiO_2 (rutile) surface, which seems to be an In_2TiO_5 like structure.

Regime III. This regime is related to bulk lattice diffusion of In in TiO_2.

Regime IV. This regime represents the background composition of In in TiO_2.

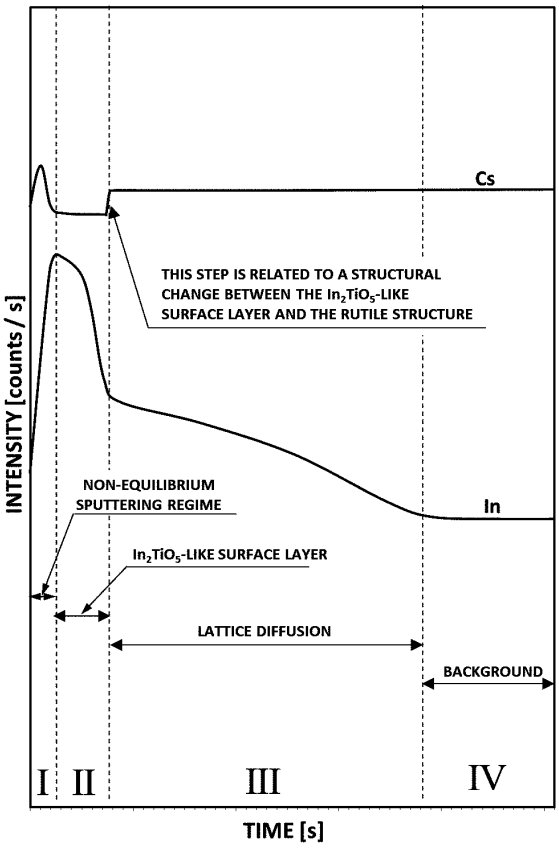

Figure 7-5. Schematic representation of the intensity vs. time profiles within the regimes I – IV (described in text).

The isothermal depth profiles of indium annealed in air, including the regimes II-IV, are shown in **Figure 7-6** in terms of the intensity ratio (I_{In}/I_{Ti}) vs. distance from the surface. As seen, these depth profiles involve three parts with distinctively different shapes:

The steepest part is related to the surface in the form of an indium titanate like phase (regime II). The second part, which exhibits a smaller slope, is related to the diffusion-induced concentration gradient of indium in the rutile structure (regime III). This part may be considered is terms of the background composition (regime IV).

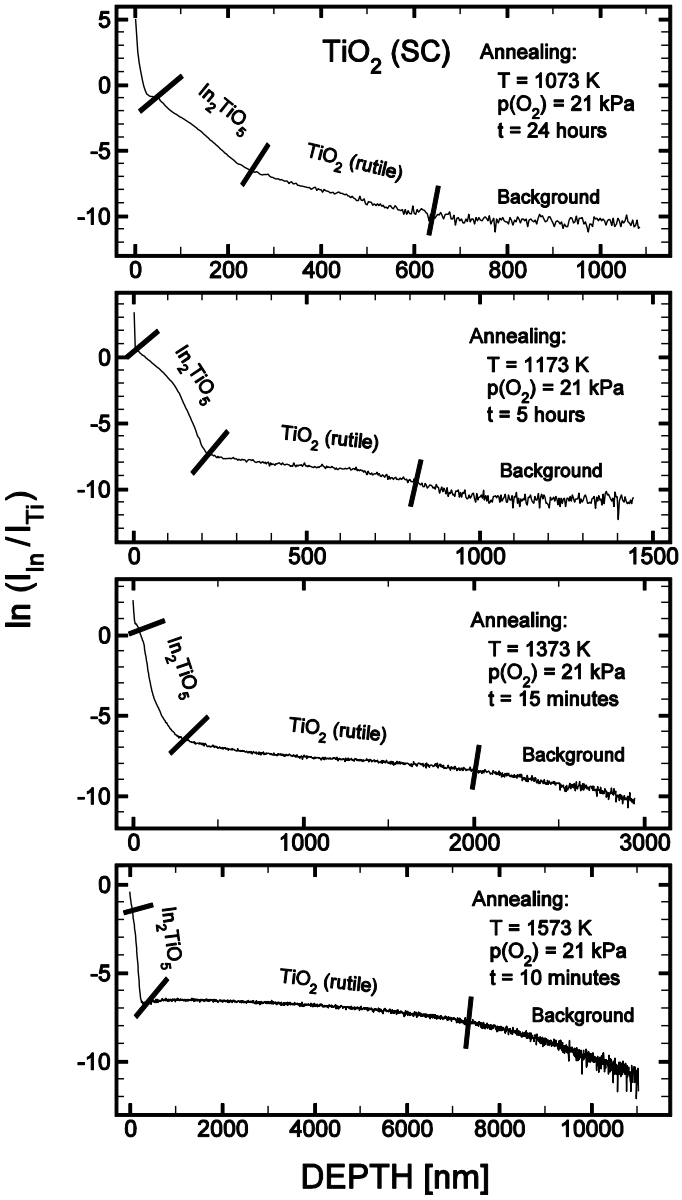

Figure 7-6. The ratio of intensity profiles $\ln(I_{In}/I_{Ti})$ vs. distance from the surface.

The depth profiles associated with lattice diffusion, plotted in terms of $\ln(I_{In}/I_{Ti})$ intensity profiles vs. square of the distance for the surface layer of In_2TiO_5 (regime II), are shown in **Figure 7-7**.

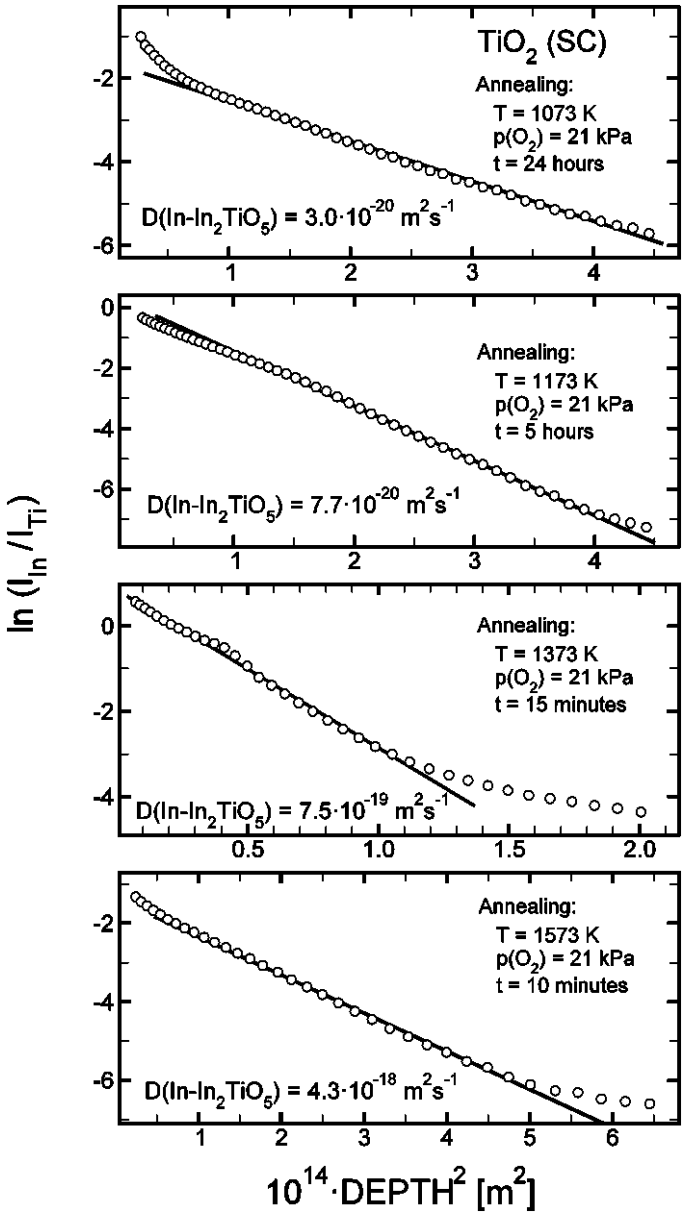

Figure 7-7. The ratio of intensity profiles $\ln(I_{In}/I_{Ti})$ vs. square of the distance from the surface for In-doped In_2TiO_5.

As seen, the parts of the profiles related to lattice diffusion can be described by a linear dependence. These depth profiles were used for the determination of the diffusion coefficient of indium in titanium-doped indium oxide using Equation (8).

The depth profiles associated with lattice diffusion, plotted in terms of $\ln(I_{In}/I_{Ti})$ intensity profiles vs. square of the distance for TiO_2 (regime III), are shown in **Figure 7-8**. As seen, also in this regime the parts of the profiles related to lattice diffusion can be described by a linear dependence. These depth profiles were used for the determination of the diffusion coefficient of indium in rutile using **Equation (7-8)**.

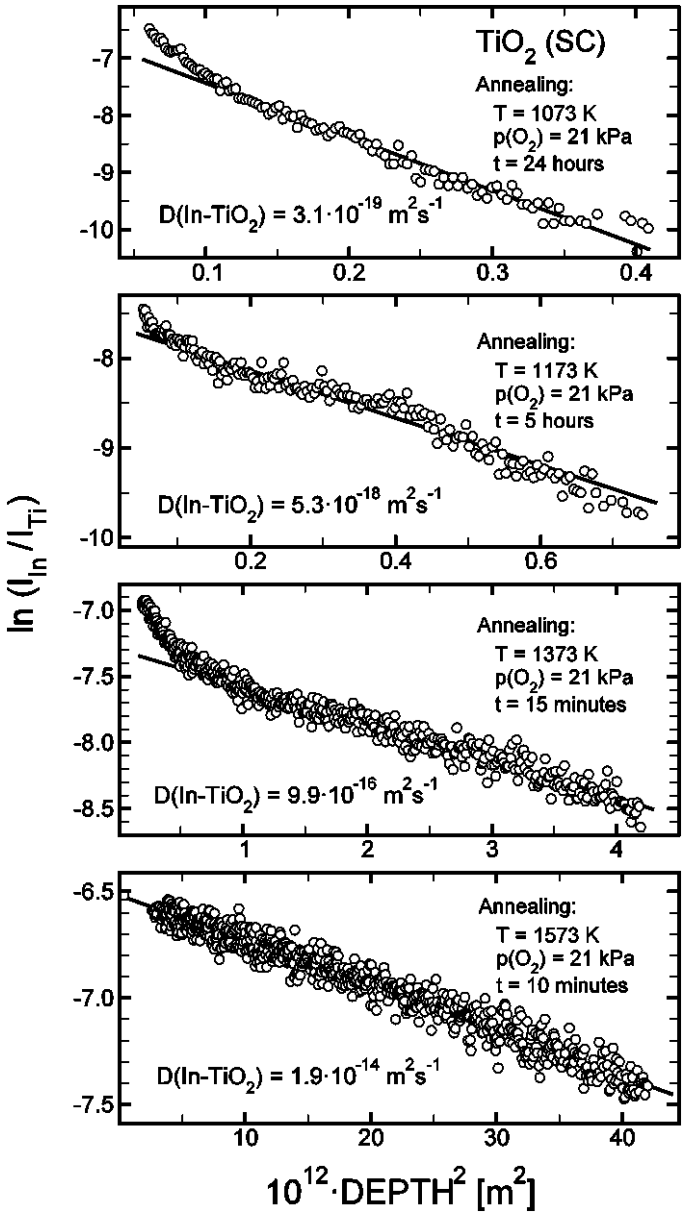

Figure 7-8. The ratio of intensity profiles $\ln(I_{In}/I_{Ti})$ vs. square of the distance from the surface for In-doped TiO_2.

The obtained diffusion coefficients, determined at four temperatures, are shown in **Figure 7-9**.

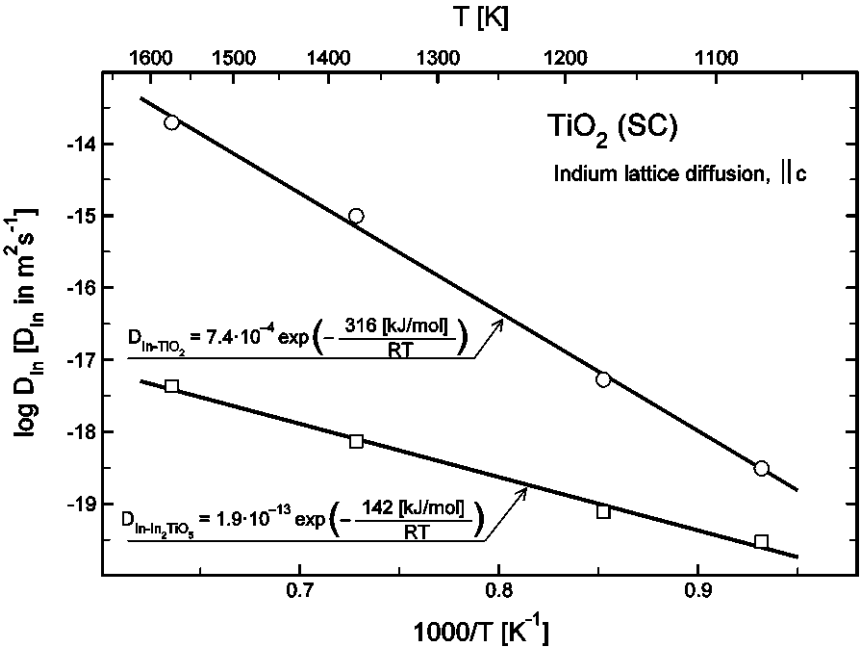

Figure 7-9. The Arrhenius plots of the self-diffusion coefficient of indium in both In_2TiO_5 and TiO_2.

These diffusion data may be expressed by the following functions of temperature:

$$D_{In-In_2TiO_5} = 1.9\times10^{-13}\exp\left(-\frac{142\,kJ/mol}{RT}\right)\left[m^2s^{-1}\right] \quad \textbf{(7-10)}$$

$$D_{In-TiO_2} = 7.4\times10^{-4}\exp\left(-\frac{316\,kJ/mol}{RT}\right)\left[m^2s^{-1}\right] \quad \textbf{(7-11)}$$

It is important to note that the diffusion data and associated function (7-10) for the diffusion of indium in indium titanate requires further experimental verification for a system that is well-defined.

According to Peterson and Sasaki [ref], tri-valent ions, such as scandium and chromium, are incorporated into the rutile structure substitutionally (into titanium sites) and are transported according to interstitialcy mechanism. Their transport is associated with the simultaneous transport of interstitial titanium ions. The same mechanism is expected also in the case of indium diffusion. The interstitialcy transport mechanism is consistent with the report of Nakamura et al. [ref] who observed that indium is incorporated into the rutile structure partly into titanium sites and partly into interstitial sites.

7.5 Conclusions

The present work determined diffusion-induced concentration-related profiles for indium in a TiO_2 lattice of rutile. It is shown that assessment of the physical meaning associated with the intensity vs. depth profiles requires careful analysis of the character of the profiles for titanium

and oxygen as well cesium. The obtained intensity profiles were used to determine the diffusion coefficient of indium in high purity TiO_2 single crystal in the range 1073 K - 1573 K in air. This diffusion data, involving eight independently determined data points, obeys a linear relationship very well. The obtained data indicate that the activation energy of diffusion is profoundly influenced by ionic radius. As seen, the activation energy for indium (316 kJ/mol) and zirconium (325 kJ/mol) are similar as they have similar ionic radii (0.081 nm and 0.080 nm, respectively). On the other hand, the activation energy for titanium (251 kJ/mol) and niobium (244 kJ/mol) are substantially lower as the ionic radii are smaller (0.068 nm and 0.070 nm, respectively).

7.6 References

(1) Fujishima, A.; Honda, K. "Electrochemical Photolysis of Water at a Semiconductor Electrode". Nature (1972), 238, 37-38.

(2) Karakitsou, K. E.; Verykios, X. E. "Effects of altervalent cation doping of titania on its performance as a photocatalyst for water cleavage". The Journal of Physical Chemistry (1993), 97 [6], 1184-1189.

(3) Khan, S. U. M.; Al-Shahry, M.; Ingler Jr, W. B. "Efficient photochemical water splitting by a chemically modified n-TiO_2". Science (2002), 297, 2243-2245.

(4) Mavroides, J. G.; Tchernev, D. I.; Kafalas, J. A.; Kolesar, D. F. "Photoelectrolysis of water in cells with TiO_2 anodes". Mater. Res. Bull. (1975), 10 [10], 1023-1030.

(5) Morisaki, H.; Watanabe, T.; Iwase, M.; Yazawa, K. "Photoelectrolysis of water with TiO[sub 2]-covered solar-cell electrodes". Appl. Phys. Lett. (1976), 29 [6], 338-340.

(6) Nowotny, J.; Bak, T.; Nowotny, M. K.; Sheppard, L. R. "Titanium dioxide for solar-hydrogen I. Functional properties". International Journal of Hydrogen Energy (2007), 32 [14], 2609-2629.

(7) Ohnishi, T.; Nakato, Y.; Tsubomura, H. "Quantum yield of photolysis of water on titanium dioxide electrodes". Berichte der Bunsengesellschaft für physikalische Chemie (1975), 79, 523-525.

(8) Wrighton, M. S.; Ellis, A. B.; Wolczanski, P. T.; Morse, D. L.; Abrahamson, H. B.; Ginley, D. S. "Strontium titanate photoelectrodes. Efficient photoassisted electrolysis of water at zero applied potential". Journal of the American Chemical Society (1976), 98 [10], 2774-2779.

(9) Nowotny, J.; Bak, T.; Nowotny, M. K.; Sheppard, L. R. "Chemical diffusion in metal oxides. Example of TiO_2". Ionics (2006), 12 [3], 227-243.

(10) Akse, J. R.; Whitehurst, H. B. "Diffusion of titanium in slightly reduced rutile". J. Phys. Chem. Solids (1978), 39 [5], 457-465.

(11) Hoshino, K.; Peterson, N. L.; Wiley, C. L. "Diffusion and point defects in TiO_{2-x}". J. Phys. Chem. Solids (1985), 46 [12], 1397-1411.

(12) Lundy, T. S.; Coghlan, W. A. "Cation self diffusion in rutile". Journal de Physique Colloques (1973), C9, 299-302.

(13) Venkatu, D. A.; Poteat, L. E. "Diffusion of titanium of single crystal rutile". Materials Science and Engineering (1970), 5 [5], 258-262.

(14) Sasaki, J.; Peterson, N. L.; Hoshino, K. "Tracer impurity diffusion in single-crystal rutile (TiO_{2-x})". J. Phys. Chem. Solids (1985), 46 [11], 1267-1283.

(15) Millot, F.; Blanchin, M. G.; Tetot, R.; Marucco, J. F.; Poumellec, B.; Picard, C.; Touzelin, B. "High-temperature nonstoichiometric rutile TiO_{2-x}". Progress in Solid State Chemistry (1987), 17 [4], 263-293.

(16) Peterson, N. L.; Sasaki, J. Mechanisms of impurity diffusion in rutile. In Transport in Nonstoichiometric Compounds; Simkovich, G., Stubican, V. S., Eds.; Plenum Press: New York, (1985); pp 269-284.

(17) Sheppard, L. R.; Atanacio, A. J.; Bak, T.; Nowotny, J.; Prince, K. E. "Bulk diffusion of niobium in single-crystal titanium dioxide". Journal of Physical Chemistry B (2007), 111 [28], 8126-8130.

(18) Johnson, W. "One-Dimensional Diffusion of Li in Rutile". Phys. Rev. (1964), 136, A284-292.

(19) Johnson, O. W.; Paek, S. H.; DeFord, J. W. "Diffusion of H and D in TiO_2: Suppression of internal fields by isotope exchange". Journal of Applied Physics (1975), 46 [3], 1026-1033.

(20) Wittke, J. P. "Diffusion of transition metal ions into rutile (TiO_2)". J. Electrochem. Soc. (1966), 113, 193-194.
(21) Arita, M.; Hosoya, M.; Kobayashi, M.; Someno, M. "Depth profile measurement by secondary ion mass-spectrometry for determining the tracer diffusivity of oxygen in rutile". Journal of the American Ceramic Society (1979), 62 [9-10], 443-446.
(22) Bagshaw, A. N.; Hyde, B. G. "Oxygen tracer diffusion in the magnéli phases TinO2n-1". J. Phys. Chem. Solids (1976), 37 [9], 835-838.
(23) Derry, D. J.; Lees, D. G.; Calvert, J. M. "A Study of Oxygen Self-Diffusion in The c-Direction of Rutile Using a Nuclear Technique". J. Phys. Chem. Solids (1981), 42 [1], 57-64.
(24) Deskocil, J.; Pospisil, Z. "Measurements of oxygen self diffusion coefficient in some titanate ceramics". Silikaty (1972), 2, 113-121.
(25) Gruenwald, T. B.; Gordon, G. "Oxygen diffusion in single crystals of titanium dioxide". Journal of Inorganic and Nuclear Chemistry (1971), 33 [4], 1151-1155.
(26) Haul, R.; Dümbgen, G. "Sauerstoff-selbstdiffusion in Rutilkristallen". J. Phys. Chem. Solids (1965), 26 [1], 1-10.
(27) Millot, F.; Picard, C. Oxygen self-diffusion in non-stoichiometric rutile TiO_{2-x} at high-temperature". Solid State Ion. (1988), 28, 1344-1348.
(28) Bak, T.; Nowotny, J.; Prince, K.; Rekas, M.; Sorrell, C. C. "Grain boundary diffusion of magnesium in zirconia". Journal of the American Ceramic Society (2002), 85 [9], 2244-2250.
(29) Sheppard, L. R.; Zhou, M. F.; Atanacio, A.; Bak, T.; Nowotny, J.; Prince, K. E. "Determination of niobium diffusion in titania and zirconia using secondary ion mass spectrometry". Adv. Appl. Ceram. (2007), 106 [1-2], 89-94.
(30) Crank, J. The Mathematics of Diffusion, 2nd ed.; Oxford Science Publications, 1997.

CHAPTER 8

Effect of Oxygen Activity on Surface Composition of In-Doped TiO_2 at Elevated Temperatures

8.1 Abstract

The present work reports the effect of oxygen activity on segregation-induced indium surface concentration in In-doped TiO_2 annealed at 1273 K for different annealing time intervals (5-120 h) and $p(O_2)$ = 21 kPa and $p(O_2) = 10^{-10}$ Pa. It is shown that equilibrium segregation of indium in oxidising conditions, $p(O_2)$ = 21 kPa, is established within 20 h. However, annealing in reducing conditions, $p(O_2) = 10^{-10}$ Pa, could not establish equilibrium segregation due to indium evaporation, which becomes substantial at $p(O_2) < 1.8x10^2$ kPa. In these conditions, annealing results in an initial rise of surface concentration due to segregation followed by a subsequent decrease due to evaporation. The data may be used for modification of the surface vs. bulk composition of In-doped TiO_2 in a controlled manner.

8.2 Introduction

The interest in TiO_2-based systems continues to increase due to its promising photocatalytic and photoelectrochemical properties. The research is primarily aimed at the formation of high-performance photocatalysts for water purification [1-3] and photoelectrodes for photoelectrochemical water splitting [4-6]. These two applications are closely related to the photoreactivity of TiO_2 with water.

A critical step in the photoreactivity of the TiO_2 surface with water is charge transfer. The mechanism and kinetics of photoreactivity at the TiO_2/water interface (i.e. TiO_2 surface) is dependent on surface properties. The surface properties can be entirely different to that of the bulk phase as a result of segregation [7]. Therefore, the effect of doping, which consists of the incorporation of aliovalent ions as donors and acceptors [8], should be considered in terms of both bulk and surface properties. Consequently, the phenomenon of segregation may be applied as a method for controlling the surface concentration of dopants. Although segregation in oxides is still not well understood, it has been shown that segregation-induced surface enrichment in metal oxides strongly depends on oxygen activity during segregation [7,9,10]. Therefore, the imposition of a gas phase with variable oxygen activity may be used to tailor the surface concentration of dopants in a well-defined and reproducible manner.

The present work aims to understand the effect of oxygen activity on the segregation of indium in polycrystalline In-doped TiO_2 during prolonged annealing in a gas phase of controlled composition. The ultimate aim is to assess the time required to reach equilibrium segregation at elevated temperatures.

8.2.1. Brief literature overview

8.2.1.1. Segregation

The surface properties are different from those in the bulk phase, in terms of both chemical composition and structure, as a result of segregation. Therefore, there has been an increasing interest in studies on the segregation of oxides, including TiO_2 [11-14]. However, most of the segregation-related data reported so far, does not correspond to gas/solid equilibrium and, therefore, are not well-defined and not reproducible.

Bernasik *et al.* [11] studied the effect of oxygen activity on iron segregation in Fe-doped TiO_2 single crystal using SIMS. Their data showed that the segregation-induced surface enrichment of iron is enhanced by the imposition of increased oxygen activity in the gas phase during annealing at 1673 K.

Gulino et al. [12] reported Sb segregation in polycrystalline specimens of Sb-doped TiO_2 at 1273 K. Their data determined that the segregation-induced enrichment factor increases substantially with a decreasing bulk content of Sb.

Ruiz *et al.* [14] studied chromium segregation in polycrystalline Cr-doped TiO_2 at 873 K and 1173 K in air using XPS surface analysis. They observed that the segregation-induced surface enrichment of chromium at 1173 K was two times larger than that at 873 K.

Conflicting data have also been reported for the segregation of niobium in Nb-doped TiO_2 in a recent review by Nakajima et al. [13].

8.2.1.2. Effect of indium doping on properties of TiO_2

Karakitsou et al. [15] reported on the photocatalytic water splitting performance for In-doped TiO_2 as well as other aliovalent ions of higher and lower valence cations such as W^{6+}, Ta^{5+}, Nb^{5+}, In^{3+}, Zn^{2+} and Li^{+}. They observed that donor cations with valence higher than Ti^{4+} enhanced the photocatlytic water splitting performance, while lower valence cations, including In^{3+} had the opposite effect.

Shchukin et al. [16] examined the photocatalytic properties of In_2O_3-TiO_2 bicomponent powders of varying ratios and reported greatly enhanced photocatalytic activity compared with undoped TiO_2. They attributed this to increased surface acidity as well as favourable band-gap modification which improved charge separation. Studies by Wang et al. [17] found that In-doped TiO_2 improved photo-generated charge separation as well as photocatalytic activity. They determined that this was due to the formation of unique O-In-Cl_x chemical species at the surface. It is certainly evident from the conflicting literature reports, that the need for further investigation of indium doped TiO_2 is warranted.

It has become increasingly clear that the surface plays a critical; even controlling role in the resulting functional properties of oxides. However there is often a failure to recognize that the surface composition can be entirely different from that of the bulk phase due to the phenomenon of segregation. Consequently, the contribution of surface segregation must also be taken into account when deriving theoretical models relating to the effect of dopants on functional properties.

The aim of the present work is to determine the effect of indium segregation on the surface composition of In-doped TiO_2. The main effort is centered on establishing the effect of annealing conditions (time and oxygen activity) on indium segregation.

8.2.1.3. Effect of Indium on Defect Disorder of TiO_2

The effect of foreign ions on the properties of TiO_2 can be described by defect chemistry models [8]. The mechanism of indium incorporation into the TiO_2 lattice in reducing conditions may be represented, using the Kröger-Vink notation [18] (**Table 8-1**) by the following reaction:

$$In_2O_3 \leftrightarrow 2In'_{Ti} + 3O_O + V_O^{\bullet\bullet} \qquad \textbf{(8-1)}$$

As seen, the reaction results in the formation of both negatively charged indium ions and positively charged oxygen vacancies (relative to the lattice). Consequently, the resulting defect disorder is governed by the following ionic charge compensation:

$$[In'_{Ti}] = 2[V_O^{\bullet\bullet}] \quad \textbf{(8-2)}$$

On the other hand, the incorporation of indium in oxidising conditions is different:

$$In_2O_3 + \frac{1}{2}O_2 \leftrightarrow 2In'_{Ti} + 2h^{\bullet} + 4O_O^x \quad \textbf{(8-3)}$$

The defect disorder in this case is governed by the following charge compensation:

$$p = [In'_{Ti}] \quad \textbf{(8-4)}$$

Therefore, the rightward shift of reaction (8-3), which is associated with oxygen consumption by the oxide lattice, is favoured at higher oxygen activity. **Reactions (8-1)** and **(8-3)** show that the effect of oxygen activity on indium incorporation may be explained using the concepts of defect chemistry. The aim of the present work is to assess the effect of oxygen activity on the segregation-induced surface enrichment of rutile in indium.

Table 8-1. The Kröger-Vink [18] and the traditional notations of point defects in TiO_2

Traditional Notation	**Description**	**Kröger-Vink notation**
$\mathbf{Ti_{Ti}^{4+}}$	Ti_{Ti}^{4+} ion in the titanium lattice site	Ti_{Ti}^{x}
$\mathbf{Ti_{Ti}^{3+}}$	Ti_{Ti}^{3+} ion in the titanium lattice site (quasi-free electron)	e'
$\mathbf{V_{Ti}}$	Titanium vacancy	V_{Ti}''''
$\mathbf{Ti_i^{3+}}$	Ti_i^{3+} in the interstitial site	$Ti_i^{\bullet\bullet\bullet}$
$\mathbf{Ti_i^{4+}}$	Ti_i^{4+} in the interstitial site	$Ti_i^{\bullet\bullet\bullet\bullet}$
$\mathbf{O_O^{2-}}$	O_O^{2-} ion in the oxygen lattice site	O_O^x
$\mathbf{V_O}$	Oxygen vacancy	$V_O^{\bullet\bullet}$
$\mathbf{O_O^-}$	O_O^- ion in oxygen lattice site (quasi-free electron hole)	$h^{\bullet}$

8.3 Experimental

8.3.1. Powder preparation

Indium doped TiO_2 powder was prepared via the sol gel technique using the following precursors: (i) titanium isopropoxide, $Ti[OCH(CH_3)_2]_4$ (97% Aldrich), (ii) indium chloride, $InCl_3$ (99.999% Aldrich), (iii) anhydrous ethanol, (iv) Milli-Q water and (v) acetic acid. The

volume of titanium isopropoxide was calculated based on the required final mass of TiO_2 powder (25 g). The required amount of $InCl_3$ powder was then calculated to achieve the desired nominal 0.03 at% dopant concentration. The volume of acetic acid (necessary to slowdown gelation) and Milli-Q H_2O was determined from the CH_3COOH:Ti and H_2O:Ti ratios of 1.5:1 and 4:1 respectively according to the work of Doeuff et al. [19]. Finally, the total volume of anhydrous ethanol was determined to achieve a final solution concentration of 0.8 mol/L.

To prepare the sol-gel, a small amount of the total calculated ethanol volume (typically ~50 ml) was first combined with the $InCl_3$ powder in a beaker (B1) under vigorous stirring for at least 30 mins until the $InCl_3$ was completely dissolved in solution. In a separate beaker (B2) the $Ti[OCH(CH_3)_2]_4$ was combined with the acetic acid under vigorous stirring for 1 hour (covered with a plastic film to minimise any moisture absorption from atmosphere). In a third separate beaker (B3) the remaining ethanol was combined with the H_2O and placed under constant stirring. After 30 mins the (B1) solution was slowly added to the (B2) solution and allowed to continue stirring for 1 hour. After 1 hour, the (B3) solution was added drop-wise to the B2 solution and left to stir until the viscosity of the gel formation hindered rotation of the stirring bar. At this stage the stirrer was stopped and the beaker of gel placed on a hot place at approximately 80^{o}C and left in the fume hood to dry for 2-3 days. The resulting crystals were then ground into a fine (talc-like) powder using an agate mortar and pestle.

8.3.2. Powder consolidation

The ground TiO_2 powder was placed in a Pt lined alumina boat and calcined in air at 1173K using a tube furnace to remove any water and organics as well as inducing the anatase-to-rutile phase transition.

The calcined samples were then pressed uniaxially into cylindrical pellets using a 10 mm diameter hardened stainless steel die at ~50-60 MPa without the addition of a binding agent. The pressed pellets were then carefully vacuum sealed into thin latex tubes and cold isostatically pressed (CIP) to a pressure of 400 MPa with dwell at full pressure for 2 minutes. The resulting pellets were sintered in air at 1773 K for 5 hours for densification into a polycrystalline solid. After sintering, ~30 - 50 µm of the sample surface was removed by mechanical grinding and polishing, using a series of diamond pads and diamond suspension liquids (Struers LaboSystem). The aim of this was to eliminate any segregation enriched surface layers formed during the sintering process and return the surface to the bulk dopant concentration. The sample at this stage will be referred to as "as-polished". A precision diamond saw was then used to

section each as-polished pellets into the brick-like shapes used in the different annealing conditions examined in the present work. A micrograph of the as-polished specimen is shown in **Figure 8-1**.

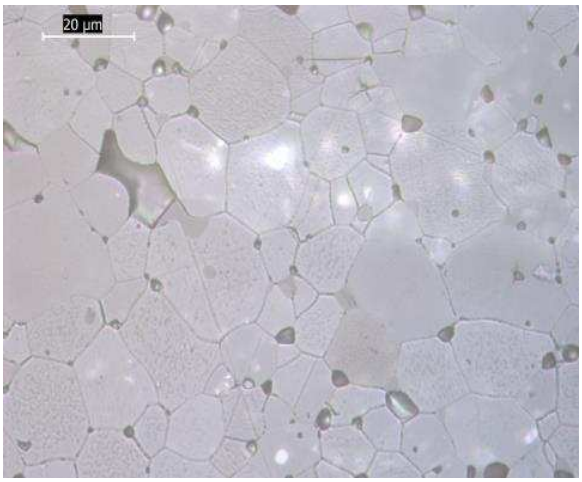

Figure 8-1. Micrograph of the polycrystalline as-polished sample of In-doped TiO_2

8.3.3. Annealing

Reducing Conditions: The gas phase involving 1%H_2/Ar gas mixture was used to impose the p(O_2) of 10^{-10} Pa. This was achieved with gas flow rate of 100 ml/min velocity. This gas was initially put through a dual bubbler system submerged in a thermally insulated ice box filled with ice and water. The small ice box was used to maintain a consistent and reproducible partial pressure related to water vapour. The first bubbler in the ice box was fitted with an aerator and filled with Milli-Q water while the second bubber was left empty and used primarily as a condensation trap. The gas was then flowed through a gasket sealed tube furnace (reactor vessel) held at 1273 K and containing the doped TiO_2 specimen. The p(O_2) of the reactor vessel output gas was continuously monitored using a zirconia oxygen probe held at 1023 K after which the gas exited through a final water filled bubbler used to stop any back flow of air into the system. Samples were inserted into the tube furnace by removing the gasket seal (on the downstream gas flow side); rapidly pushing the sample into the heat zone and replacing the gasket seal. After the required annealing time had been reached, the downstream gasket was again removed and the sample pulled from the central heat zone as quickly as possible to a pre-defined position near the end of the tube (but not directly to room temperature) in order to quench the sample whilst not imposing thermal shock.

Oxidising Conditions: The oxygen activity of p(O_2) = 21 kPa was achieved by flowing artificial air through the tube furnace during annealing.

8.3.4. Sample characterisation

8.3.4.1. X-ray Diffraction (XRD)

XRD (Siemens D500) analysis was performed on the calcined samples using a Co $K\alpha_{1,2}$ radiation source and a graphite monochromator. Data was collected in the angular range of 5° to 80° with a 2θ step size of 0.05 and a five second dwell time. All data was analysed using the PANalytical XRD analysis package (High Score Pro) to identify the crystalline phases related to the obtained peak positions. As seen in **Figure 8-2**, all of the X-ray diffraction peaks for the studied specimen of In-doped TiO_2 relate to the rutile phase. This pattern indicates that indium incorporation into the TiO_2 lattice resulted in the formation of a solid solution as no additional peaks, which would suggesting the formation of another phase has been observed.

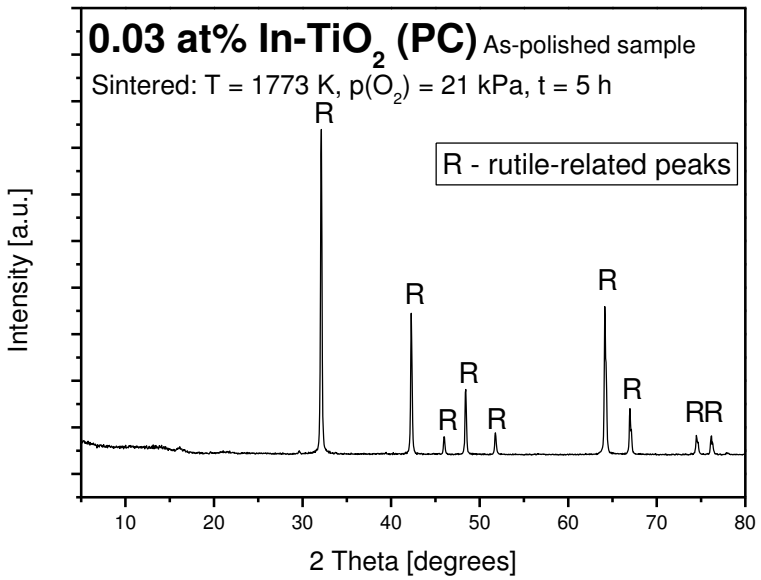

Figure 8-2. The X-ray diffraction pattern of In-doped TiO_2 powder calcined in air at 1173 K. The presence of only rutile peaks confirms the incorporation of indium (In^{3+}) ions as a solid solution.

8.3.4.2. Proton Induced X-ray Emission (PIXE)

PIXE analysis was used to perform elemental bulk phase analysis of the studied In-doped TiO_2 specimen. The analysis was performed using the 2MV STAR tandem accelerator at the Australian Nuclear Science and Technology Organisation. A 2.6 MeV proton beam of 10-15nA beam current and collimated to 3 mm was applied at a normal angle of incidence to the as-polished sample surface for analysis. The X-rays were recorded using a Si(Li) detector fitted with 25 µm thick Be window at the 45º angle. Due to the limitation of the Si(Li) detectors ability

to cope with very high count rates resulting from solid samples, an additional pin-hole filter (1700 µm thick acrylic) with 2% hole area, was used. The pin-hole filter was placed over the x-ray detector to minimise pile-up and dead time during sample analysis. The pin-hole filter was also fitted with an additional 4µm thick mylar film to further decrease the intensity of the low energy X-rays excited with high cross-sections. The collected charge generated by the ion beam for each sample was 30µC. The acquired X-ray spectra were processed using the GUPIXWIN software package (Version 2.1.4, University of Guelph, Canada) to determine the elemental concentration.

The PIXE spectrum of the as-polished In-doped TiO_2 annealed at 1773 K for 5 h in air is shown in **Figure 8-3**. The quantitative analysis of the indium-related peak indicates that the content of indium in the bulk phase is 0.03 ± 0.004 at%.

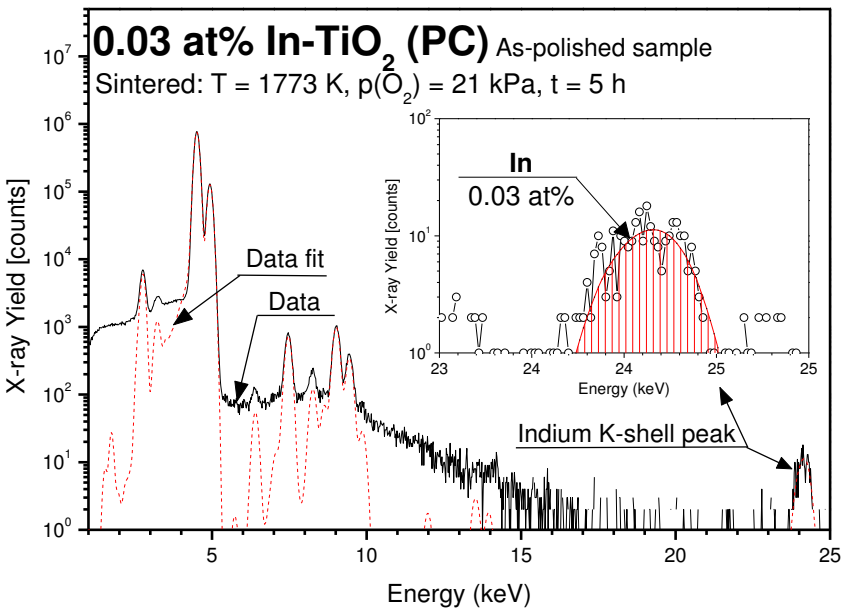

Figure 8-3. Proton-induced X-ray emission (PIXE) spectra for an as-polished sample of In-doped titanium dioxide.

8.3.4.3. Secondary Ion Mass Spectrometry (SIMS)

The SIMS technique is one of the most sensitive surface analytical tools, however, it only provides the depth profiles in terms of qualitative ion intensity rather than absolute concentration unless matrix matched reference materials are available. The SIMS sputtering technique essentially enables layer-by-layer lattice removal from the specimen. Therefore, variations in ion intensity can be detected within the individual lattice layers. The thickness of the removed layers is dependent on the sputtering rate which is related to the primary ion beam and net impact

energy used. The maximum penetration depth, to which the SIMS depth profile is limited, depends on the geometry of the incident beam. Beyond this certain depth the results of the analysis may be influenced by the top edge of the crater wall. In the present work the maximum analysis depth is ~10 µm.

Depth profiling was performed using secondary ion mass spectrometry, SIMS (Cameca ims 5f). A Cs^+ primary ion beam of 5nA current and 5 keV net impact energy was rastered over a 250 x 250 µm area to sputter secondary ions from the sample surface. Lens and aperture settings were used to restrict secondary ion analysis to a 55µm circular area within the rastered region and analysis kept below 10 µm to avoid any influence of crater edge effects on the results.

The SIMS analysis is applied in the present work to determine the indium depth profile after different annealing times in the gas phase of controlled oxygen activity.

8.3.4.4. X-ray Photoelectron Spectroscopy (XPS)

Quantitative surface concentration was determined using XPS (ESCALAB 250 xi). The spectra were induced with a monochromatic Al Kα (1486.6 eV) excitation source operated at 15 kV and 160 W. The X-ray spot was approximately 0.5 mm in diameter. A take-off angle of 90º relative to the sample surface was used for all analyses which results in an analysis depth of approximately 6 nm. A pass energy of 100 eV was used for survey scans and 20 eV for elemental region scans. A 20 second argon sputtering etch was required prior to XPS analysis of the as-polished sample to remove surface carbon likely remaining from the polishing/lubrication medium used. The energy of the Ar^+ ion beam used for the sputtering etch was 3 keV. The etching rate was approximately 0.4 nm/s calibrated using a Ta_2O_5/Ta reference sample. XPS analysis was used in the present work to determine the quantitative indium surface concentration at certain stages of the annealing process.

8.4 Results and Discussion

The raw data representing the effect of annealing time on the SIMS depth profiles are shown in **Figure 8-4 (a)-(b)** in terms of indium intensity (counts) vs. depth profiles as a function of imposed annealing time. This figure also includes the profile of the gold surface layer, which was deposited (by evaporation) onto each sample prior to SIMS analysis to eliminate sample charging.

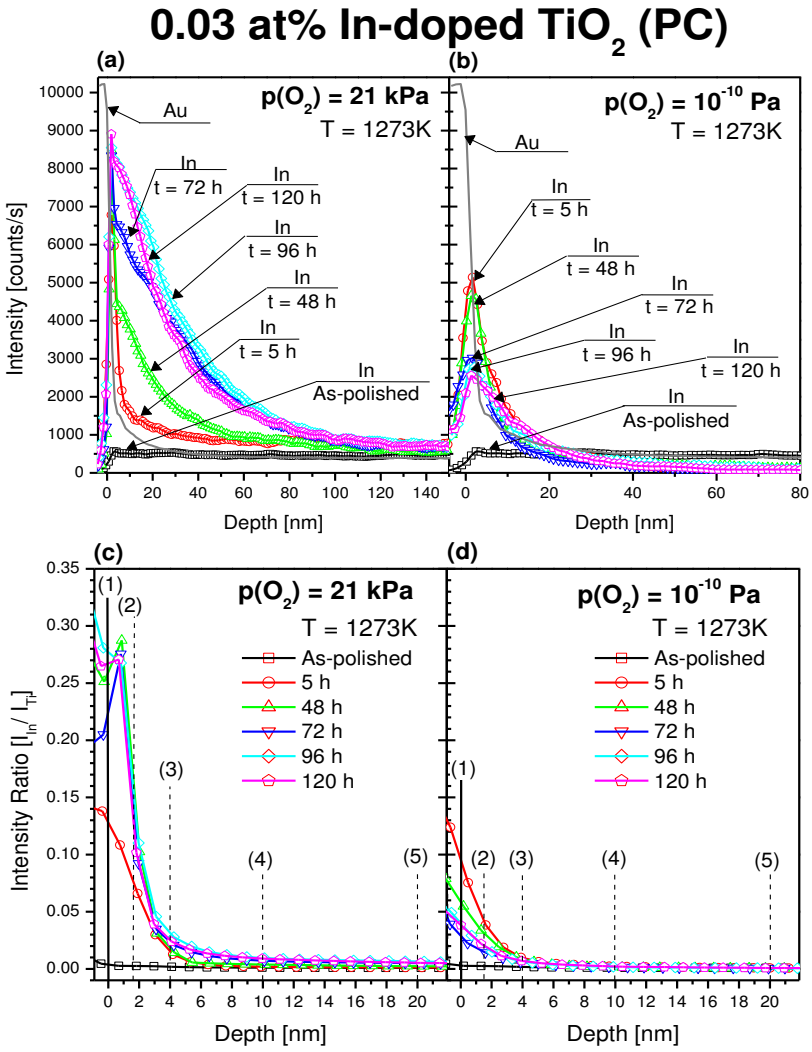

Figure 8-4. Effect of annealing time in oxidising and reducing conditions at 1273 K on SIMS profiles in terms of (a)-(b) intensities vs. depth and (c)-(d) intensity ratio for In-doped TiO_2.

The related zero of the depth scale in **Figure 8-4** has been associated with the part of the depth profile at which gold drops rapidly to the background level. In other words, the part of the profile, which is related to the gold surface layer should not be taken into account in quantitative analysis of indium segregation.

A negative characteristic of SIMS analyses are experimental uncertainties which occur at the initial stages of analysis due to non-equilibrium sputtering conditions. These uncertainties may be minimized when the depth profiles are plotted in terms of the intensity ratios [I_{In} / I_{Ti}], which are shown in **Figure 8-4 (c)-(d)**. In other words, the absolute values of the intensity profiles within the oxide lattice may be normalised to a host lattice ion such as Ti or one of the predominant cations which form the lattice, whose concentration is relatively stable as a function

of depth within each samples and also expected to be of consistent intensity across different samples, such as titanium.

Figure 8-4 (c)-(d) represents the depth profiles, in terms of the [I_{In} / I_{Ti}] ratio, at different time intervals of annealing ranging between 5 h and 120 h as well as the as-polished specimens, in both oxidising and reducing environments related to $p(O_2)$ = 21 kPa and $p(O_2) = 10^{-10}$ Pa, respectively. The data for as-polished specimen serves as a reference. The intensity ratio data shown in **Figure 8-4(c)-(d)**, and free from non-equilibrium sputtering fluctuations, will be analysed further in the present work. The associated penetration depth was determined from calibration using the relationship between the total sputtering time and total crater depth. The total depth of the crater generated by the sputtering process was measured accurately using high precision stylus profilometer (Alpha step 2000, KLA Tencor).

The depth profiles in **Figure 8-4 (c)-(d)** have been considered within the following ranges (1)-(5):

(1) The first range, demarcated by the solid line (1) corresponds to the initial part of the intensity profile related to the gold surface layer. Therefore, the line (1) is considered to correspond to the zero level of the depth scale. Consequently, the indium intensity profile on the left side of the solid line (1) is not taken into account.

(2) The second range is demarcated by the dotted line (2). This range exhibits the maximum intensity of the profile, which corresponds to approximately 1.5 nm depth. As seen in **Figure 8-4 (c)-(d)**, the indium intensity of the as-polished specimen remains constant within across the entire analysis depth.

(3) The third range is demarcated by the lines (2) and (3). The latter corresponds to d = 4 nm. This layer exhibits the strongest indium concentration gradient.

(4) The subsequent ranges (4) and (5), selected arbitrarily, correspond to d =10 nm and d = 20 nm depth from the Au/TiO_2 interface, respectively.

Figure 8-4 (c) represent the depth profiles of In-doped TiO_2 annealed at $p(O_2)$ = 21 kPa during different periods of time, including 5h, 48 h, 72 h, 96 h, and 120 h, respectively. The intensity ratios at the solid line (1), which is related to the depth at which the gold profile drops to background, are associated with the concentrations at the outermost surface layer.

The intensity profiles for In-doped TiO_2 annealed in strongly reducing conditions, $p(O_2) = 10^{-10}$ Pa, during 5h, 48 h, 72 h, 96 h, and 120 h, respectively, as well as the as-polished specimen

of In-doped TiO_2 are shown in **Figure 8-4 (d)**. As seen, the intensity profiles related to the surface layer in reducing conditions, denoted by solid line (1), are markedly lower than at the same point in **Figure 8-4 (c)**.

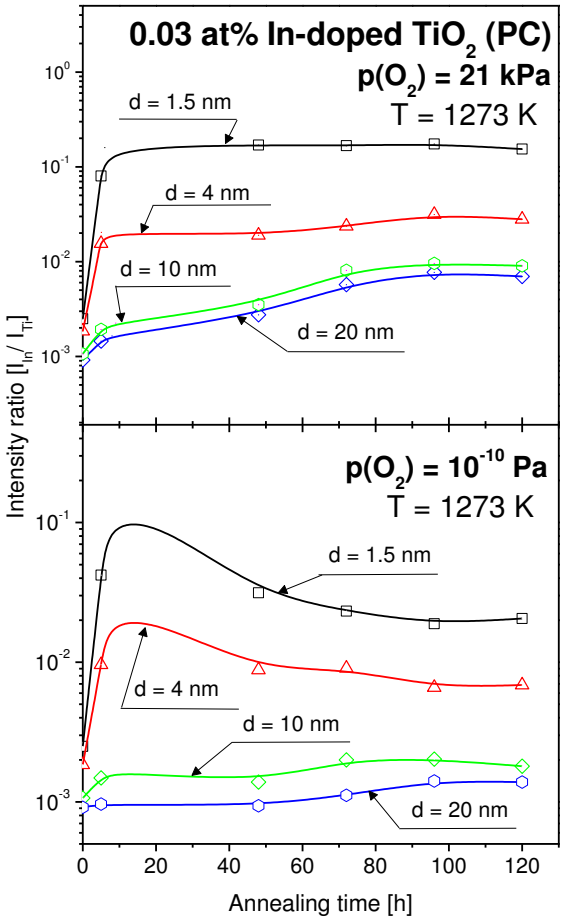

Figure 8-5. Effect of annealing time at 1273 K in oxidising and reducing gas phase on the concentration of indium for In-doped TiO_2 at different depths.

The effect of annealing on the concentration of indium at specific depths from the surface, in both oxidising and reducing environment, is shown in **Figure 8-5** in terms of the intensity ratios vs. annealing time at 1273 K in both oxidising and reducing environments (upper and lower part, respectively). The associated surface concentration values determined by XPS are shown in **Figure 8-6**.

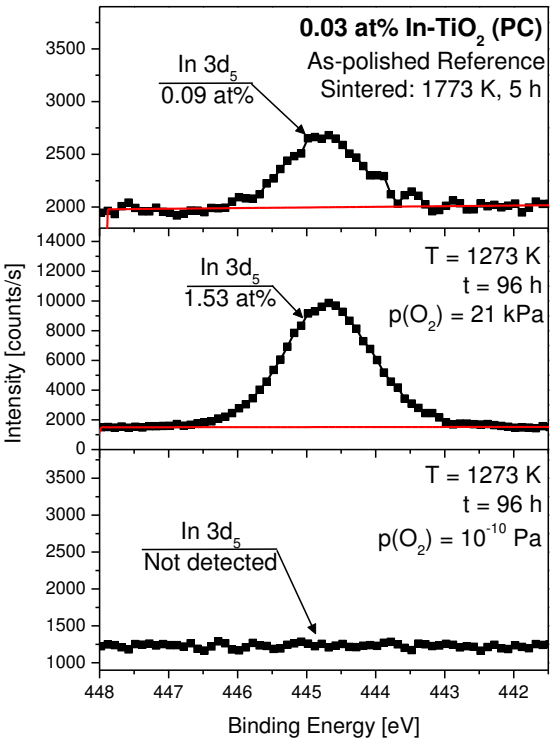

Figure 8-6. The effect of annealing in oxidising and reducing environments at 1273 K on surface concentration of indium for In-doped TiO_2 along the data for as-polished specimen.

These two sets of data represented in **Figure 8-5** and **Figure 8-6** can be used to derive a general picture on the effect of segregation in both oxidising and reducing environments.

8.4.1. Oxidising Conditions

As seen in **Figure 8-5**, the outermost surface layer, related to approximately 1.5 nm, in oxidising conditions assumes a stable concentration within approximately 20 h and then remains constant as a function of time. The shape of the annealing curve associated with the deeper layer (4 nm) is similar. According to the XPS analysis, the surface concentration of indium in this case is 1.53 at% indicating that the segregation-induced enrichment of the surface layer is approximately f = 50. It is interesting to note that even polishing the surface results in an enrichment of f = 3. Furthermore, the annealing curves corresponding to deeper layers indicate that segregation still takes place at t > 80 h.

8.4.2. Reducing Conditions

As is also seen in **Figure 8-5**, the profiles corresponding to $p(O_2)=10^{-10}$ Pa assume a maximum at approximately 10 h and then the intensity ratio value decreases as the annealing time increases. This correlates well with the results shown in **Figure 8-6**, where the surface indium concentration after 96 hours in reducing environment is below the detectability limit of the XPS analysis. This effect may be considered in terms of two possible scenarios:

(1) The segregation driving force of indium in low oxygen activity is either reduced to zero or indium has the tendency to desegregate resulting in an impoverishment of the surface layer.

(2) The segregation driving force of indium is still high enough to produce indium segregation; however, the surface concentration of indium is diminished by evaporation.

The increasing trend of the intensity ratio vs. annealing time curve for $p(O_2) = 10^{-10}$ Pa within the first 10 h, indicates that the segregation driving force is strong enough. However, the subsequent decreasing trend indicates that the reduced surface indium content is most likely due to the evaporation of In_2O_3. This observed effect of oxygen activity on indium evaporation is consistent with the report of Valderrama-N and Jacobs [20]. They have documented that at low oxygen activity In_2O_3 in converted into highly volatile phase of In_2O. They have shown that the decomposition pressure of In_2O_3 at 1373 K is 10^{-7} Pa. Therefore, one should expect that indium oxide will evaporate in the reducing conditions applied in the present work.

8.5 Conclusions

The present work reported segregation-induced concentration profiles for indium in In-doped TiO_2 annealed in both oxidising environment, $p(O_2)$ = 21 kPa, and in strongly reducing environment, $p(O_2) = 10^{-10}$ Pa. The obtained data allow the following points to be made:

- Indium has the tendency to segregate to the surface of In-doped TiO_2 (rutile). The time required to reach ~90% of the equilibrium concentration at the surface in oxidising conditions, $p(O_2)$ = 21 kPa, at 1273 K is 20 h. The segregation-induced enrichment in these conditions is f = 50.
- Annealing In-doped TiO_2 in highly reducing conditions does not allow equilibrium segregation to be reached due to strong effect of indium evaporation from the surface.

The reported effects of oxygen activity on dopant segregation may be used as a technology for imposing specific surface chemistry and related chemically-induced electric fields, which have an essential role in separation of light-induced charge carriers.

8.6 References

(1) Liu, Y.; Li, J.; Qiu, X.; Burda, C. "TiO_2 nanocatalysts for water purification: tapping energy from the sun". Water Science and Technology (2006), 54, 47-54.

(2) Robert, D.; Malato, S. "Solar photocatalysis: a clean process for water detoxification". Sci. Total Environ. (2002), 291 [1-3], 85-97.

(3) Skorb, E. V.; Ustinovich, E. A.; Kulak, A. I.; Sviridov, D. V. "Photocatalytic activity of TiO_2 : ln2O3 nanocomposite films towards the degradation of arylmethane and azo dyes". J. Photochem. Photobiol. A-Chem. (2008), 193 [2-3], 97-102.

(4) Fujishima, A.; Honda, K. "Electrochemical Photolysis of Water at a Semiconductor Electrode". Nature (1972), 238, 37-38.

(5) Ni, M.; Leung, M. K. H.; Leung, D. Y. C.; Sumathy, K. "A review and recent developments in photocatalytic water-splitting using TiO_2 for hydrogen production". Renew. Sust. Energ. Rev. (2007), 11 [3], 401-425.

(6) Nowotny, J.; Sorrell, C. C.; Sheppard, L. R.; Bak, T. "Solar-hydrogen: Environmentally safe fuel for the future". International Journal of Hydrogen Energy (2005), 30 [5], 521-544.

(7) Cabane, J.; Cabane, F. Equilibrium segregation in interfaces. In Interface segregation and related processes in materials; Nowotny, J., Ed.; Trans Tech Publications Ltd.: Zurich, (1991); pp 1-150.

(8) Kofstad, P. Nonstoichiometry, diffusion and electrical conductivity in binary metal oxides; Wiley: New York, 1972.

(9) Nakajima, T.; Sheppard, L. R.; Prince, K. E.; Nowotny, J.; Ogawa, T. "Niobium segregation in TiO_2". Adv. Appl. Ceram. (2007), 106 [1], 1-7.

(10) Sikora, I.; Stolze, F.; Hirschwald, W. "Segregation of chromium in CoO-Cr_2O_3 solid-solutions and $CoCr_2O_4$ spinel phases studied by SIMS and ESCA ". Surface and Interface Analysis (1987), 10 [8], 424-429.

(11) Bernasik, A.; Rekas, M.; Sloma, M.; Weppner, W. "Electrical surface versus bulk properties of Fe-doped TiO_2 single crystals". Solid State Ion. (1994), 72 [Part 2], 12-18.

(12) Gulino, A.; Condorelli, G. G.; Fragalà, I.; Egdell, R. G. "Surface segregation of Sb in doped TiO_2 rutile". Applied Surface Science (1995), 90 [3], 289-295.

(13) Nakajima, T.; Sheppard, L. R.; Prince, K. E.; NOwotny, J.; Ogawa, T. Adv. Appl. Ceram. (2007), 106, 82-88.

(14) Ruiz, A. M.; Sakai, G.; Cornet, A.; Shimanoe, K.; Morante, J. R.; Yamazoe, N. "Cr-doped TiO_2 gas sensor for exhaust NO_2 monitoring". Sens. Actuator B-Chem. (2003), 93 [1-3], 509-518.

(15) Karakitsou, K. E.; Verykios, X. E. "Effects of altervalent cation doping of titania on its performance as a photocatalyst for water cleavage". The Journal of Physical Chemistry (1993), 97 [6], 1184-1189.

(16) Shchukin, D.; Poznyak, S.; Kulak, A.; Pichat, P. "TiO_2-In_2O_3 photocatalysts: preparation, characterisations and activity for 2-chlorophenol degradation in water". Journal of Photochemistry and Photobiology A - Chemistry (2004), 162 [2-3], 423-430.

(17) Wang, E. J.; Yang, W. S.; Cao, Y. A. "Unique Surface Chemical Species on Indium Doped TiO_2 and Their Effect on the Visible Light Photocatalytic Activity". Journal of Physical Chemistry C (2009), 113 [49], 20912-20917.

(18) Kröger, F. A. The chemistry of imperfect crystals North Holland, Amsterdam, 1974.

(19) Doeuff, S.; Henry, M.; Sanchez, C.; Livage, J. "Hydrolysis of titanium alkoxides - modification of the molecular precursor by acetic-acid ". J. Non-Cryst. Solids (1987), 89 [1-2], 206-216.

(20) Valderrama-N, J.; Jacob, K. T. "Vapor pressure and dissociation energy of (In_2O)". Thermochimica Acta (1977), 21 [2], 215-224.

CHAPTER 9

Effect of Indium Segregation on Surface vs. Bulk Chemistry for In-Doped TiO_2

9.1 Abstract

This work reports the effect of indium segregation on surface vs. bulk composition of In-doped TiO_2. The studies are performed using proton-induced X-ray emission (PIXE), secondary ion mass spectrometry (SIMS), X-ray photoelectron spectroscopy (XPS), and Rutherford backscattering (RBS). The PIXE and XPS results indicate that annealing 0.3 at% In-doped TiO_2 at 1273 K in the gas phase of controlled oxygen activity [$p(O_2)$ = 75 kPa and $p(O_2)$ = 10 Pa] results in surface enrichment of 2.95 at% In and 2.61 at% In, respectively. The obtained segregation data are considered in terms of the transport of indium ions from titanium sites in the bulk phase to the surface where these ions are incorporated into interstitial sites. The effect of oxygen activity on segregation-induced surface enrichment results in the formation of a 1-2 nm low-dimensional surface structure and a sub-layer, which are charged negatively. The latter formed as a result of strong interactions between titanium vacancies and interstitial indium ions leading to the formation of defect complexes. The data obtained in this work may be used for engineering of TiO_2-based semiconductors with enhanced performance in solar energy conversion.

9.2 Introduction

TiO_2 is a promising candidate for photocatalytic removal of toxic organic contaminants from water [1,2] and photoelectrochemical generation of hydrogen fuel from water [3]. The first

successful experiment of Fujishima and Honda [3] on photoelectrochemical water splitting has resulted in intensive research, aimed at modifying TiO_2 in order to enhance its performance. The ultimate goal of the research is to form a TiO_2-based system which is able to perform at the level of efficiency that is required for commercialization.

The most common way to modify the performance-related properties of oxides including TiO_2, such as electronic structure, flat band potential and surface properties, is by incorporation of aliovalent ions into the TiO_2 lattice (doping) [4-8]. The process of doping, which results in the formation of donor and/or acceptor centres, leads to a change in the concentration of electronic charge carriers and the related semiconducting properties in a controlled manner. So far, the effect of doping on the properties of oxides has been mainly been assessed in terms of bulk properties. Awareness is growing, however, that the mechanism of incorporating foreign ions and the resulting properties in the bulk and surface phase can be entirely different [9-12]. Clarification of this effect is crucial for correctly understanding the effect of doping on the performance of photoelectrodes and photocatalysts, which is determined by surface vs. bulk properties. So far, however, little is known in this matter.

There has been an accumulation of reports indicating that solutes present in the bulk phase segregate to the surface, however, the reported enrichment data are conflicting [13]. Moreover, awareness is growing that solute segregation in metal oxides is profoundly influenced by intrinsic defect disorder and the related oxygen activity [9-11]. Therefore, there is an increasingly urgent need to understand the effect of segregation on both the bulk and surface properties of oxides and, specifically the effect of oxygen activity on segregation-induced enrichment.

The present work is a part of a larger research program to investigate the effect of segregation on surface properties of photosensitive oxide semiconductors, including chemical composition and the associated performance-related properties of TiO_2 solid solutions with donor- and acceptor-type ions.

Our previous work for In-doped TiO_2 has revealed that the effect of indium segregation on surface composition is a compromise between indium evaporation and segregation [14]. That work resulted in the following conclusions:

Equilibrium Segregation. The determination of equilibrium segregation requires knowledge of the time needed to establish equilibrium. It was shown that equilibrium segregation of indium in the TiO_2 lattice in oxidising atmosphere can be reached within 20 h at 1273 K.

Evaporation. Annealing of In-doped TiO_2 in a strongly reducing environment cannot achieve equilibrium segregation due to indium evaporation. In this case the resulting surface concentration of indium is a compromise between the rate of segregation and the rate of evaporation. Knowledge of these effects may be used to set-up appropriate processing conditions for the formation of well-defined In-doped TiO_2 in terms of surface vs. bulk composition.

The purpose of the present work is, using the experimental framework established previously [14], to determine the effect of indium segregation on surface vs. bulk composition of In-doped TiO_2 in an oxidising environment. In this environment the segregation-induced surface composition is not affected by evaporation. In order to establish the effect of segregation on the local indium concentration within the surface layer, it seems appropriate to use the following range of analytical tools, which exhibit different sensitivity to surface vs. bulk composition:

Secondary ion mass spectrometry, SIMS. This destructive method is extremely sensitive to chemical composition. It is able to analyse the composition-related intensity of species within lattice layers of approximately 1 nm in thickness and removed layer-by-layer up to 10 µm in depth from the surface. However, quantitative assessment of the SIMS intensity data in terms of absolute elemental concentration vs. depth requires calibration, which is awkward. Furthermore, SIMS can be strongly influenced by matrix-related effects which add further complexity. Consequently, SIMS is typically utilised for qualitative depth profiling.

X-ray photoelectron spectroscopy, XPS. This method, which is non-destructive, provides the absolute concentration of the surface layer composition within 4-6 nm depth from the surface, depending on angle of incidence.

Rutherford backscattering spectroscopy, RBS. The analysis depth of this method, which is also non-destructive, is of the order of tens of nanometers and, therefore, is larger than that of SIMS and XPS. In the case of RBS the smallest analysis depth can be as low as 20-30 nm and the probing depth is on the order of several micrometers depending on the incident particle energy and target matrix. Therefore, RBS is a comparatively less surface sensitive technique than SIMS and XPS.

Proton-induced X-ray emission, PIXE. The analysis depth of PIXE is of the order of tens of micrometers and provides no information in relation to elemental concentration as a function of depth. Therefore, compared with SIMS, XPS and RBS, PIXE is considered to be mainly sensitive to the composition of the bulk phase.

Since these techniques have varying sensitivities to the surface composition, the combination of data may be used for deriving a reliable model of the effect of segregation on surface vs. bulk composition. The experimental part of this work is preceded by a brief analysis of literature reports and definition of basic terms.

9.2.1. Literature Reports

There have been several attempts to understand the effect of indium on a wide range of TiO_2 properties.

Nakamura et al. [15] reported the effect of indium introduced into the TiO_2 lattice by implantation. They observed that implantation and subsequent annealing results in the formation of titanium interstitials. This effect suggests that indium is incorporated predominantly into titanium sites forming acceptors, which in turn are compensated by titanium interstitials and oxygen vacancies. They claim that when the concentration of indium in titanium sites surpasses a certain critical limit (72%-88%), the remaining fraction of indium ions are incorporated into interstitial sites.

Chandra Babu et al. [16] reported that the formation of a TiO_2 solid solution with In_2O_3 (by powder sintering during 24 h at 1273 K) results in a change of a wide range of properties, including (i) reduction of the band gap, (ii) shift in the flat band potential, (iii) increase in surface area, and (iv) enhanced photo-assisted hydrogen evolution.

Sasikala et al. [17] observed that co-doping of TiO_2 with indium and nitrogen results in band gap narrowing due to mixing of energy levels and leading, in consequence, to enhanced photocatalytic activity. On the other hand, Wang et al. [18] reported that indium doping does not result in a change of the band gap of TiO_2. Instead, they observed the formation of a surface chemical structure O-In-Cl_x, with the energy level 0.3 eV below the conduction band. They claim that this structure allows more efficient utilisation of visible light and enhancement of charge separation.

Rodriguez-Gonzales et al. [19] studied two mixed oxide systems; (i) one formed by mixing TiO_2 and In_2O_3 by sol-gel (calcined at 773 K), and (ii) the other In_2O_3/TiO_2 system formed by impregnating TiO_2 gel (calcined at 773 K) with a solution of indium acetylacetonate-acetone. They observed that the mixed and the impregnated systems exhibit the band gaps of 3.5 eV and 3.1 eV, respectively. They also observed that the mixed system, involving highly dispersed In_2O_3, exhibited higher photocatalytic activity, which they attributed to better charge separation.

Similar effects were reported by Rangel-Porras et al. [20] who reported that indium incorporated during the formation of TiO_2 by sol-gel, resulted in a highly mesoporous microstructure.

Using the Periodic Plane Wave Density Functional Theory, Iwaszuk and Nolan [21] determined that the incorporation of indium into the lattice of TiO_2 results in the formation of acceptor centres that are compensated by oxygen vacancies. The substitutional mechanism of indium incorporation into the bulk phase has been confirmed by recent studies on the effect of indium on semiconducting properties in terms of both electrical conductivity and thermoelectric power data. [22]

In summary, the literature reports indicate that indium in the bulk phase of TiO_2 is incorporated predominantly into titanium sites, leading to the formation of acceptors. However, the experiment of Nakamura et al. [15] suggests that a small fraction of indium is incorporated into interstitial sites.

9.2.2. Definition of Terms

9.2.2.1. Defect Disorder

This section considers TiO_2 defect disorder using Kröger-Vink [23] notation, which is defined in **Table 1**. The related defect equilibria are defined in **Table 2** [1].

It is known that the photoreactivity of oxide semiconductors, such as TiO_2, are closely related to defect disorder. Therefore, their photoreactivity and the related performance can be modified by shifting the defect equilibria.

Table 9-1. The Kröger-Vink [23] and traditional notation of defects for TiO_2

Traditional Notation	**Description**	**Kröger-Vink notation**
$\mathbf{Ti_{Ti}^{4+}}$	Ti_{Ti}^{4+} ion in the titanium lattice site	Ti_{Ti}^{x}
$\mathbf{Ti_{Ti}^{3+}}$	Ti_{Ti}^{3+} ion in the titanium lattice site (quasi-free electron)	e'
$\mathbf{V_{Ti}}$	Titanium vacancy	V_{Ti}''''
$\mathbf{Ti_{i}^{3+}}$	Ti_{i}^{3+} in the interstitial site	$Ti_{i}^{\bullet\bullet\bullet}$
$\mathbf{Ti_{i}^{4+}}$	Ti_{i}^{4+} in the interstitial site	$Ti_{i}^{\bullet\bullet\bullet\bullet}$
$\mathbf{O_{O}^{2-}}$	O_{O}^{2-} ion in the oxygen lattice site	O_{O}^{x}
$\mathbf{V_{O}}$	Oxygen vacancy	$V_{O}^{\bullet\bullet}$
$\mathbf{O_{O}^{-}}$	O_{O}^{-} ion in oxygen lattice site (quasi-free electron hole)	$h^{\bullet}$

Table 9-2. Basic defect equilibria in TiO_2 [1] described using the Kröger-Vink [23] notation.

	Defect reaction	Equilibrium constant	ΔH^O [kJ/mol]	ΔS^O [J/(mol.K)]
1	$O_O^x \Leftrightarrow V_O^{\bullet\bullet} + 2e' + {}^1/_2\, O_2$	$K_1 = [V_O^{\bullet\bullet}]n^2 p(O_2)^{1/2}$	493.1	106.5
2	$Ti_{Ti}^x + 2O_O^x \Leftrightarrow Ti_i^{\bullet\bullet\bullet} + 3e' + O_2$	$K_2 = [Ti_i^{\bullet\bullet\bullet}]n^3 p(O_2)$	879.2	190.8
3	$Ti_{Ti}^x + 2O_O^x \Leftrightarrow Ti_i^{\bullet\bullet\bullet\bullet} + 4e' + O_2$	$K_3 = [Ti_i^{\bullet\bullet\bullet\bullet}]n^4 p(O_2)$	1025.8	238.3
4	$O_2 \Leftrightarrow V_{Ti}'''' + 4h^{\bullet} + 2O_O^x$	$K_4 = [V_{Ti}'''']p^4 p(O_2)^{-1}$	354.5	-202.1
5	$nil \Leftrightarrow e' + h^{\bullet}$	$K_i = np$	222.1	44.6
	$\mathbf{lnK = [(\Delta S^o)/R] - [(\Delta H^o)/RT]}$			

The effect of indium on the semiconducting properties of TiO_2 depends on the mechanism of its incorporation. The incorporation of indium into TiO_2 may be represented by the reaction:

$$In_2O_3 \rightarrow 2In_{Ti}^{'} + 3O_O^X + V_O^{\bullet\bullet} \qquad \textbf{(9-1)}$$

This defect disorder is governed by the following ionic charge compensation of In:

$$[In_{Ti}^{'}] = 2[V_O^{\bullet\bullet}] \qquad \textbf{(9-2)}$$

Combination of the equilibrium constants K_1 and K_i, and the relation described by Equation (9-2**)** results in the following relationship between the concentration of electronic charge carriers and oxygen activity:

$$p = K_i\left(\frac{[In_{Ti}^{'}]}{2K_1}\right)^{1/2} p(O_2)^{1/4} \qquad \textbf{(9-3)}$$

The incorporation of indium into the TiO_2 lattice in high oxygen activities leads to the formation of electron holes:

$$In_2O_3 + \frac{1}{2}O_2 \rightarrow 2In_{Ti}^{'} + 2h^{\bullet} + 4O_O^X \qquad \textbf{(9-4)}$$

Consequently, this regime is governed by the following charge compensation:

$$[In_{Ti}^{'}] = p \qquad \textbf{(9-5)}$$

The effect of acceptor-type ions, such as In^{3+}, on the bulk defect disorder of TiO_2 can be considered in terms of a Brouwer-type defect diagram [24].

The relationships expressed in **Equations (9-1) – (9-5)** represent the theoretical background for the effect of indium doping on bulk properties of TiO_2 in terms of defect chemistry.

However, the effect of indium doping on surface properties of TiO_2 may be entirely different than that of the bulk due to the effect of segregation. The aim of the present work is to determine the effect of indium segregation on the bulk vs. surface composition of TiO_2. This will be achieved by the determination of indium concentration in the bulk phase and at the surface using a range of complimentary analytical techniques: SIMS, XPS, RBS and PIXE. The related data will be considered in terms of defect chemistry independently for the bulk phase and the surface layer.

9.2.2.2. Diffusion of Indium in TiO_2 (Rutile)

The effect of doping with a foreign ion is well-defined only when the transport kinetics of this ion, resulting in its lattice incorporation, is well-defined. Therefore, this work was preceded by the determination of the diffusion kinetics of indium in the TiO_2 lattice [25]. The obtained diffusion data can be used in assessing appropriate annealing conditions that allows homogeneous distribution of indium in the specimen.

9.2.2.3. Segregation

Surface segregation is the diffusion of certain lattice elements from the bulk phase to the surface leading to surface enrichment in these elements. The driving force of segregation is an excess of surface energy.

The studies of segregation in oxides, such as NiO and CoO, indicate that both intrinsic defects such as oxygen and cation vacancies, and extrinsic defects such as dopants, segregate to the surface [11]. Therefore, interaction between both types of defects should be taken into account when considering the kinetics of segregation and its effect on surface properties. It has been documented that segregation-induced enrichment of the surface layer of oxide solid solutions, such as Cr-doped CoO, may substantially surpass the bulk solubility limit [26]. In certain cases, the segregation-induced enrichment of the surface layer results in the formation of low-dimensional surface structures [10,27]. This is the case when the local concentrations surpass certain critical limits. The critical concentrations depend not only on the surface structure, which is different than that of the bulk phase as a result of the broken crystalline periodicity, but also depends on the intrinsic defect disorder. The latter, in the case of metal-oxides, is also profoundly influenced by oxygen activity.

The purpose of the present work is to assess the segregation-induced surface concentration of indium in In-doped TiO_2, understand the predominant driving force of segregation, and determine the effect of oxygen activity on segregation.

9.3 Experimental

9.3.1. Specimens

In-doped TiO_2 was prepared by the sol gel technique using titanium isopropoxide, indium chloride, acetic acid, ethanol and water. The amount of acetic acid, water and titanium isopropoxyde were calculated to achieve the final molar ratio of acetic acid to titanium 1.5:1 and water to titanium 4:1 [28]. The total amount of ethanol was calculated to achieve 0.8 mol/L in the final solution [28]. The total amount of $InCl_3$ powder was calculated to achieve several concentrations of indium in the range 0.02 at% - 2.5 at%.

The $InCl_3$ powder was mixed with a small amount of the total calculated ethanol volume in beaker (B1) and stirred until fully dissolved. The titanium isopropoxide was combined under stirring with acetic acid (used as a chelating agent) in separate beaker (B2). In a third separate beaker (B3), the remaining amount of ethanol was mixed with the deionised water. The (B1) solution was slowly added to the (B2) solution under stirring and after 1 hour the (B3) solution was added (drop-wise) to solution (B2). The resulting liquid formed a viscous gel after approximately 30 minutes after which it was placed on a hot plate (80^{o}C) and left to dry for 2-3 days. The crystal-like solid product (solid solution) was then ground into a fine powder using an agate mortar and pestle, placed in a Pt lined alumina boat and calcined in air at 1173 K using a tube furnace. The calcined powder was subsequently pressed into cylindrical pellets, initially using a uniaxial press (~40 MPa) followed by a cold isostatic pressing (CIP) to a pressure of 400 MPa. The pressed pellets were then sintered in air at 1773 K for 5 hours. As a final step, a surface layer (~50 µm) was removed by grinding and polishing to a ~1µm finish. The resulting as-polished specimen was considered to be the reference specimen.

The as–polished specimens were then annealed at 1273 K for 24 hours in a gas phase of well-defined oxygen activity to induce segregation:

- Pure oxygen, $p(O_2)$ = 75 kPa
- Pure argon, $p(O_2)$ = 10 Pa

The required oxygen activity was imposed by flowing appropriate gases through the tube furnace with a continuous flow rate of 100 ml/min. The oxygen activity of the gas leaving the tube furnace was monitored electrochemically during the entire experiment using the yttria-stabilised zirconia oxygen probe.

9.3.2. Bulk Analysis

X-Ray Diffraction, XRD. The XRD analysis (Siemens D500) was performed using a Co $K\alpha_{1,2}$ radiation source and graphite monochromator. Data was collected over an angular range of 5^o to 80^o with a 2θ step size of 0.05 and a five second dwell time. The PANalytical software package (High Score Pro) was used for identification of the crystalline phases. The obtained X-ray diffraction patterns are shown in **Figure 9-1.** As seen, the peaks in the spectra are reflective of the rutile structure for In-doped TiO_2 up to 0.4 at% of indium. As also seen, traces of the In_2O_3 phase are detected at both 1 at% and 2.5 at%. This data suggest that the solubility of indium in rutile is between 0.4 at% and 1 at% of indium. It is important to note that this solubility limit is related to the bulk phase.

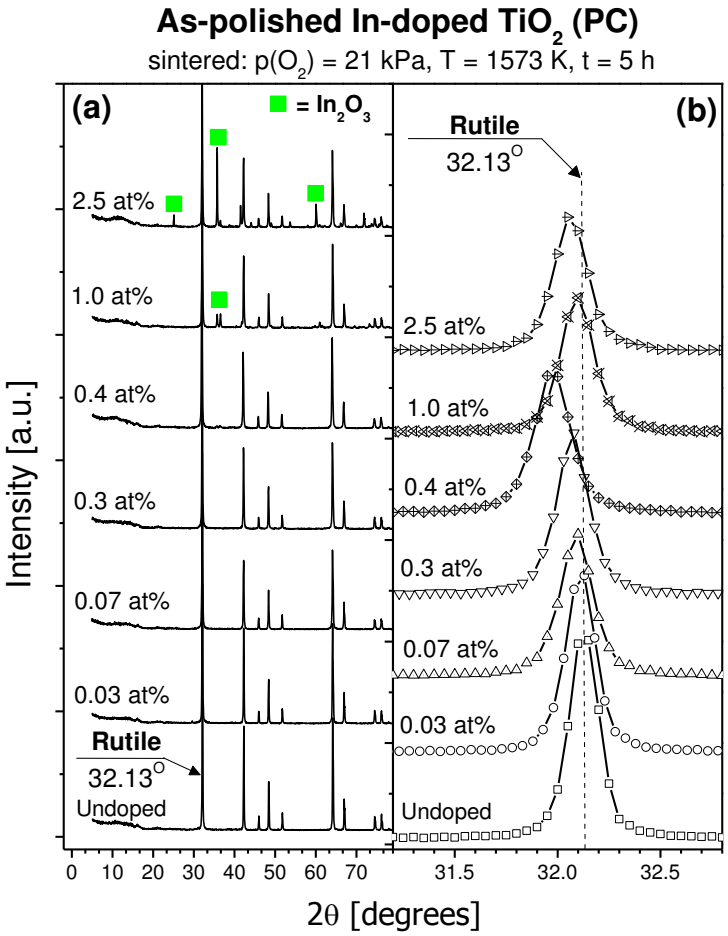

Figure 9-1. X-ray diffraction patterns for In-doped TiO_2. This pattern, showing the peaks related to an alternative phase than rutile, indicates that the solubility range of indium in rutile is approximately 1 at%.

Proton-Induced X-Ray Emission, PIXE. PIXE analysis was performed at the Australian Nuclear Science & Technology Organisation using the 2MV STAR tandem accelerator. The technical specifications for the PIXE analysis were as follows:

- **Sample Charge.** The charge collected for each sample was 30 µC.
- **Detector.** The X-rays were recorded at 45° angle using a Si(Li) detector fitted with a 25 µm Be window and multichannel energy analyser.
- **Filter.** An additional pin-hole acrylic filter, 1700 µm thick, with a 2% hole area and 4 µm thick mylar film, was used to decrease the intensity of low energy X-rays excited with high cross sections in order to minimise pile-up and dead time during analysis.

- **Data Processing.** The PIXE spectra were processed using the GUPIXWIN (Version 2.1.4, University of Guelph, Canada) software package for the determination of elemental concentrations. The quantitative analysis of the indium peaks is related to a depth of 42 µm (based on the proton penetration range in TiO_2 determined using the SRIM software program [29]).

9.3.3. Surface Analysis

9.3.3.1. Secondary Ion Mass Spectrometry (SIMS)

Depth profiles were determined using secondary ion mass spectrometry (Cameca - IMS 5f). A Cs^+ primary ion beam of 5nA current and 5 keV net impact energy was used to raster an area of 250 x 250 µm from which secondary ions were sputtered. Sample charging during analysis was controlled by the deposition of a thin layer of gold (~5 nm) on the sample surface. The depth of the crater after analysis (measured using a stylus profilometer) was used for to determine the average sputter rate. The sputter rate was 0.012 nm/s. SIMS electronic gating settings were used to restrict secondary ion analysis to a 55µm circular area within the rastered region to avoid any influence of crater edge effects on the results.

The SIMS technique provides depth profiles in terms of ion intensity (counts). The absolute concentration values can be determined from the intensity of the species of interest divided by those for species whose intensity remains relatively constant throughout the specimen such as the host (matrix) species (TiO). The atom proportion of indium-to-titanium can be determined from the peak height proportion of $^{115}In/(^{48}Ti+^{16}O)$ in the mass spectrum, according to the following formula:

$$\frac{C_{In}}{C_{TiO}} = \frac{I_{In} K^+_{TiO} h_{TiO}}{I_{TiO} K^+_{In} h_{In}} \qquad \textbf{(9-6)}$$

where I is the ion intensity, K^+ is the secondary ion yield (defined as the number of secondary ions produced per incident primary ion of mass m and charge $z\pm$) and h is the isotopic abundance.[30] Equation ((9-6) may be reduced to the following form:

$$[C_{In}] = \frac{I_{In}}{I_{TiO}} F_{In} \qquad \textbf{(9-7)}$$

where F_{In} is a calibration factor (also known as a relative sensitivity factor). The calibration factor is not solely related to the species of interest, but is also influenced by a complex

contribution of the host matrix composition and structure (including density, crystal orientation or grain boundaries) as well as SIMS sputtering conditions used (including primary ion, beam current and impact energy). Consequently, determination of the calibration factor typically requires generation of a calibration curve using reference samples containing known concentrations of the species of interest in the same matrix as the unknown samples and analysed under the same SIMS conditions. However, without the calibration factor, the SIMS depth profiles can still be used for semi-quantitative analysis.

9.3.3.2. X-Ray Photoelectron Spectroscopy (XPS)

XPS analysis was performed using a Thermo Scientific ESCALAB 250 xi instrument. A monochromatic Al Kα source of 1486.6 eV X-ray energy, operating at 15 kV and 160 W, was applied for collecting the XPS spectra. The X-ray spot was approximately 0.5 mm in diameter. A take-off angle of 90^{o} relative to the sample surface was used for the analysis, resulting in an analysis depth approximately 6 nm. The spectrometer pass energy filter was set at 100 eV for survey scans and 20 eV for elemental regional scans. A 20 second argon sputtering etch was required prior to analysis of as-polished samples to remove surface carbon. The energy of the Ar^{+} ion beam was 3 keV and the etching rate was approximately 0.4 nm/s calibrated using a Ta_2O_5/Ta reference sample. The relative surface concentrations of different species were determined by integrating their related peak areas above the linear background.

For SIMS analysis, the intensity data corresponds to the local concentration at a specific depth, while in the case of XPS analysis the data is reflective of the average concentration within the analysed depth of 6 nm.

9.3.3.3. Rutherford Backscattering (RBS)

The STAR 2MV tandem accelerator (Australian Nuclear Science and Technology Organisation) was used for RBS analysis. 2MeV He^{+} ions were applied at a normal angle of incidence to the sample surface in the form of a 3 mm diameter collimated beam. The backscattered ions were detected at an angle of 162^{o} using a silicon surface-barrier detector (4mm diameter active area) and multi-channel energy analyser. A charge of 40 μC was acquired for each sample. The RBS data corresponding to a region of interest (ROI) depth of approximately 84 nm (from the surface) was fit using multilayer models generated by SIMNRA software (Version 6.05, Max-Planck Institut Fur Plasmaphysik, Germany). Consequently, the RBS results relate to an average indium concentration over this 84 nm depth.

9.4 Results and Discussion

9.4.1. Proton induced X-ray Emission (PIXE)

The results of PIXE analysis are shown in **Figure 9-2**, for the as-polished specimen containing 0.3 at% In in the bulk. The insert on this drawing is an enlargement of the indium-related peak. It is important to note that the analysis depth of PIXE is on the order of micrometers and the resultant peaks reflect the average concentration within that analysis depth. Consequently, the method is predominantly sensitive to the bulk phase and the related concentration data are considered as bulk related.

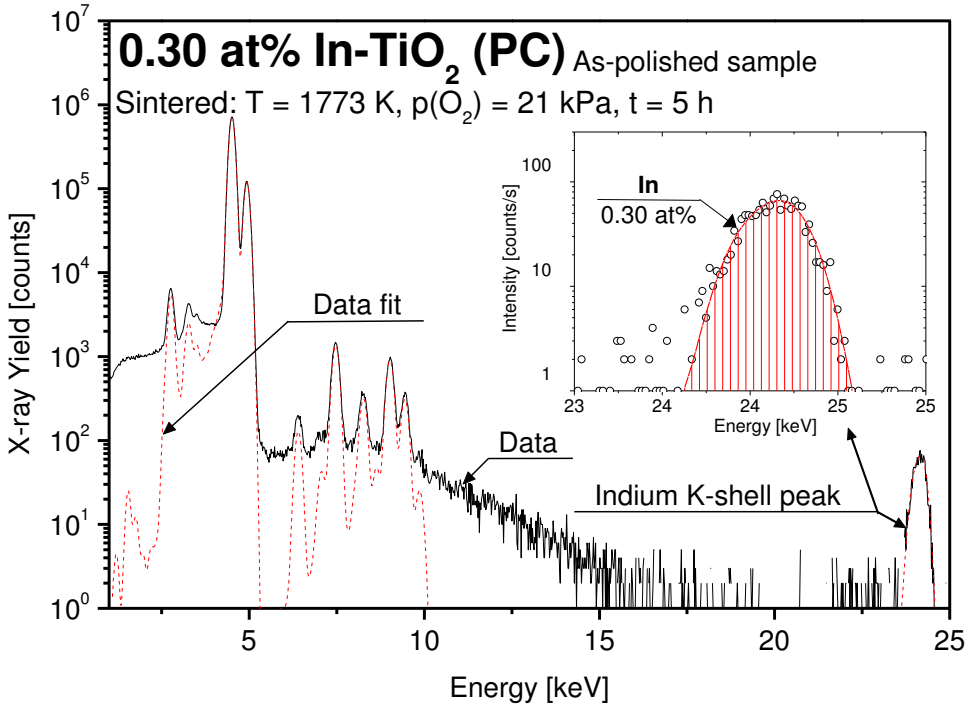

Figure 9-2. X-ray yield vs. energy for the In-doped TiO_2 (0.3 at%) specimen annealed in the gas phase of $p(O_2)$ = 75 kPa (the insert shown the indium-related peak).

9.4.2. Secondary Ion Mass Spectrometry (SIMS)

The SIMS spectra, represented in the form of intensity ratio of indium to TiO, are shown in **Figure 9-3.** The data can be considered in the following terms:

- Equilibrium vs. non-equilibrium depth profile
- Bulk composition
- Surface composition

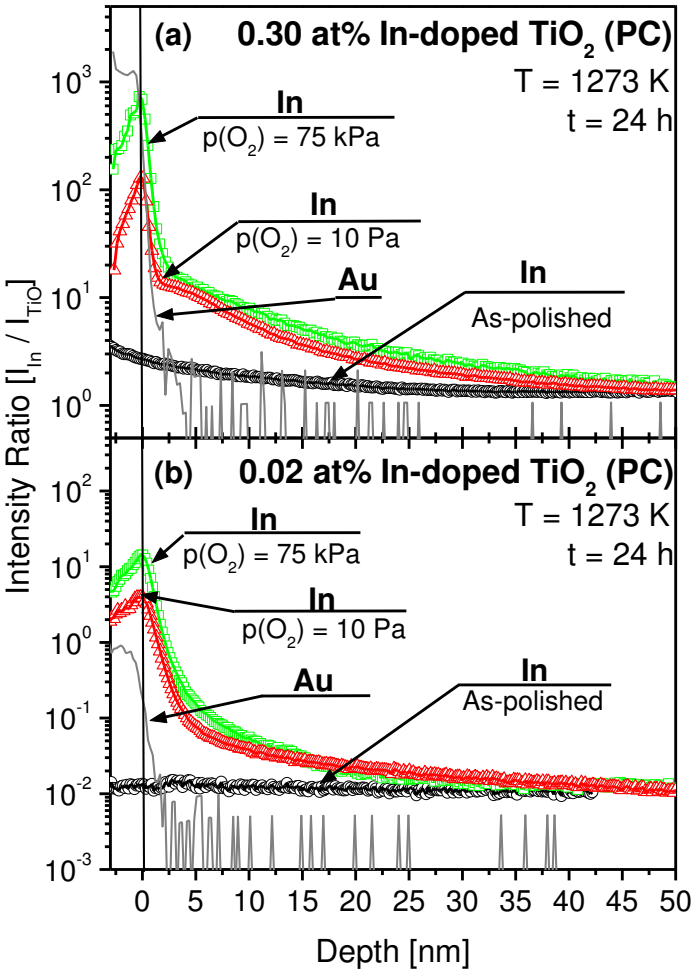

Figure 9-3. SIMS depth profile for In-doped TiO_2, including the specimen containing 0.3 at% In (a) and 0.02 at% In (b), in terms of the intensity ratio of In/TiO secondary ions the for as-polished (the reference specimen), and specimens annealed in the gas phase of $p(O_2)$ = 75 kPa, and $p(O_2)$ = 10 Pa.

Equilibrium vs. non-equilibrium depth profile. The data on the left side of the vertical line at depth = 0 nm (**Figure 9-3)** can be considered as non-equilibrium data, which are mainly reflective of the gold layer deposited for the purpose of suppressing surface charge that is formed during sputtering. The intensity profiles to the right of this line are reflective of the segregation-induced enrichment of indium (gold profiles are shown as well).

Bulk composition. The spectrum in **Figure 9-3** relating to the as-polished specimen is relatively flat, and essentially corresponds to the bulk phase composition annealed in air during sintering. Therefore, the intensity data for these samples are considered in the present work as reference data which reflect the bulk phase. The observed insignificant increase of the intensity

near the surface suggests some minor indium segregation induced by the applied surface polishing procedure and is considered to be non-equilibrium segregation.

Surface composition. As seen in **Figure 9-3**, the segregation-induced intensity of indium depends on oxygen activity. The 0.3 at% specimen annealed for 24 h at $p(O_2)$=75 kPa and 1273 K, exhibits the strongest surface enrichment (I_{Ti}/I_{TiO}=~10^3). The specimen annealed at lower oxygen activity (10 Pa) exhibits lower surface enrichment (I_{in}/I_{TiO}=~$1.2x10^2$). As seen, in both cases a steep initial decrease of the intensity is followed by a change of the slope I_{In}/I_{Ti} vs. depth at 2 nm. The initial part of the intensity vs. depth slope, within 1-2 nm, can been considered in terms of a local surface structure, which is different from the rutile structure beneath. For the latter case the slope is less steep. The two differing intensity vs. depth slopes observed in the SIMS profiles may also be related to the different matrix structures.

As seen, the enrichment-related profiles converge with the bulk-related profile at 40-50 nm. This value is reflective of the thickness of the surface layer enriched by segregation.

The effect of oxygen activity on indium segregation observed for the 0.3 at% In specimen is confirmed for the specimen of 0.02 at%, although the related maxima of the intensity ratios are lower.

The indium enrichment factor in the outermost surface layer may be determined from the intensity ratios between the levels related to the maxima and the level related to the bulk phase (reference specimens). As seen in **Table 9-3**, the enrichment factors for the 0.3 at% specimen assume 486 and 85.3 at higher and lower oxygen activity, respectively. The related enrichment factors for the 0.02 at% specimen are even larger. These factors are consistent with the tendency of the surface layer to assume specific composition, independent of the bulk content.[10] However, the enrichment values obtained for the outermost surface layer with SIMS are markedly larger than those related to XPS. The difference between the two sets of data may be explained in terms matrix effects between the low-dimensional surface structure, forming one matrix in the outermost surface layer, and the rutile matrix beneath. In this case, the matrix effect difference which influences the SIMS analysis does not affect the XPS analysis.

Taking into account the results of the previous work [14], the low-dimensional surface structure is stable in oxidizing conditions. However, imposition of strongly reducing gas phase environment results in its evaporation.

9.4.3. Photoelectron Spectroscopy (XPS)

The XPS spectra for the In-doped TiO_2 specimens, including the as-polished specimen, and the specimens annealed in oxygen and argon, are shown in **Figure 9-4.** The related concentration data are shown in **Table 9-3**. These data indicate that the surface of the as-polished specimen is slightly enriched in indium to the level of 0.4 at%. This effect, which is known as non-equilibrium segregation, is related to the applied polishing procedure.

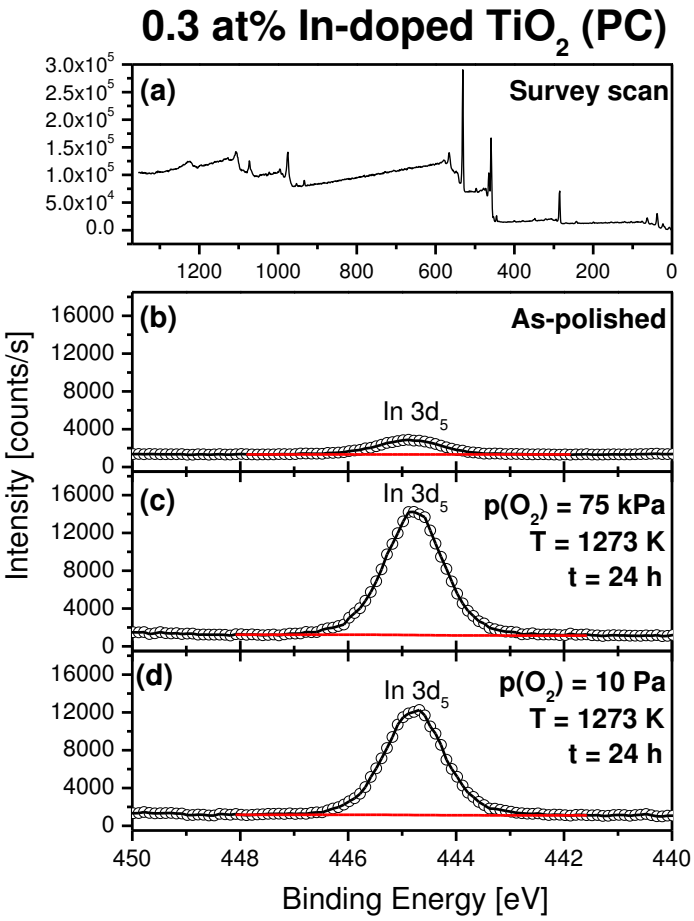

Figure 9-4. XPS intensity vs. binding energy spectra for In-doped TiO_2 (0.3 at% In), including the survey scan for (a) as-polished (reference specimen), and elemental region scans for (b) as-polished (reference specimen), (c) annealed in the gas phase of $p(O_2)$ = 75 kPa, and (d) annealed at $p(O_2)$ = 10 Pa.

Annealing of the 0.3 at% specimens at $p(O_2)$ = 75 Pa and $p(O_2)$ = 10 Pa (T=1273 K) results in surface enrichment to the level of 2.95 at% In and 2.61 at% In, respectively. The respective enrichment factors (10.2 and 9.0) are substantially smaller than those resulting from SIMS (484 and 128, respectively). The difference between these two sets of data reflect a very substantial concentration gradient within the surface layer, which is consistent with the postulated structure consisting of a low-dimensional surface structure within the outermost surface layer and the rutile structure beneath.

9.4.4. Rutherford Backscattering (RBS)

The RBS spectra are shown in **Figure 9-5** for the as polished reference specimen as well as the specimens annealed in the oxidising gas phase of controlled oxygen activity. The backscattered energy regions of the spectra, which are related to indium, have been enlarged for better clarity.

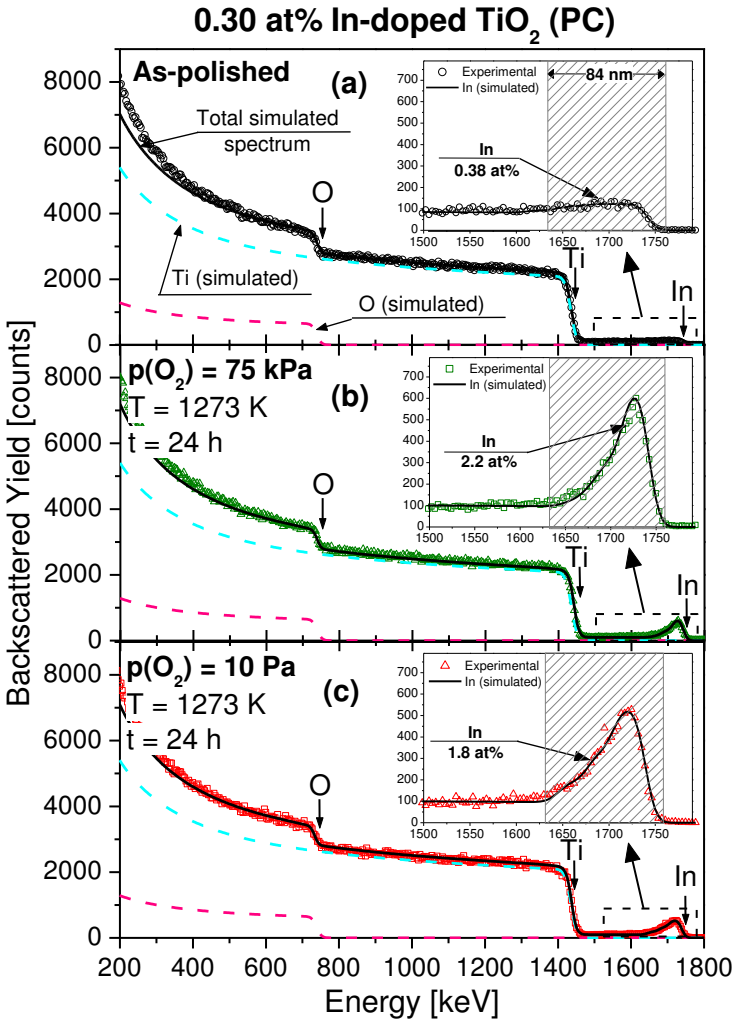

Figure 9-5. RBS yield vs. energy spectra for the following In-doped TiO_2 (0.3 at%) specimens: (a) as-polished (the reference specimen), (b) annealed in the gas phase of $p(O_2)$ = 75 kPa, and (c) annealed in the gas phase of $p(O_2)$ = 10 Pa.

The as-polished specimen exhibits 0.38 at% of indium. This value, which is slightly lower that that related to the XPS analysis (0.4 at% In), is consistent with the larger RBS analysis depth of 84 nm.

Annealing the specimen at $p(O_2)$ = 75 Pa and $p(O_2)$ = 10 Pa (T = 1273 K) results in surface concentration 2.2 at% and 1.8 at%, respectively. These factors are substantially smaller than

those related to XPS. Again, the difference is consistent with the depth resolution of XPS (6 nm) and RBS (84 nm).

In summary, the determined enrichment factors are influenced by the surface sensitivity of the applied analytical techniques and the related depth resolution.

Table 9-3. Collection of PIXE, SIMS, XPS and RBS data on indium concentration in TiO_2 (rutile) and the related enrichment factors.

Bulk content	**p(O_2) [Pa]**	**Concentration of indium [at%] Enrichment factor $f = [In]_{surface}/[In]_{PIXE}$**			**SIMS $[I_{In} / I_{TiO}]$**
		PIXE	**XPS**	**RBS**	
0.30 at%	As polished	0.30 ± 0.02	0.40 ± 0.08 f_{XPS} = 1.3	0.38 ± 0.08 f_{RBS} = 1.3	1.5
	75 x 10^{3}	0.29 ± 0.02	2.95 ± 0.6 f_{XPS} = 10.2	2.2 ± 0.4 f_{RBS} = 7.6	729.1 f_{SIMS} = 486
	10	0.29 ± 0.02	2.61 ± 0.5 f_{XPS} = 9.0	1.8 ± 0.4 f_{RBS} = 6.2	128.0 f_{SIMS} = 85.3
0.02 at%	As polished	0.02 ± 0.004			0.01
	75 x10^{3}				14.2 f_{SIMS} = 1420
	10				3.9 f_{SIMS} = 390

9.4.5. Theoretical Model

It has been documented in the present work that annealing In-doped TiO_2 in an oxidising environment results in indium segregation to the surface. All applied surface sensitive tools clearly show that segregation-induced In enrichment is enhanced by increased oxygen activity. The most obvious questions that should be addressed at this point are:

- Why does indium segregate to the surface of TiO_2?
- Why indium segregation is favoured by an increase in oxygen activity?

9.4.5.1. Segregation Driving Force

In the first approximation, segregation in oxide solid solutions may be described by the following commonly assumed model, based on a regular solution model [12]:

$$\frac{X_2^s}{X_1^s} = \frac{X_2^b}{X_1^b} \exp \frac{-\Delta H_{seg}}{kT} \quad \textbf{(9-8)}$$

where X is the equilibrium concentration (in mole fraction) of the i-th component at the surface (s) and in the bulk phase (b), ΔH_{seg} denotes the heat of solute segregation and (1) and (2) corresponds to solvent and solute, respectively. The principal contributions to the heat of segregation involve the surface energy contribution and the elastic strain energy contribution. This approach seems plausible since there is a substantial mismatch between ionic radii of In^{3+} and Ti^{4+} ions (0.081 nm and 0.068 nm, respectively). While the mismatch explains the tendency for the removal of indium from the bulk due to strain energy, it does not explain why indium segregation is enhanced by an increase of oxygen activity.

9.4.5.2. Effects of Oxygen Activity on Indium Segregation

If indium is incorporated into the cation sublattice of TiO_2, the indium ions are charge negatively as expected by **Equation (9-4)**. The segregation of negatively charged indium may be enhanced by increased oxygen activity, if associated with an increase of a positive charge. This is not the case, since an increase of oxygen activity results in an increase of a negative charge associated with the following two effects:

1. The formation of negatively charge titanium vacancies, which are located in the outermost surface layer [1], and
2. Negatively charged chemisorbed oxygen species, which are located in the adsorbed layer.

The effect of oxygen chemisorption on segregation at elevated temperature may be ignored because the reactivity between oxygen and the TiO_2 lattice in these conditions results in the formation of titanium vacancies. Therefore, only effect (1) can be taken into consideration. This effect is represented schematically by the surface model in **Figure 9-6** showing the concentration of indium vs. distance from the surface. This model involves (i) a negatively charged low-dimensional surface structure, which consists of predominantly of indium and oxygen, (ii) a negatively charge sub-surface layer of TiO_2 enriched in indium, and (iii) a bulk phase of In-doped TiO_2.

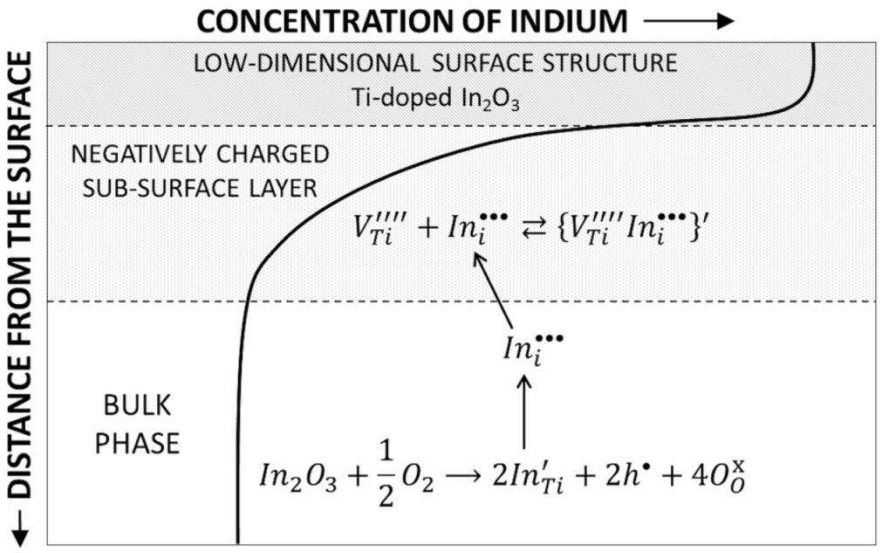

Figure 9-6. The model representing the surface vs. bulk concentration of In-doped TiO_2, in terms of the low-dimensional surface structure, the sub-surface layer enriched in indium, and the bulk phase.

9.4.5.3. Formation of Titanium Vacancies

It has been documented that titanium vacancies are formed at the TiO_2/O_2 interface following the reaction described by equation ((9-4) in **Table 9-2.** However, these vacancies are quenched within the outermost surface layer due to the kinetics reason. Taking into account the related diffusion data, the diffusion distance of titanium vacancies during the annealing time used in the present work (24 h at 1273 K) is limited to a thin surface layer, while their concentration in the bulk is substantially lower. However, the presence of titanium vacancies at the surface may result in indium segregation only when the effective charge of indium ions is positive. The effect of oxidation on surface vs. bulk equilibration of the TiO_2 lattice with respect to titanium vacancies is represented in **Figure 9-7** [31].

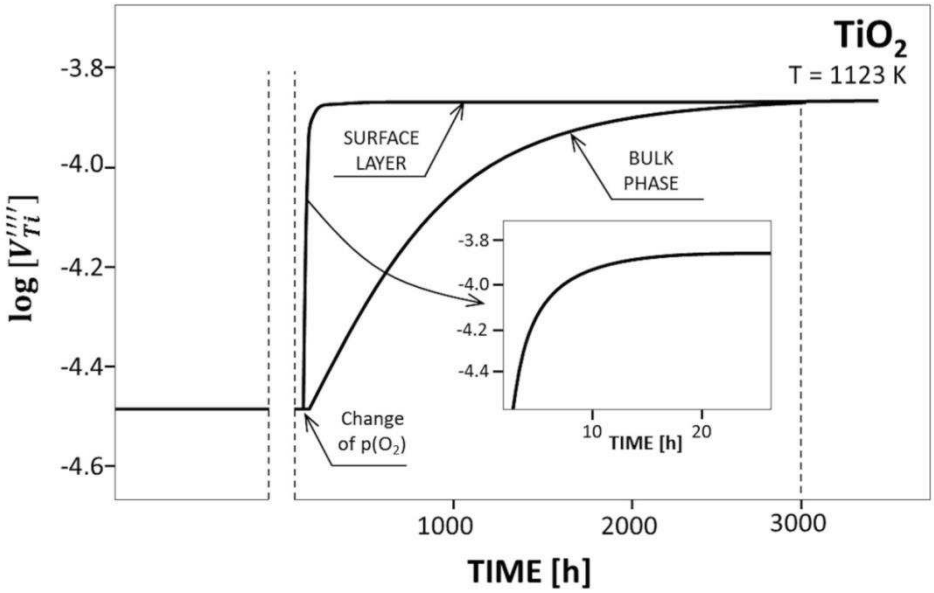

Figure 9-7. The effect of TiO_2 oxidation on the concentration of titanium vacancies at the surface and in the bulk phase as a function of time at 1123 K [31].

9.4.5.4. Surface Mechanism of Indium Incorporation

The reported experimental data indicate that indium is incorporated substitutionally into the bulk phase of the TiO_2 lattice resulting in the formation of negative species. However, the work of Nakamura et al. [15] has shown that a small portion of indium is incorporated into interstitial sites. In the latter case, the incorporation mechanisms may be represented by the following equilibria:

$$2In_2O_3 \rightarrow 4In_i^{\bullet\bullet\bullet} + 3V_{Ti}^{''''} + 6O_O \qquad \textbf{(9-9)}$$

$$In_2O_3 \rightarrow 2In_i^{\bullet\bullet\bullet} + 6e' + \frac{3}{2}O_2 \qquad \textbf{(9-10)}$$

The respective charge neutrality conditions require that:

$$4[In_i^{\bullet\bullet\bullet}] = 3[V_{Ti}^{''''}] \qquad \textbf{(9-11)}$$

$$4[In_i^{\bullet\bullet\bullet}] = 12n \qquad \textbf{(9-12)}$$

As seen, the mechanism represented by expression **(8-9)**, which is plausible in the experimental conditions applied in the present work and the associated ionic charge compensation, does not lead to a change in the concentration of electronic charge carriers. On

the other hand, indium incorporation according to the mechanism represented by equilibrium **(9-11)**, which is plausible in reducing conditions, results in the formation of electrons.

According to Nakamura et al. [15] only a small fraction of indium (11% - 24%) incorporates into the bulk phase according to the mechanism **(8-9)**. We postulate in the present work that this mechanism is the predominant within the surface layer due to the excess of surface energy and the related deformations of the surface layer [10,11]. We believe that this is plausible taking into account the effect of excess of surface free energy on the crystal field and related structural deformations.

It has been reported that defect disorder of the surface layer of metal oxides may be entirely different than that in the bulk phase [10,11]. For example, it has been documented that lithium ions are incorporated into cation sites in the bulk phase of NiO, forming acceptors. On the other hand, lithium is incorporated into interstitial sites forming donors within the surface layer of NiO [11]. Similarly, it has been shown that cobalt ions may be present in interstitial sites within the surface layer of CoO, forming donors, while in the bulk such defects are not stable at all [11].

The solubility limit has been commonly considered as a material-related property. This is the case as far as the bulk phase is concerned. The analysis of the effect of segregation on diffusion indicates that the term solubility limit for foreign ions in metal oxides must be considered as the property that is the function of the distance from the surface [11]. The studies of surface vs. bulk properties for Cr-doped CoO have shown that the solubility limit of Cr in the bulk phase at 1000 K is 1 at% while its solubility within the surface layer is 14 at% Cr [27].

In summary, due to the excess of surface energy and the related structural deformations, the surface layer may accommodate extraordinary defect disorder and related properties. The experimental data obtained in the present work indicate that the interstitial mechanism **(8-9)** should be considered to explain the effect of indium on the properties of the surface layer of TiO_2. At the same time, the substitutional mechanisms, described by the relations **(9-1)** and (9-4**)**, is valid for the bulk phase, the process of segregation can be considered as a transition of indium from the titanium sites in the bulk to interstitial sites at the surface. This can be described by the following reaction:

$$(In_{Ti}^{'})_B \rightarrow (In_i^{\bullet\bullet\bullet})_S + (V_{Ti}^{''''})_S \qquad \textbf{(9-13)}$$

The incorporation mechanisms represented by reactions **(9-9) - (9-13)** assume that that the defects in the TiO_2 lattice are isolated and form an ideal solid solution. However, according to

Stoneham [32], increasing the defect concentration above the level of 0.1 at% results in substantial defect interactions leading to the formation of larger defect aggregates. In the case of the present work, the predominant defects at the surface are negatively charged titanium vacancies, which are formed in oxidising conditions, and positively charged indium ions. These defects are expected to react and lead to the formation of defect complexes:

$$In_i^{\bullet\bullet\bullet} + V_{Ti}^{''''} \rightarrow \{In_i^{\bullet\bullet\bullet} V_{Ti}^{''''}\}' \qquad \textbf{(9-14)}$$

These complexes have a tendency to form a negatively charged low-dimensional surface structure. The surface composition data according to SIMS analysis, as well as other techniques, indicate that the low-dimensional surface structure, which is formed at the outermost surface layer, is an oxide structure that in the first approximation may be considered as Ti-doped In_2O_3.

9.4.5.5. Surface vs. Bulk Properties

The present work indicates that the mechanism of indium incorporation in the bulk is different than that at the surface. The predominant bulk mechanism results in the formation of acceptor-type centres, which lead to a decrease of Fermi level in the bulk phase. On the other hand, indium segregation to the surface layer leads to the formation of donor-type ions.

The bulk solubility limit of indium in TiO_2 is in the range 0.4 at% - 1 at% at 1273 K. The determined enrichment data indicates, however, that indium solubility within the surface layer is markedly larger than that in the bulk phase. The substantially enlarged enrichment factor obtained with SIMS and attributed to matrix effects suggests the presence of a Ti-doped In_2O_3-type low-dimensional surface structure (1-2 nm thick). This layer is negatively charged.

The near-to-surface layer, just beneath the low-dimensional surface structure, is a solid solution of indium in the rutile structure. Its solubility limit seems to be enhanced at the surface above the level of approximately 1 at% In. The predominant intrinsic defects in this layer are titanium vacancies and indium incorporated into interstitial sites. The resulting interactions between titanium vacancies and indium ions results in the formation of defect complexes, which have a net negative charge. The thickness of the surface layer enriched with indium is approximately 40 nm.

9.5 Conclusions

It has been shown that the surface composition of In-doped TiO_2 is entirely different from that of the bulk phase as a result of segregation. The phenomenon of segregation leads to the

formation of a strong concentration gradient of indium, which is profoundly influenced by oxygen activity – the larger the oxygen activity the larger the segregation-induced enrichment of indium.

Indium incorporates into titanium sites of the TiO_2 lattice leading to the formation of acceptors in the bulk phase. The related solubility limit of indium in the bulk is in the range 0.4 at% - 1 at%. Indium has a strong tendency to segregate to the surface when annealed in an oxidising gas phase environment. The process of segregation involves the removal of indium ions from their titanium lattice sites where they are transported by the interstitialcy mechanism towards the surface and incorporated into interstitial sites.

The solubility of indium in the surface layer is enhanced to the level of approximately 3 at%. The segregation-induced enrichment of the outermost surface layer results in the formation of a low-dimensional surface structure, which is approximately 2 nm thick, and a sublayer involving defect complexes and larger defect aggregates. Both the low-dimensional surface structure and the sublayer are charged negatively compared to the bulk phase. This negative surface charge is the predominant driving force of indium segregation.

The data reported in the present work show that doping of the TiO_2 lattice by indium results in different effects for the bulk phase and the surface layer. While the photoreactivity of TiO_2-based semiconductors and the related charge transfer is determined by the surface properties, knowledge of the difference between the bulk and the surface is essential in engineering of appropriate electric field that is need for charge separation.

9.6 References

(1) Bak, T.; Nowotny, J.; Sucher, N. J.; Wachsman, E. "Effect of Crystal Imperfections on Reactivity and Photoreactivity of TiO_2 (Rutile) with Oxygen, Water, and Bacteria". The Journal of Physical Chemistry C (2011), 115 [32], 15711-15738.

(2) Fujishima, A.; Hashimoto, K.; Watanabe, T. TiO_2-Photocatalysis, Fundamentals and Applications; BKC Inc.: Tokyo, 1999.

(3) Fujishima, A.; Honda, K. "Electrochemical Photolysis of Water at a Semiconductor Electrode". Nature (1972), 238, 37-38.

(4) Carp, O.; Huisman, C. L.; Reller, A. "Photoinduced reactivity of titanium dioxide". Progress in Solid State Chemistry (2004), 32, 33-177.

(5) Carpentier, J. L.; Lebrun, A.; Perdu, F. "Point-Defects and Charge Transport in Pure and Chromium-Doped Rutile at 1273-K". J. Phys. Chem. Solids (1989), 50 [2], 145-151.

(6) Karakitsou, K. E.; Verykios, X. E. "Effects of altervalent cation doping of titania on its performance as a photocatalyst for water cleavage". The Journal of Physical Chemistry (1993), 97 [6], 1184-1189.

(7) Linsebigler, A. L.; Lu, G.; Yates, J. T. J. "Photocatalysis of TiO_2 Surfaces: Principles, Mechanisms, and Selected Results". Chem. Rev. (1995), 95, 735-758.

(8) Wilke, K.; Breuer, H. D. "The influence of transition metal doping on the physical and photocatalytic properties of titania". J. Photochem. Photobiol. A-Chem. (1999), 121 [1], 49-53.

(9) Burggraaf, A. J.; Winnubst, A. J. A. Segregation in Oxide Surfaces, Solid Electrolytes and mixed Conductors. In Surface and Near-Surface Chemistry of Oxide Materials; Elsevier: Amsterdam, (1988); pp 448-477.

(10) Cabane, J.; Cabane, F. Equilibrium segregation in interfaces. In Interface segregation and related processes in materials; Nowotny, J., Ed.; Trans Tech Publications Ltd.: Zurich, (1991); pp 1-150.

(11) Nowotny, J. Inteface defect chemistry and its impact on properties of oxide ceramic materials. In Science of Ceramic Interfaces; Nowotny, J., Ed.; Elsevier Science Publishers B.V., (1991); pp 79-204.

(12) Wynblatt, P.; McCune, R. C. Surface Segregation in Metal Oxides. In Surface and Near-Surface Chemistry of Oxide Materials; Elsevier Science Publishers, (1988); pp 247-279.

(13) Nakajima, T.; Sheppard, L. R.; Prince, K. E.; Nowotny, J.; Ogawa, T. Adv. Appl. Ceram. (2007), 106, 82-88.

(14) Atanacio, A. J.; Nowotny, J.; Prince, K. E. "Effect of Oxygen Activity on Surface Composition of In-Doped TiO_2 at Elevated Temperatures". Journal of Physical Chemistry C (2012), 116 [36], 19246-19251.

(15) Nakamura, S.; Yagi, E.; Osaka, T.; Iwaki, M. "Lattice disorder and behavior of implanted atoms in In-implanted TiO_2 (rutile)". Nuclear Instruments and Methods in Physics Research Section B: Beam Interactions with Materials and Atoms (1988), 33 [1-4], 729-733.

(16) Babu, K. S. C.; Singh, D.; Srivastava, O. N. "Investigations on the mixed oxide material TiO_2-In_2O_3 in regard to photoelectrolytic hydrogen production". Semicond. Sci. Technol. (1990), 5 [4], 364-368.

(17) Sasikala, R.; Shirole, A. R.; Sudarsan, V.; Jagannath; Sudakar, C.; Naik, R.; Rao, R.; Bharadwaj, S. R. "Enhanced photocatalytic activity of indium and nitrogen co-doped TiO_2 Pd nanocomposites for hydrogen generation". Applied Catalysis A: General (2010), 377 [1-2], 47-54.

(18) Wang, E. J.; Yang, W. S.; Cao, Y. A. "Unique Surface Chemical Species on Indium Doped TiO_2 and Their Effect on the Visible Light Photocatalytic Activity". Journal of Physical Chemistry C (2009), 113 [49], 20912-20917.
(19) Rodriguez-Gonzalez, V.; Moreno-Rodriguez, A.; May, M.; Tzompantzi, F.; Gomez, R. "Slurry photodegradation of 2,4-dichlorophenoxyacetic acid: A comparative study of impregnated and sol-gel In_2O_3-TiO_2 mixed oxide catalysts". Journal of Photochemistry and Photobiology A: Chemistry (2008), 193 [2-3], 266-270.
(20) Rangel-Porras, G.; Ramos-Ramirez, E.; Torres-Guerra, L. M. "Mesoporous characteristics of crystalline indium-titania synthesized by the sol-gel route". J. Porous Mat. (2010), 17 [1], 69-78.
(21) Iwaszuk, A.; Nolan, M. Journal of Physical Condensed Matter (2011), 23, 1-11.
(22) Bak, T.; Nowotny, J.; Atanacio, A. J. (In progress).
(23) Solid State Physics; Kröger, F. A.; Vink, H. J., Eds.; Academic Press: New York, (1956); Vol. 3, pp 307.
(24) Brouwer, G. "A general asymptotic solution of reaction equations common in solid-state chemistry". Phyllips Res Reps (1954), 9, 366-376.
(25) Atanacio, A. J. PhD Thesis (in progress), University of Western Sydney, 2012.
(26) Nowotny, J.; Sikora, I.; Wagner, J. B. "Segregation and near-surface diffusion for undoped and cr-doped CoO". Journal of the American Ceramic Society (1982), 65 [4], 192-196.
(27) Haber, J.; Nowotny, J.; Sikora, I.; Stoch, J. "Electron-Spectroscopy in Studies of Surface Segregation of Cr in Cr-Doped CoO". Applied Surface Science (1984), 17 [3], 324-330.
(28) Doeuff, S.; Henry, M.; Sanchez, C.; Livage, J. "Hydrolysis of titanium alkoxides - modification of the molecular precursor by acetic-acid ". J. Non-Cryst. Solids (1987), 89 [1-2], 206-216.
(29) Ziegler, J. SRIM - The Stopping Range of Ions in Matter (www.srim.org), 2013.
(30) Hirschwald, W.; Loechel, B.; Nowotny, J.; Oblakowski, J.; Sikora, I.; Stolze, F. "SIMS studies of segregation for NiO-Cr_2O_3 solid-solution". Bulletin De L Academie Polonaise Des Sciences-Serie Des Sciences Chimiques (1981), 29 [7-8], 369-375.
(31) Nowotny, M. K.; Bak, T.; Nowotny, J. "Electrical properties and defect chemistry of TiO_2 single crystal. IV. Prolonged oxidation kinetics and chemical diffusion". Journal of Physical Chemistry B (2006), 110 [33], 16302-16308.
(32) Stoneham, M. "Theory of Defect Processes". Physics Today (1980), 33, 34-37.

CHAPTER 10

Effect of Niobium Segregation on Surface Chemistry and the Related Electric Field Light-Induced Charge Carrier Separation in Nb-Doped TiO_2

10.1 Abstract

This work studied the effect of niobium segregation on the surface and near-surface composition of Nb-doped TiO_2 (0.18 at% Nb and 0.018 at% Nb). The studies were performed using a range of analytical techniques of different depth resolution, including secondary ion mass spectrometry (SIMS), X-ray photoelectron spectroscopy (XPS), Rutherford backscattering (RBS), and Proton-Induced X-Ray Emission (PIXE). According to the XPS analysis, annealing the 0.18 at% Nb specimens at 1273 K in oxidising conditions results in segregation-induced niobium surface enrichment of 2.83 at% and 2.35 at% in $p(O_2)$=75 kPa and $p(O_2)$= 10 Pa, respectively. However, annealing in strongly reducing conditions of $p(O_2)=10^{-10}$ Pa leads to impoverishment of niobium at the surface down to 0.05 at% (desegregation). The derived theoretical model considers that (i) the predominant driving force of niobium segregation in oxidising conditions is a negative surface charge associated with the formation of titanium vacancies in the surface layer, and (ii) the effect of desegregation is induced by a positive surface charge related to a Magneli-type surface structure formed in strongly reducing conditions. The derived theoretical model shows the effect of surface vs. bulk composition on the formation of chemically-induced electric field for separation of light-induced charge carriers. The established influence of oxygen activity on niobium segregation/desegregation may be used as a technology for the imposition of (i) chemically-induced electric field required for charge separation and (ii)

controlled surface composition required to achieve the desired performance of TiO_2 as photocatalytic electrode for solar energy conversion.

10.2 Introduction

Titanium dioxide (TiO_2) is a candidate material for the conversion of solar energy into the chemical energy via water oxidation [1-3]. Its performance, which is determined by photoreactivity of TiO_2 with water, is closely related to surface properties. Therefore, the performance of TiO_2 in solar energy conversion may be modified by changing its surface properties. Consequently, intensive research efforts have been aimed at identifying the specific surface properties responsible for the reactivity and photoreactivity of TiO_2 with water.

The surface properties of solids are substantially different from those of the bulk phase as a result of segregation. The difference concerns chemical composition, structure and the related semiconducting properties [4-6]. To date, the theory of segregation has been derived for metals and alloys [7-9]. However, the picture of segregation for metal oxides is more complex. First, segregation-induced enrichment in oxides depends on oxygen activity in the gas phase environment [10]. Moreover, unlike metallic solids, the surface charge compensation in oxides can occur over a long distance from the surface, approximately 50 nm – 100 nm, compared to 1 nm in metals. As a consequence, the thickness of the surface layer enriched by segregation in oxides is substantially larger than that in metallic solids [10].

Knowledge of the effect of segregation on surface properties is essential for correctly understanding the functional properties of oxides. The present work shows that the effect of segregation may be used for tailoring the surface composition in order to impose the specific properties that are needed to achieve the desired performance, including reactivity and photoreactivity.

So far, little is known about the effect of segregation on the surface vs. bulk chemistry of metal oxides and the reported segregation data in oxides are scarce and often conflicting. The main reason for the reported discrepancies is that quantitative analysis of segregation-induced enrichment in oxides is complex. Furthermore, segregation-induced concentration gradients in metal oxides are only well-defined when the studied specimen is equilibrated with the gas phase of controlled oxygen activity, and subsequently cooled down from the equilibrium temperature to analysis temperature in a controlled manner. Such experimental details are usually not provided in reports on segregation in oxides.

The present work is a part of a larger research program studying the effect of segregation of both acceptor- and donor-type ions on surface composition of TiO_2 and its solid solutions. The overall aim of the research is to use the phenomenon of segregation as a surface engineering technology in the formation of electrodes, photoelectrodes and photocatalysts with enhanced performance. In other words, the phenomenon of segregation may be used for imposing a controlled chemical composition within the surface and near-surface layer. Segregation may also be used for the imposition of a chemically-induced electric field at the surface for increased charge separation in solar energy conversion. In the latter case, the recombination related energy losses may be reduced substantially.

The reported studies on the effect of niobium on the properties of TiO_2 have been limited to the determination of bulk properties [11-13] and so far, little is known on surface properties of Nb_2O_5-TiO_2 solid solutions. The aim of the present work is to address this matter and examine the effect of niobium segregation on the surface and near-surface composition of Nb-doped TiO_2 annealed in the gas phase of controlled oxygen activity. The main effort of this work is the imposition of segregation-induced concentration gradients in well-defined conditions of temperature and oxygen activity. The outcomes are expected to have implications on several applied aspects in processing TiO_2-based systems for the conversion of solar energy into chemical energy related to both the partial and total oxidation of water.

The difference between partial and total water oxidation is associated with the number of electrons removed from water molecule. Partial water oxidation results in the formation of hydroxyl radicals, HO*, according to the following reaction:

$$H_2O - e' \leftrightarrow HO^* + H^+ \qquad \textbf{(10-1)}$$

where e' denotes an electron. These radicals have the capacity to oxidise contaminants present in water. Total water oxidation results in the formation of protons, H^+, according to the following anodic reaction:

$$2H_2O - 4e' \leftrightarrow O_2 + 4H^+ \qquad \textbf{(10-2)}$$

Segregation-induced effects have a substantial impact on the photoreactivity of TiO_2 and the recombination-related energy losses in the relation to both processes.

In a former work, the authors studied the effect of indium segregation on surface properties of In-doped TiO_2 [14]. Typically, indium ionization results in the formation of tri-valent ions. It has been shown that the mechanisms of indium incorporation into the bulk and the surface

layer of TiO_2 are different. In the bulk phase, indium incorporates into titanium sites leading to the formation of acceptors. On the other hand, indium at the surface is incorporated predominantly into interstitial sites leading to the formation of donors. It was shown that indium exhibits a very strong segregation driving force in the rutile structure. The substantial segregation-induced enrichment of the surface layer results in substantial interactions between point defects leading to the formation of a new low-dimensional surface structure, which exhibits outstanding properties [14].

The aim of the present work is to assess the effect of niobium segregation on surface vs. bulk chemistry of Nb-doped TiO_2.

10.2.1. Brief Literature Overview

Niobium is a strong donor in the TiO_2 lattice when incorporated into titanium sites as well as interstitial sites [11-13]. Therefore, as pure TiO_2 is a good insulator, niobium doping has been widely used to enhance the charge transport of TiO_2.

Several attempts have been made to determine niobium segregation in Nb-doped TiO_2 [15-20]. However, the reported data are conflicting in terms of the niobium surface enrichment factor and its temperature dependence. Analysis of these reports indicates that the studied specimens are not well-defined in terms of the processing conditions and subsequent cooling process. The observed discrepancies are commonly related to:

- Lack of equilibrium. In other words, the reported data correspond to the kinetic regime rather than thermodynamic equilibrium.
- Annealing in the gas phase that is not well-defined in terms of oxygen activity.
- A cooling process that is not well-defined in terms of the cooling rate and the gas phase composition.

Awareness is growing that the key factor in the formation of segregation-induced concentration gradients of solutes in metal oxides is oxygen activity [21-24]. The effect of oxygen activity on segregation-induced enrichment in oxides has been reported by Black and Kingery [21] for Cr-doped MgO and Fe-doped MgO as well as Sikora et al. [22] for Cr-doped CoO. Bernasik et al. [23] reported that TiO_2 exhibits iron segregation mainly in reducing conditions of $p(O_2) = 2$ Pa. The studies of Sheppard et al. [24], using the SIMS analysis, indicate that increased oxygen activity results in decreased segregation of niobium in Nb-doped TiO_2.

An extensive overview on surface properties of TiO_2, including both rutile and anatase, has been reported by Diebold [25]. This report mainly considers the surface properties determined

in vacuo for specific crystal orientations. It is shown that titanium interstitials play an important role in reactivity with gaseous oxygen.

Recently Sheppard et al. [26] reported a study on niobium segregation in Nb-doped TiO_2 using secondary ion mass spectrometry (SIMS). These authors observed that the surface is depleted in niobium in reducing environment. However, no explanation for the reported effect of oxygen activity on segregation was offered. The reducing environment was imposed using the gas mixture involving 99% of argon and 1% of hydrogen. The authors claim that the resulting oxygen activity, $p(O_2)= 10^{-15}$ Pa, is independent of the applied temperature in the range 1173 K - 1673 K. The latter effect is in conflict with the mass action law.

The bulk solubility range of Nb_2O_5 in TiO_2 at 1000 K is approximately 19 at% [14].

10.2.2. Postulation of the Problem

The present study aims to determine well-defined data on Nb segregation in Nb-doped TiO_2. The critical issues in addressing this aim include (i) the formation of solid solutions, which are well-defined, and (ii) imposition of segregation-induced concentration gradients by annealing in the gas phase that is well-defined. In order to achieve this, the following points must be addressed:

1. Processing
2. Equilibrium
3. Oxygen activity
4. Cooling
5. Chemical analysis

10.2.2.1. Processing

The aim of processing is to form well-defined Nb_2O_5-TiO_2 solid solutions, which are free of concentration gradients within the bulk phase. Selection of appropriate processing conditions requires knowledge of the Nb diffusion rate in TiO_2. Additionally, the temperature of the process must be high enough to allow homogeneous distribution of the solute (niobium) within the entire lattice of solvent (TiO_2).

10.2.2.2. Surface vs. Bulk Equilibrium

The surface layer is not autonomous. It remains in continuous interactions with the bulk phase on one side and the gas phase on the other side. Therefore, the chemical composition of the surface layer is well-defined only when the entire gas/solid system is in thermodynamic equilibrium. Consequently, segregation-induced concentration gradients are well-defined only

when in equilibrium and the electrochemical potential of the lattice species, X, within the specimen remains constant:

$$\eta_X(d) = \text{const} \quad \textbf{(10-3)}$$

where η denotes the electrochemical potential and d denotes a distance from the surface. The electrochemical potential for the species X can be expressed as:

$$\eta_X = \mu_X + ez\Psi_X \quad \textbf{(10-4)}$$

where μ_x and ψ_x denote the chemical potential and the electrical potential, respectively; e is the elementary charge and z is the valence. Therefore, the excess of surface energy results in a change of both $\mu_X(d)$ and $\psi_X(d)$, leading to the formation of a chemical potential gradient and related electrical potential gradient at the surface as represented schematically in **Figure 10-1**.

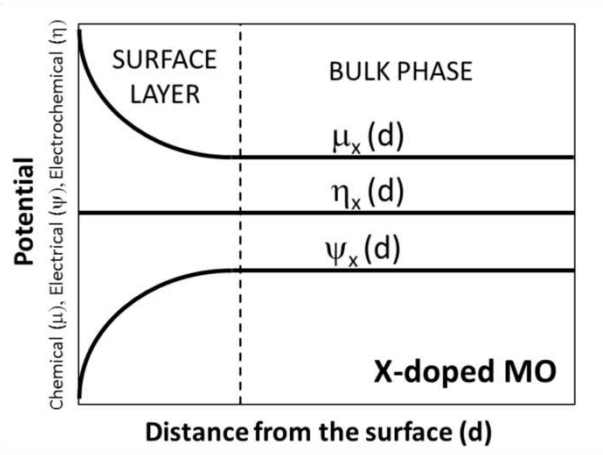

Figure 10-1. Schematic representation of the chemical potential, electrochemical potential and electrochemical potential as a function of the distance from the surface enriched in X species.

The segregation-induced concentration gradient, which can be assessed using surface sensitive techniques, may be used in the determination of the related chemical potential:

$$\mu_X = \mu_X^o + kT\ln c_X \quad \textbf{(10-5)}$$

where c denotes concentration, k is Boltzman constant and T is the absolute temperature. The resulting electrical potential barrier is:

$$\Psi_X(d) = \frac{\eta_X - \mu_X(d)}{ez} \quad \textbf{(10-6)}$$

The quantities η_X, $\mu_X(d)$ and $\psi_X(d)$ are well-defined only when in equilibrium. The time and the temperature required for equilibration should be determined using the diffusion data, including self-diffusion data related to the incorporation of niobium and the chemical diffusion data associated with oxygen penetration in the lattice.

The surface analytical tools applied in this work operate at room temperature. Therefore, there is a need to cool down the system from the temperature of equilibrium to room temperature in reproducible manner, including the cooling rate and the associated gas phase composition.

10.2.2.3. Oxygen Activity

The defect disorder of metal oxides and the associated properties are closely related to oxygen activity. The latter may be imposed when the oxide specimen is equilibrated with the gas phase of well-defined oxygen activity, which must be monitored during the entire experiment, including annealing and cooling. The equilibration process results in imposition of the required oxygen activity at the surface followed by its propagation into the oxide lattice until a new equilibrium is established.

10.2.2.4. Cooling

The specimen equilibrated with the gas phase at elevated temperature must then be cooled down from the equilibrium conditions to the temperature of the chemical analysis. The cooling must be performed in a controlled manner in terms of the cooling rate and the associated gas phase composition. Again, oxygen activity should be monitored during the entire cooling process.

10.2.2.5. Chemical Analysis

The reported segregation profiles are complex as the shape of the concentration gradients exhibit a change with the distance from the surface. The largest changes occur in the outermost surface layer and enrichment/depletion drops with the distance from the surface. The shape of the concentration gradient depends on equilibrium conditions. The determination of this concentration gradient is not a simple matter and cannot be properly assessed using a single surface sensitive technique. Therefore, the present work applies a range of analytical tools of different depth resolution and sensitivity.

The commonly used surface sensitive tool, X-ray photoelectron spectroscopy (XPS), usually informs only of an average chemical composition within a certain thickness, which, depending on the applied angle of incidence is 4 – 6 nm. Therefore, while XPS is surface sensitive, this technique does not allow the determination of depth profiles.

The surface sensitive technique that allows the determination of concentration-related intensity profiles vs. time of sputtering is secondary ion mass spectrometry (SIMS). However, the determination of quantitative depth profiles, in terms of the chemical composition, requires complex calibrations of the SIMS intensity data against concentrations using precise reference standards. If quantitative calibrations are not performed, SIMS can still be utilised for qualitative analysis. Both SIMS and XPS applied independently provide complementary information.

An alternative technique of larger depth resolution is Rutherford backscattering (RBS). This technique, which provides information on elemental composition, is less surface sensitive than XPS and SIMS.

The analytical technique which is predominantly bulk-sensitive in elemental analysis is proton-induced X-ray emission (PIXE). The analysis depth of this technique is approximately 50 μm.

Consequently, the most reliable approach for determination of surface vs. bulk chemical composition is through application of all of the above analytical techniques.

10.2.2.6. Recommended Research Strategy

The determination of well-defined data on segregation in metal oxides requires the criteria (1) – (5) (in section **10.2.2**) to be addressed. Only then can the segregation-induced data be considered as material-related data.

The aim of the present work is to determine well-defined data on Nb segregation in Nb-doped TiO_2 using a range of complimentary analytical techniques, which exhibit different depth resolution and sensitivity; SIMS, XPS, RBS and PIXE. The related analysis penetration depths are represented schematically in **Figure 10-2**.

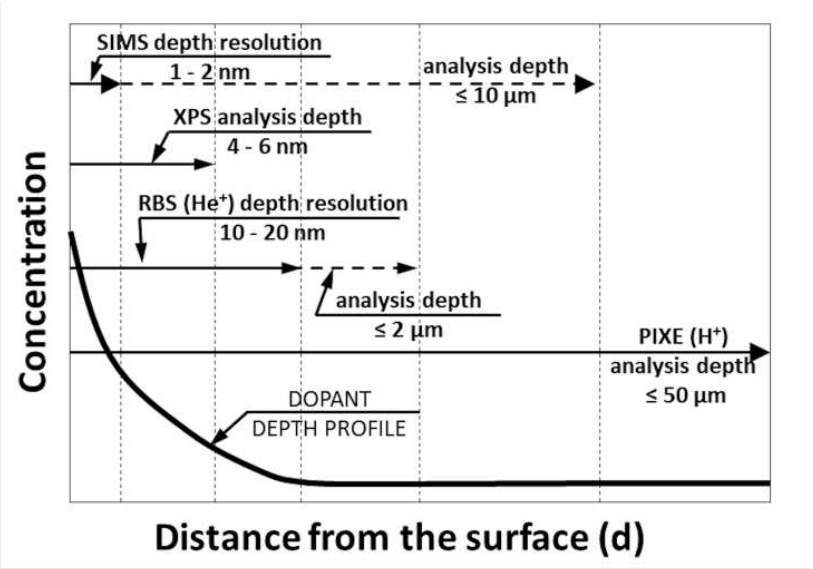

Figure 10-2. Schematic representation of approximate penetration of depth of SIMS, XPS, RBS and PIXE.

10.2 3. Definition of Terms

10.2.3.1. Defect Disorder

It has been documented that the semiconducting properties of TiO_2 are closely related to defect disorder [10,27]. The defect disorder for pure TiO_2 is represented by the defect equilibria in **Table 10-1**.

Table 10-1. Basic defect equilibria in TiO_2 (n and p denote the concentration of electronic and electron holes, respectively) [3].

	Defect reaction	Equilibrium constant	ΔH^O [kJ/mol]	ΔS^O [J/(mol.K)]
1	$O_O^x \Leftrightarrow V_O^{\bullet\bullet} + 2e' + {}^1/_2\, O_2$	$K_1 = [V_O^{\bullet\bullet}]n^2p(O_2)^{1/2}$	493.1	106.5
2	$Ti_{Ti}^x + 2O_O^x \Leftrightarrow Ti_i^{\bullet\bullet\bullet} + 3e' + O_2$	$K_2 = [Ti_i^{\bullet\bullet\bullet}]n^3p(O_2)$	879.2	190.8
3	$Ti_{Ti}^x + 2O_O^x \Leftrightarrow Ti_i^{\bullet\bullet\bullet\bullet} + 4e' + O_2$	$K_3 = [Ti_i^{\bullet\bullet\bullet\bullet}]n^4p(O_2)$	1025.8	238.3
4	$O_2 \Leftrightarrow V_{Ti}^{''''} + 4h^{\bullet} + 2O_O^x$	$K_4 = [V_{Ti}^{''''}]p^4p(O_2)^{-1}$	354.5	-202.1
5	$nil \Leftrightarrow e' + h^{\bullet}$	$K_i = np$	222.1	44.6

$$\mathbf{lnK} = [(\Delta \mathbf{S^o})/\mathbf{R}] - [(\Delta \mathbf{H^o})/\mathbf{RT}]$$

The incorporation of niobium into the TiO_2 lattice in oxidising conditions may be represented, using the Kröger-Vink notation [28], by the following reaction leading to the formation of titanium vacancies:

$$2Nb_2O_5 \rightarrow 4Nb_{Ti}^{\bullet} + V_{Ti}^{''''} + 10O_O^X \quad \textbf{(10-7)}$$

Consequently, this regime is governed by the following charge compensation:

$$4[V_{Ti}^{''''}] = [Nb_{Ti}^{\bullet}] \quad \textbf{(10-8)}$$

The relationship between the concentration of electronic charge carriers and oxygen activity in this regime is:

$$n = K_i \left(\frac{[\,Nb^{\bullet}{}_{Ti}\,]}{4K_4} \right)^{1/4} p(O_2)^{-1/4} \quad \textbf{(10-9)}$$

where n is the concentration of electrons, K_i is the intrinsic equilibrium constant and K_4 is the equilibrium constant of the reaction between TiO_2 and oxygen resulting in the formation of titanium vacancies.

The incorporation of niobium in reducing conditions results in the following reaction leading to the formation of electronic defects (electrons) and the release of oxygen:

$$Nb_2O_5 \rightarrow 2Nb_{Ti}^{\bullet} + 2e' + 4O_O^X + \tfrac{1}{2}O_2 \quad \textbf{(10-10)}$$

The resulting defect disorder is governed by electronic charge compensation of niobium:

$$n = [\,Nb^{\bullet}{}_{Ti}\,] \quad \textbf{(10-11)}$$

The charge neutrality expressed by Equation **(10-11)** indicates that electrical conductivity in this regime is controlled by the concentration of niobium incorporated into the TiO_2 lattice and is essentially independent of the $p(O_2)$.

In the case of Nb-doped TiO_2 In strongly reduced conditions, the concentration of oxygen vacancies becomes significantly larger than the concentration of niobium ions. Consequently, the effective contribution of Nb ions can essentially be ignored and the defect disorder represented by the following defect reaction:

$$O_O \leftrightarrow V_O^{\bullet\bullet} + 2e' + \frac{1}{2}O_2 \quad \textbf{(10-12)}$$

The simplified charge neutrality condition therefore assumes the following form:

$$2[V_O^{\bullet\bullet}] = n \quad \textbf{(10-13)}$$

Equations **(10-7)** – **(10-13)** represent the bulk defect disorder of Nb-doped TiO_2 within a wide range of oxygen activities.

It is essential to note at this stage that the effect of oxygen activity on the concentration of defects should be considered independently for the bulk phase and the surface layer.

10.2.3.2. Segregation

The phenomenon of segregation can be described as a thermal diffusive transport of selected lattice species from the bulk phase to interfaces, such as the external surface and grain boundaries. The driving force for segregation is the difference in free energy between the bulk phase and the interface. Therefore, segregation results in a decrease of the free energy of the system. In some cases, annealing oxide specimens result in the transport of selected species from the surface into the bulk phase leading to a depletion of the surface layer in these species. This is termed desegregation.

Both adsorption and segregation can be described by the same concepts and laws. The main difference between the two processes is the kinetics related to mass and charge transport. The process of adsorption is fast and its equilibrium may therefore be reached at room temperature relatively fast. On the other hand, segregation equilibrium, involving the transport of ionic/atomic species in crystalline solids, can only be established at elevated temperatures at which the mobility of these lattice species is high enough.

10.3 Experimental

10.3.1. Specimens and Procedure

The Nb-doped TiO_2 polycrystalline specimens, of nominal concentrations of 0.2 at% Nb and 0.02 at % Nb, were prepared using the sol-gel method. The basic reactants included titanium Isopropoxide (97%-Aldrich) and $NbCl_5$ (99%-Aldrich) of appropriate proportions. The resulting solid solution was ground to a fine powder and calcined at 1173 K in air. The powder was then pressed into cylindrical pellets with a uniaxial press (50 MPa) followed by cold isostatic pressing (CIP) at much higher pressure (400 MPa). These pellets were then sintered at 1773 K for 5 h in air. The specimens was then ground and polished to remove at least ~50 µm from the surface. The resulting as-polished specimens were used as a reference. The as-polished specimens were subsequently annealed at 1273 K for 24 hours in order to induce segregation.

The specimens were annealed in the gas phase of controlled oxygen activity, which was monitored during the entire time of annealing using an electrochemical oxygen probe based on yttria-stabilised zirconia.

This probe is essentially composed of an alumina tube closed on one end with a zirconia disc as it is schematically represented in **Figure 10-3**. Platinum is attached to both sides of the zirconia disc. Artificial air (21% of oxygen and 79% of nitrogen) was used as a reference gas. Oxygen activity was determined from the Nernst equation:

$$E = \frac{kT}{4} \ln \frac{p(O_2)_x}{p(O_2)_{air}} \qquad \textbf{(10-14)}$$

Where k is Boltzman constant, T absolute temperature, and $p(O_2)_x$ and $p(O_2)_{air}$ denote the oxygen activity in the studied gas flowing through the reactor and the reference gas (air), respectively.

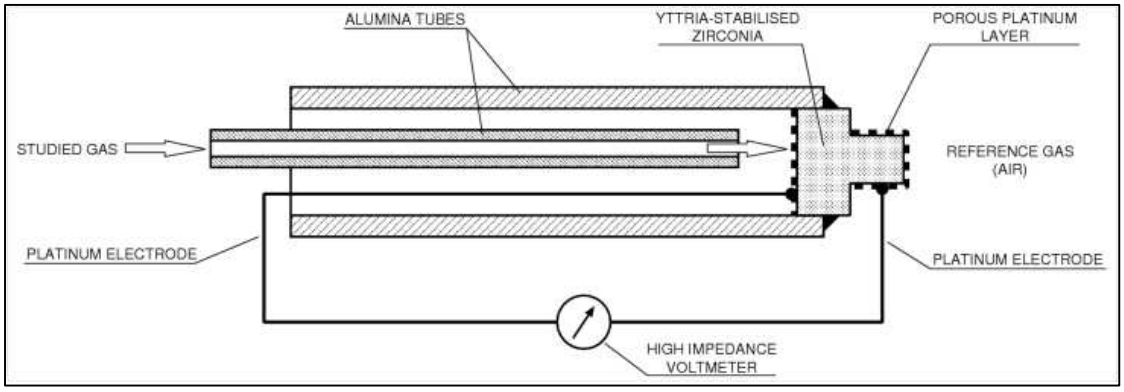

Figure 10-3. Schematic representation of the zirconia-based electrochemical oxygen sensor

Specimen annealing took place in the following gas phases of controlled oxygen activity:

- Pure oxygen. Its oxygen activity determined electrochemically is $p(O_2)$ = 75 kPa.
- Pure argon. Its related oxygen activity is $p(O_2)$ = 10 Pa.
- Argon-hydrogen mixture, involving 1% of hydrogen and 99% of argon. The oxygen activity of this mixture at 1273 K is approximately $p(O_2) = 10^{-10}$ Pa.

10.3.2. Bulk vs. Surface Chemical Analysis

10.3.2.1. Proton-Induced X-ray Emission (PIXE)

The PIXE technique was used to determine the elemental composition of the bulk phase. PIXE was performed using a 2 MV tandem accelerator. Analysis was performed with a 3mm collimated proton beam, with 2.6 MeV energy and 10 nA beam current, applied at normal angle

of incidence to the sample surface. The X-rays were detected at an angle of 45 degrees from normal with a Si (Li) detector fitted with at 25 µm thick Be window. A 10 µC charge was acquired for each sample. A pin-hole filter (1700 µm thick Acrylic with 2% hole area) fitted with an additional 4µm thick mylar film was utilised to further decrease the intensity of the low energy X-rays excited with high cross-sections in order to control dead-time and pile-up during analysis. The PIXE spectra were processed using GUPIXWIN software (Version 2.1.4, University of Guelph, Canada) to determine the concentration of elements in the sample.

10.3.2.2. Secondary Ion Mass Spectrometry (SIMS)

The surface vs. bulk depth profiles were determined by SIMS (Cameca IMS 5f). Sample charging was reduced by the deposition of gold coat (~5 nm). A Cs^+ primary ion beam of 5 keV net impact energy and 5 nA beam current rastered the area of approximately 250 µm x 250 µm. Insturment settings were applied to limit the analysis of secondary ions to a 55 µm circular area within the rastered region to avoid contributions from crater edge effects. The crater depth, measured by stylus profilometer (Alpha-Step IQ, KLA-Tencor), was used to determine the average sputter rate (0.012 nm/s).

10.3.2.3. X-ray Photoelectron Spectrometry (XPS)

XPS analysis was performed using a Thermo Scientific ESCALAB 250 xi instrument. The spectra were collected using a monochromatic Al Kα source of 1486.6 eV X-ray energy operated at 15 kV and 160 W. The X-ray spot was approximately 0.5 mm in diameter and the take-off angle of 90^o relative to the sample surface was used for all analyses which results in an analysis depth of approximately 6 nm. A pass energy filter of 100 eV was used for survey scans and 20 eV for elemental region scans. A 20 second argon sputtering etch was required prior to analysis of as-polished samples to remove surface carbon likely remaining from the polishing/lubrication medium used. The Ar^+ beam energy was 3 keV and the related etching rate (approximately 0.4 nm/s) was calibrated using a Ta_2O_5/Ta reference sample. The relative surface concentrations of the different species were determined by integrating their respective XPS peak areas.

10.3.2.4. Rutherford Backscattering (RBS)

RBS analysis was performed on a 2MV tandem accelerator (Australian Nuclear Science and Technology Organisation). 2 MeV He^+ ions were used at normal angle of incidence to the sample surface with backscattered ions being detected at an angle of 160^o. A collimated 3mm diameter beam of approximately 10nA beam current was used for analysis and a charge of 40 µC was acquired for each sample. The backscattered ions were detected using a silicon surface-

barrier charged particle detector (4 mm diameter active area) and energy analysed using a multi-channel analyser. The RBS spectra were processed using SIMNRA software (Version 6.05, Max-Planck Institut Fur Plasmaphysik, Germany).

10.4 Results and Discussion

10.4.1. Proton-Induced X-Ray Emission

The PIXE spectrum for the as-polished specimen, including the insert for the niobium-related peak, is shown in **Figure 10-4**. According to this analysis, the bulk concentration of niobium is 0.180 at%. The PIXE analysis shows that the concentration of niobium in the second specimen is 0.018 at%. The results are shown in **Table 10-2**. As seen, niobium concentration is practically the same for the specimens annealed in different oxygen activities. This data indicates that the effect of niobium evaporation can be ignored. The concentration of niobium resulting from the PIXE analysis has been assigned as the reference concentration related to the bulk phase.

Table 10-2. Collection of PIXE, SIMS, XPS and RBS data on niobium concentration and the related enrichment factors

Bulk Nb [at%]	**$p(O_2)$ [Pa]**	**Concentration of niobium [at%] Enrichment factor, $f = [Nb]_{surface}/[Nb]_{PIXE}$**			**SIMS $[I_{Nb} / I_{TiO}]$**
		PIXE	**XPS**	**RBS**	
0.18	As polished	0.180 ± 0.004	0.17 ± 0.03 $f_{XPS} = 0.9$	0.19 ± 0.04 $f_{RBS} = 1.1$	0.19
	75×10^{3}	0.179 ± 0.004	2.83 ± 0.6 $f_{XPS} = 15.7$	0.31 ± 0.06 $f_{RBS} = 1.7$	4.1 $f_{SIMS} = 21.6$
	10	0.177 ± 0.004	2.35 ± 0.5 $f_{XPS} = 13.1$	0.32 ± 0.06 $f_{RBS} = 1.8$	2.3 $f_{SIMS} = 12.1$
	1×10^{-10}	0.181 ± 0.004	0.05 ± 0.01 $f_{XPS} = 0.3$	0.16 ± 0.03 $f_{RBS} = 0.9$	0.16 $f_{SIMS} = 0.84$
0.018	As polished	0.018 ± 0.001			0.03
	75×10^{3}				0.07 $f_{SIMS} = 2.33$
	10				0.04 $f_{SIMS} = 1.33$

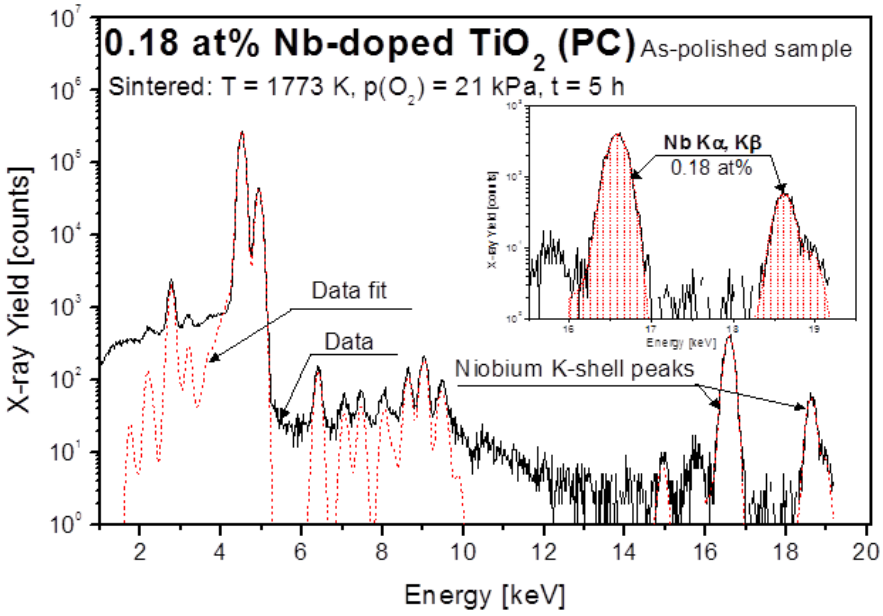

Figure 10-4. PIXE X-ray yield vs. energy spectra for Nb-doped TiO_2 (0.18 at%) as-polished specimen.

10.4.2. Secondary Ion Mass Spectrometry

The SIMS spectra are represented as the intensity ratio of niobium to TiO (matrix) species in **Figure 10-5**. These spectra were determined for the specimen of Nb-doped TiO_2 containing 0.18 at% Nb and 0.018 at% Nb after polishing as well as after annealing at 1273 K in the gas phase of controlled oxygen activity. The data for the as-polished specimen is considered as reference data reflective of the initial surface and bulk composition.

The spectra for the specimen containing 0.18 at% Nb are shown in **Figure 10-5a** along with the spectrum of gold. The data related to non-equilibrium sputtering (associated with the gold layer and demarcated by the solid vertical line) has not been taken into account. Therefore, only the part of the spectra to the right side of the vertical line is considered as meaningful and in terms of the oxide lattice. Consequently, the depth scale is related to the solid vertical line that is marked as d = 0.

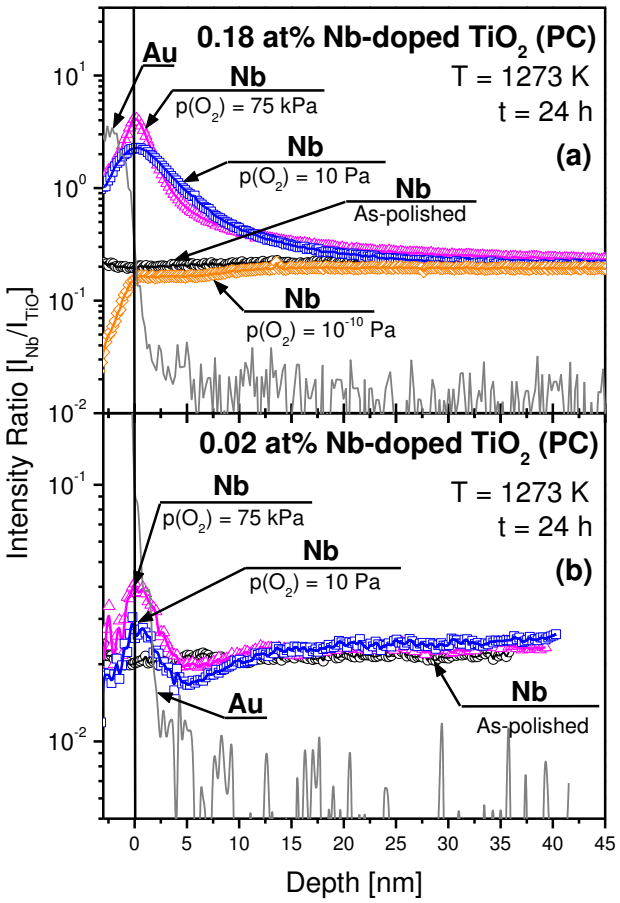

Figure 10-5. SIMS depth profile for Nb-doped TiO_2, including specimens containing 0.18 at% (a) and 0.02 at% (b) Nb, in terms of the intensity ratio of Nb/TiO secondary for the as-polished (reference) specimen, and specimens annealed in the gas phase of $p(O_2)$ = 75 kPa, $p(O_2)$ = 10 Pa and $p(O_2) = 10^{-10}$ Pa (the profile for Au has also been indicated).

The depth profiles shown in **Figure 10-5** indicate that:

- The highest intensity ratio of Nb/TiO at the surface (d = 0) is observed for the specimen annealed at $p(O_2)$ = 75 kPa. The related enrichment factor, in terms of ion intensities, is f = 21.6. This intensity ratio converges with the spectrum for the as-polished specimen (reflecting bulk composition) at d = 30 nm. This can be considered as the thickness of the segregation-induced surface layer at 1273 K and $p(O_2)$ = 75 kPa.
- The Nb/TiO intensity ratio for the specimen annealed at $p(O_2)$ = 10 Pa at d = 0 is slightly lower. The related enrichment factor is f = 12.1. As seen, the segregation-induced enrichment is reduced to the bulk level at d = 30 nm.
- The Nb/TiO depth profile for the specimen annealed at $p(O_2) = 10^{-10}$ Pa indicates that the surface layer is impoverished in niobium. The related enrichment factor of f = 0.3 is reflective of the reduced concentration of niobium at the surface.

- The SIMS depth profile for 0.018 at% Nb-doped TiO_2 (**Figure 10-5b**), essentially confirms the effects established for the specimen involving 0.18 at% Nb.

10.4.3. X-Ray Photoelectron Spectroscopy

Figure 10-6 represents the XPS spectra for the Nb-doped TiO_2 specimen containing 0.18 at% Nb, including the reference (as-polished) specimen and the annealed specimens. The related concentration data are shown in **Table 10-2**. As seen, the specimen annealed in oxygen and in argon exhibit a surface enrichment factor of f = 15.7 and f = 13.1, respectively. On the other hand, the concentration of niobium in the surface layer of the specimen annealed in strongly reducing conditions is 0.05 at%. The related enrichment factor (f = 0.3) indicates that the surface is impoverished in niobium. As seen, the XPS data are in a good agreement with the SIMS data in terms of the effect of oxygen activity on surface enrichment with niobium.

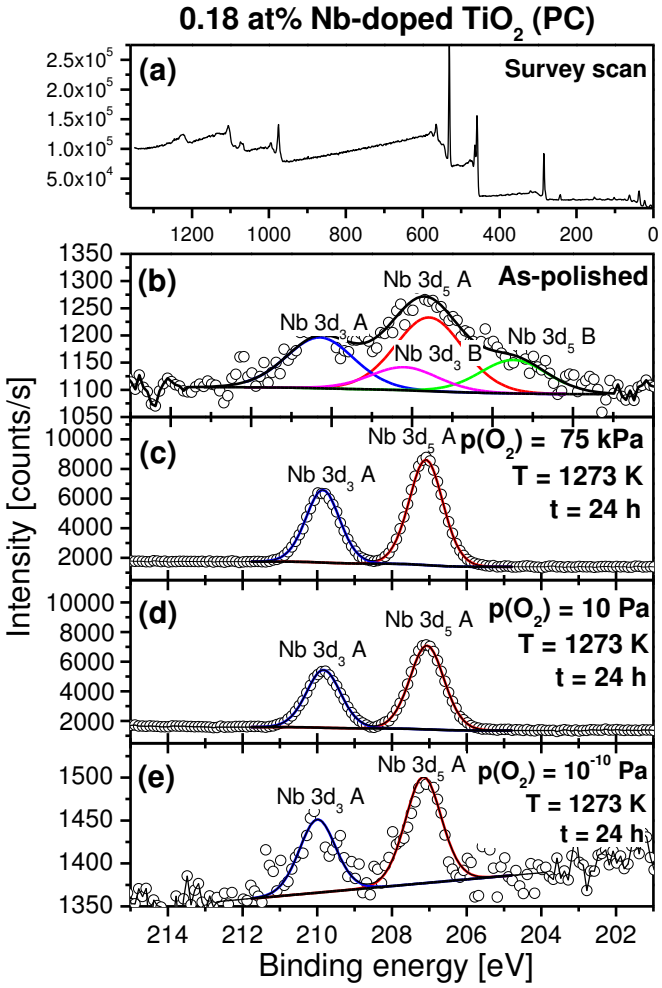

Figure 10-6. XPS intensity vs. binding energy spectra for Nb-doped TiO_2 (0.18 at% Nb) including the survey scan for (a) as-polished (reference) specimen, and elemental region scans for (b) as-polished specimen, (c) annealed in the gas phase of $p(O_2)$ = 75 kPa, and (c) $p(O_2)$ = 10 Pa, and (d) $p(O_2) = 10^{-10}$ Pa.

10.4.4. Rutherford Backscattering

Figure 10-7 represents the RBS spectra for the Nb-doped TiO_2 (0.18 at% Nb) specimens. Each of the spectra show the full backscattered energy range for the specimens annealed in the gas phase of different oxygen activity as well as the reference specimen. The data points represent the experimental data and the solid lines represent the simulated data fits obtained with SIMNRA (the backscattered energy steps at 740 keV, 1440 keV and 1690 keV correspond to oxygen, titanium and niobium, respectively). The insert plots provide an expanded view of the energy region related to niobium. The region of interest (shaded areas) corresponds to the depth of 61 nm. As seen in **Figure 10-7a**, the niobium concentration for the as-polished specimen is 0.19 at%. This concentration is consistent with the bulk content of niobium determined by PIXE (0.18 at%). As seen in **Figure 10-7b** and **Figure 10-7c**, the niobium-related peaks in the shaded areas indicate that niobium concentration for the specimens annealed at $p(O_2)$ = 75 kPa and $p(O_2)$ = 10 Pa is elevated to the level of 0.31 at% and 0.32 at%, respectively. On the other hand, annealing in strongly reducing conditions, $p(O_2) = 10^{-10}$ Pa (**Figure 10-7d**), results in a slight impoverishment of niobium to the level of 0.16 at% (the related concentration data are in **Table 10-2**). While the RBS data are less accurate than those related to XPS and SIMS, these results are well consistent.

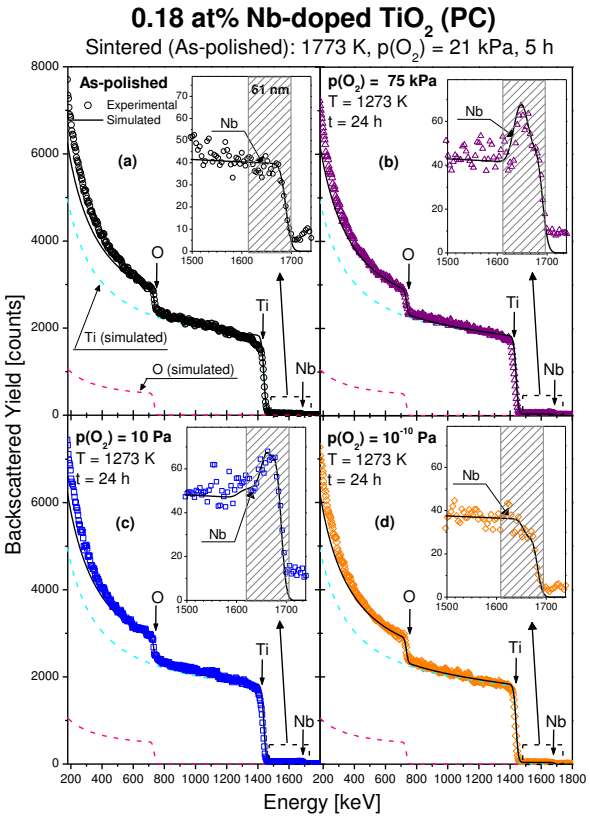

Figure 10-7. RBS yield vs. energy spectra for Nb-doped TiO_2 (0.18 at% Nb) specimens: (a) as-polished (reference), (b) annealed in the gas phase of $p(O_2)$ = 75 kPa, (c) annealed in the gas phase of 10 Pa, (d) annealed in the gas phase of 10^{-10} Pa.

10.4.5. Segregation Induced Enrichment – Comparison of Niobium and Indium

The comparison of segregation data for niobium, studied in this work, and indium, studied previously [14], may be considered in terms of the effect of charge and size of these two ions. Niobium in the lattice site of TiO_2 has a positive charge. However, indium may be incorporated both in the lattice sites and interstitial sites. Then its effective charge is negative and positive, respectively. The ionic radii for niobium (Nb^{5+}) and indium (In^{3+}) are 0.07 nm and 0.081 nm, respectively, while the ionic radius for titanium (Ti^{4+}) is 0.068 nm. Therefore, indium is expected to have much stronger driving force for segregation due to the miscibility reason.

According to SIMS data, the thickness of the surface layer enriched in niobium is in the range of 20 nm – 30 nm (**Figure 10-5**). On the other hand, the thickness of the segregation-enriched surface layer for In-doped TiO_2 is 60 nm. The SIMS-related enrichment of TiO_2 in niobium is f = 21.6 and f = 12.1 in oxygen and argon, respectively. However, the respective enrichment factors for indium are substantially larger (f = 486.1 and f = 85.3). These enrichment factors, which are reflective of the outermost surface layer, are consistent with the ionic radii of niobium

and indium compared to that of titanium. The observed huge enrichment factor of indium in the outermost surface layer is considered in terms of a low-dimensional surface structure for In-doped TiO_2 and associated SIMS matrix effect. The enrichment factor for Nb-doped TiO_2 is substantially smaller, however, the related concentration of niobium in the surface layer (> 2 at% Nb) is substantially larger than the critical concentration of 0.1 at% above which defects form larger aggregates [29].

The XPS average enrichment of niobium within 6 nm is f = 15.7 and f = 13.1 at 75 kPa and 10 Pa, respectively (**Figure 10-6**). At the same time, the XPS-related enrichment for indium is comparable (f = 10.2 and f = 9.0, respectively).

The RBS-related enrichments factors are markedly lower (f = 1.7 and f = 1.8 at 75 kPa and 10 Pa, respectively) indicating that the concentration of niobium exhibits a substantial drop within 60 nm distance from the surface (**Figure 10-7**). The enrichment data obtained in the present work for niobium are summarized in **Figure 10-8**.

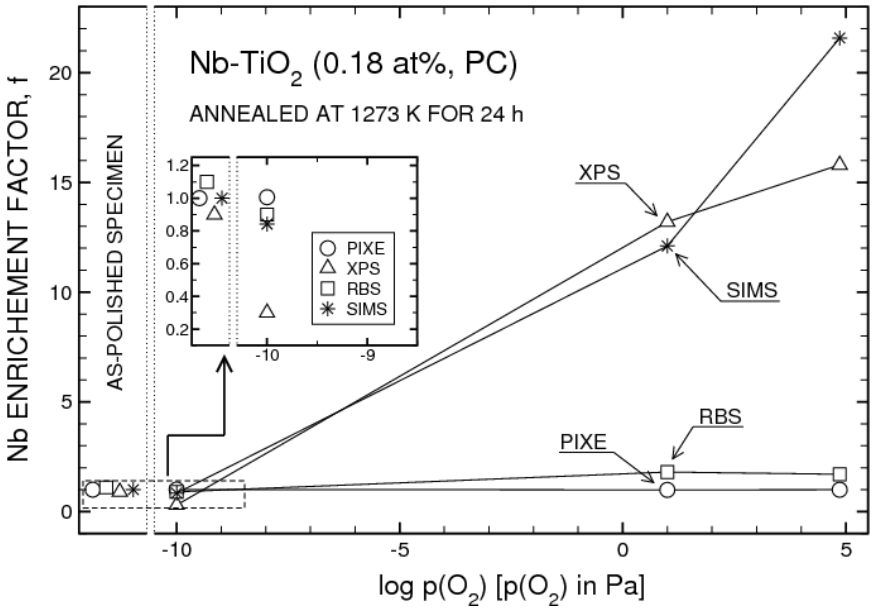

Figure 10-8. The effect of oxygen activity on the segregation-induced enrichment factor of niobium reflective of different analytical techniques.

10.4.6. Theoretical Model

10.4.6.1. Effect of Defect Disorder on Niobium Segregation

The reported effects related to niobium segregation may be considered in terms of defect disorder and the related charge neutrality requirement of the Nb-dopedTiO_2 lattice in the bulk and at the surface.

It has been documented that the full charge neutrality condition for Nb-dopedTiO_2 requires compensation of negatively charged defects (titanium vacancies and electrons) by positively charged defects (niobium ions in titanium sites and oxygen vacancies):

$$4[V_{Ti}^{''''}] + n = [Nb_{Ti}^{\bullet}] + 2[V_O^{\bullet\bullet}] \qquad \textbf{(10-15)}$$

where n denotes the concentration of electrons (the concentration of electron holes can be ignored in this case). The increase of oxygen activity results in a rapid imposition of an increased concentration of titanium vacancies [30]. These defects are initially localized at the surface. However, due to their extremely slow diffusion rate, these defects do not penetrate the bulk phase within the time frame of the experimental conditions reported in this work (24 hours, 1273 K) [30]. Therefore, these defects may be considered as quenched at the surface resulting in the formation of a quasi-isolated surface layer that is charged negatively (compared to the bulk phase). In consequence, the increase of oxygen activity in the gas phase leads to the imposition of a negative surface charge. The resulting electric field is the predominant force driving the segregation of positively charged niobium ions.

The bulk phase of Nb-doped TiO_2 may be considered as an ideal solid solution involving niobium ions distributed randomly. However, the observed enrichment of the surface layer in niobium results in substantial interactions between the defects within this layer leading to the formation of larger defect aggregates [29]:

$$4Nb_{Ti}^{\bullet} + V_{Ti}^{''''} \rightarrow \{4Nb_{Ti}^{\bullet}V_{Ti}^{''''}\}^{x} \qquad \textbf{(10-16)}$$

These complexes are the precursors for a new low dimensional surface structure, which is formed when the concentration of defects surpasses a critical concentration [29]. The effect of surface charging by the imposition of titanium vacancies at the surface is represented in **Figure 10-9a**.

The decrease of oxygen activity, resulting in imposition of a strongly reducing environment, leads to a decrease in the concentration of titanium vacancies and a decrease in negative surface charge. Consequently, the surface layer in a strongly reducing environment is mainly enriched in oxygen vacancies. Strong interactions between these defects are expected to result in the formation of a low-dimensional surface structure, similar to Magneli type structures [31]. The effect of this structure on desegregation of niobium is shown in **Figure 10-9b**.

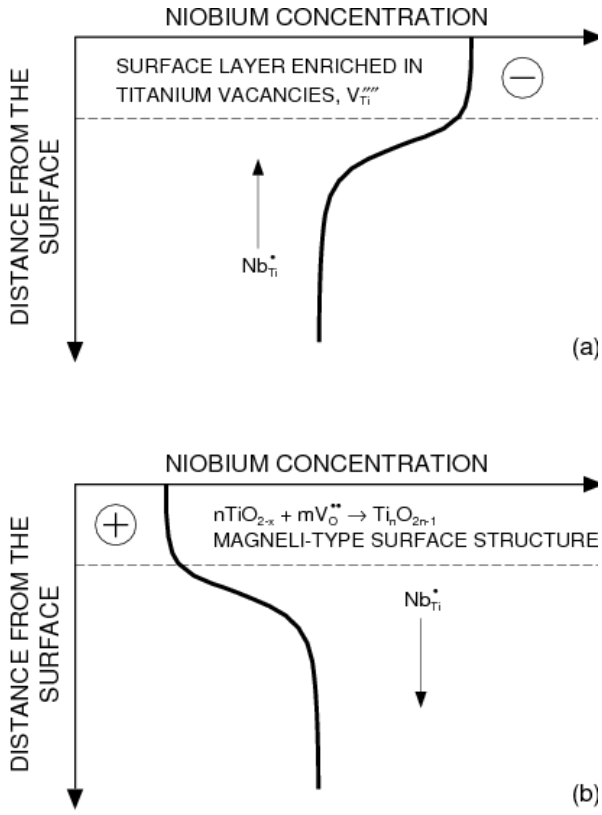

Figure 10-9. Schematic representation of niobium surface segregation in oxidising environment (a) and desegregation in strongly reducing environment (b)

10.4.6.2. Depth Resolved XPS Analysis in Strongly Reducing Conditions

The surface analysis of In-doped TiO_2 in strongly reducing conditions indicate that while indium segregates to the surface, resulting in initial strong surface enrichment, prolonged annealing (> 24 h) leads to a slow decrease in the segregation-induced enrichment due to evaporation [32,33]. Therefore, in strongly reducing conditions the segregation equilibrium cannot be reached due to indium evaporation. Consequently, the segregation-induced enrichment for In-doped TiO_2 is a compromise between evaporation and segregation, the latter phenomenon having much stronger effect on surface composition at low oxygen activities.

The effect of evaporation on surface composition of Nb-doped TiO_2 appears to be much smaller because the partial pressure of niobium oxide vapour over its solid phase is substantially lower (**Figure 10-10**) [34]. As seen, the difference at 1273 K is approximately 10 orders of magnitude. Nevertheless, it seems interesting to determine the effect of the strongly reducing environment on the concentration of niobium at the very initial stage of annealing in order to assess the extent of the desegregation phenomenon.

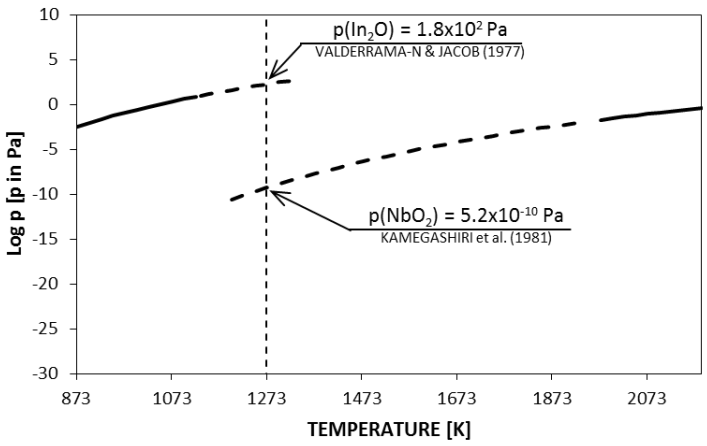

Figure 10-10. The temperature dependence of the partial pressure of indium and niobium oxides [33,34].

The effect of annealing in a strongly reducing environment on surface composition was examined using XPS surface analysis for the 0.18 at% specimen after only 30 min of annealing at 1273 K and again after a surface layer of 20 nm thick was removed by Ar^+ sputtering. As seen in **Figure 10-11**, a substantial effect of desegregation is observed already within 30 min. This result indicates that desegregation is induced by low the oxygen activity in the strongly reducing conditions. In other words, the imposition of strongly reducing conditions does not result in an initial increase of the solute concentration as has been observed for In-doped TiO_2.

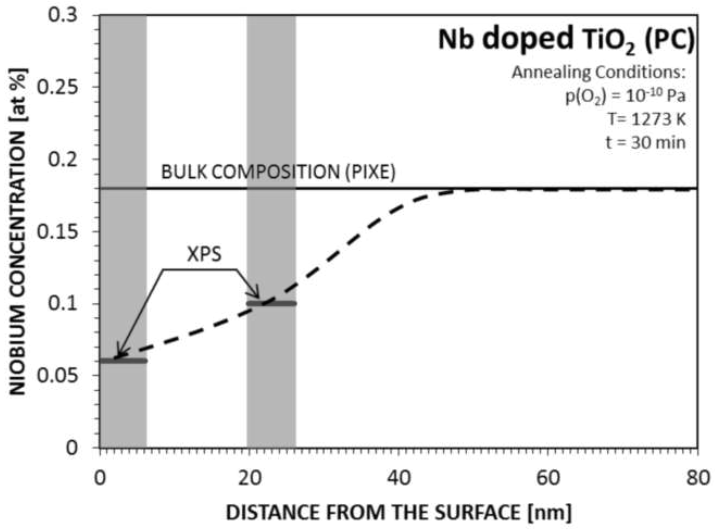

Figure 10-11. The results of XPS analysis of the Nb-doped TiO_2 specimen involving 0.18 at% Nb after 30 min annealing at 1273 K and after subsequent removal of 20 nm thick surface layer with Ar^+ sputtering.

10.4.6.3. Impact on Applications

The established effects related to niobium segregation in Nb-doped TiO_2 have an impact on a wide range of applications, which are directly or indirectly related to solar energy conversion. It has been documented that the conversion efficiency solar energy into chemical energy is determined by several key performance-related properties, including, (i) charge transport, (ii) electronic structure and band gap, (iii) flat band potential and (iv) reactivity-related surface active sites [27].

10.4.6.4. Charge Transport

Pure TiO_2 is theoretically an n-type semiconductor. However, its conduction level at room temperature is so low that TiO_2 may also be considered as a good insulator. Consequently, its performance in energy conversion is low due to substantial energy losses related to charge transport. This performance may be enhanced substantially by doping TiO_2 with donors, such as niobium. Since the donor level of niobium is close to the bottom of the conduction band, its ionisation leads to a substantial increase in conduction. The effect of niobium on the electrical conductivity of TiO_2 is shown in **Figure 10-12**. As seen, the effect of niobium on conduction is substantial.

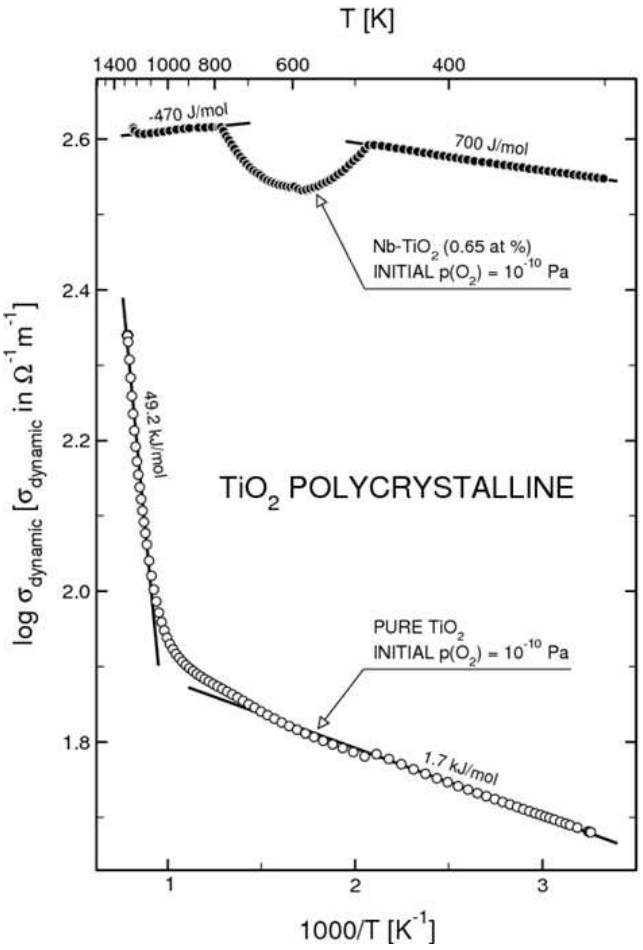

Figure 10-12. Arrhenius plot of the electrical conductivity of both pure TiO_2 and Nb-doped TiO_2 [13].

10.4.6.5. Electronic Structure

The incorporation of a high concentration of niobium into the TiO_2 lattice results in the formation of a local band. As a result, the light-induced ionization occurs via the apparent band gap between the valence band and the niobium-related band. Yang et al. [35] have shown that the incorporation of niobium into TiO_2 results in band gap reduction from 3.1 eV for pure TiO_2 to 2.9 eV for Nb-doped TiO_2 (5 at% Nb).

10.4.6.6. Flat Band Potential

The segregation-induced enrichment of Nb at the surface is substantial. The resulting electrical potential gradient can be determined from the following relation:

$$\frac{C_1}{C_2} = \exp(-ez\Psi / kT) \qquad \textbf{(10-17)}$$

where C1 and C2 denote the surface and bulk concentration, respectively, e is the elementary charge, ψ is electrical potential, z is the valence, k is Boltzman constant and T is the absolute

temperature. The effect of the segregation/desegregation-induced enrichment factor, determined by XPS and SIMS, and the related electric field are shown in **Table 10-3**. The sign + and – are reflective of the field polarity.

Table 10-3. The enrichment (depletion) coefficients of the surface layer in niobium and the related electric fields

XPS		**SIMS**	
F	**V/m**	***f***	**V/m**
15.8	-2.9×10^6	21.6	-3.2×10^6
13.8	-2.7×10^6	12.1	-2.6×10^6
0.3	1.2×10^6	0.84	1.8×10^5

The effect of the segregation-induced electric field on charge separation depends on surface vs. bulk electric charge and the related direction of this vector quantity. The surface composition effect on surface vs. bulk polarity is schematically represented in **Figure 10-13** within the following scenarios:

- The surface is enriched in titanium vacancies (**Figure 10-13a**). This scenario, which is valid in an oxidising environment, results in the formation of a negative surface charge. The latter is the driving force for niobium surface segregation and the transport of electron holes towards the surface. Therefore, the surface of Nb-doped TiO_2 in oxidising conditions exhibits anodic properties assuming that the applied annealing procedure results in the imposition of titanium vacancies while the transport of niobium is quenched.
- The imposition of segregation equilibrium in oxidising conditions leads to surface enrichment in niobium. This results in the imposition of a positive surface charge. In this case, the resulting electric field is the driving force for the transport of electrons to the surface and electron holes towards the bulk phase as shown in **Figure 10-13b**. The surface layer formed in these conditions exhibits cathodic properties.
- The imposition of reducing conditions results in niobium desegregation and impoverishment of the surface in niobium compared with the bulk phase as represented by **Figure 10-13c**. The resulting negative surface charge is the driving force for the transport of electron holes towards the surface leading to imposition of an anodic potential.

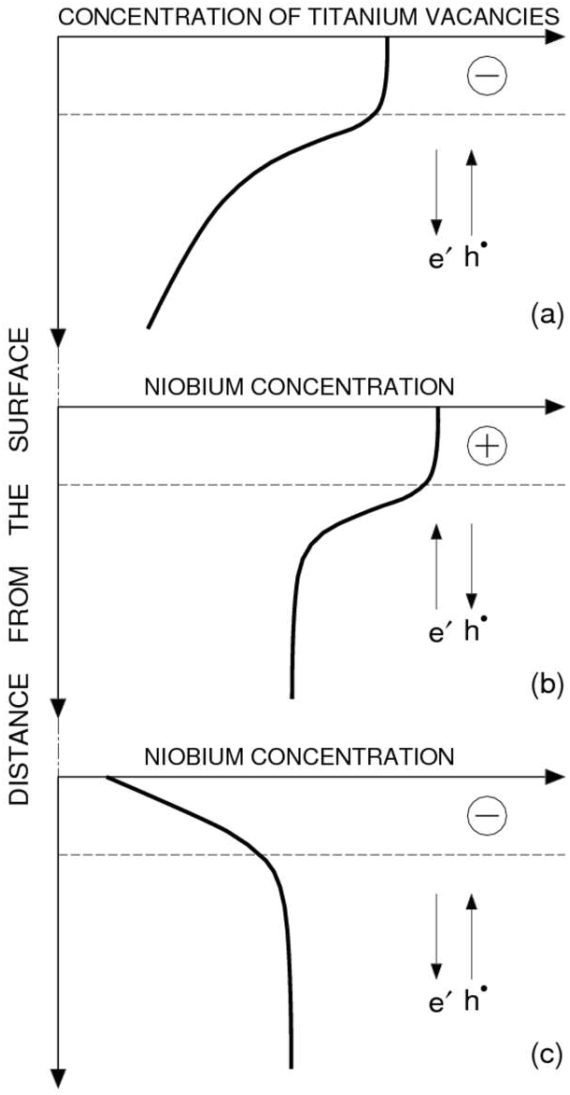

Figure 10-13. Schematic representation of three scenarios for surface vs. bulk properties and the related electric field for Nb-doped TiO_2 (a) the surface enriched in titanium vacancies in oxidising conditions - before niobium segregation, (b) surface enriched in niobium in oxidising conditions, and (c) surface depleted in niobium in strongly reducing conditions.

10.4.6.7. Reactivity-Related Surface Active Sites

The prerequisite for TiO_2 surface reactivity with water requires the adsorption of water molecules. It has been shown that titanium vacancies are the active sites required for the formation of the active complex [36].

10.5 Conclusions

Niobium has a strong tendency to segregate to the surface of TiO_2 in oxidising conditions. The predominant driving force for positively charged niobium segregation is a negatively charged surface layer predominantly enriched in titanium vacancies. It has been documented

that the imposition of strongly reducing conditions results in the impoverishment of niobium at the surface (desegregation). The predominant driving force for desegregation is the positive surface charge related to a Magneli-type surface structure. The resulting electrostatic interactions lead to the departure of positively charged niobium ions toward the bulk phase. The obtained data indicate that annealing in the gas phase of controlled oxygen activity may be used to engineer the surface composition of Nb-doped TiO_2.

10.6 References

(1) Fujishima, A.; Honda, K. "Electrochemical Photolysis of Water at a Semiconductor Electrode". Nature (1972), 238, 37-38.

(2) Linsebigler, A. L.; Lu, G.; Yates, J. T. J. "Photocatalysis of TiO_2 Surfaces: Principles, Mechanisms, and Selected Results". Chem. Rev. (1995), 95, 735-758.

(3) Carp, O.; Huisman, C. L.; Reller, A. "Photoinduced reactivity of titanium dioxide". Progress in Solid State Chemistry (2004), 32, 33-177.

(4) Wynblatt, P.; McCune, R. C. Surface Segregation in Metal Oxides. In Surface and Near-Surface Chemistry of Oxide Materials; Elsevier Science Publishers, (1988); pp 247-279.

(5) Burggraaf, A. J.; Winnubst, A. J. A. Segregation in Oxide Surfaces, Solid Electrolytes and mixed Conductors. In Surface and Near-Surface Chemistry of Oxide Materials; Elsevier: Amsterdam, (1988); pp 448-477.

(6) Cabane, J.; Cabane, F. Equilibrium segregation in interfaces. In Interface segregation and related processes in materials; Nowotny, J., Ed.; Trans Tech Publications Ltd.: Zurich, (1991); pp 1-150.

(7) Leygraf, C.; Hultquis, G.; Ekelund, S.; Eriksson, J. C. "Surface composition studies of (100) and (110) faces of monocrystalline $Fe_{84}Cr_{16}$". Surf. Sci. (1974), 46, 157-176.

(8) Kuijers, F. J.; Ponec, V. "The surface composition of the nickel-copper alloy system as determined by Auger electron spectroscopy". Surf. Sci. (1977), 68 [0], 294-304.

(9) Rolland, A.; Aufray, B. "Superficial composition in binary solid solutions A(B): Drastic effect of pure element surface tensions". Surf. Sci. (1985), 162 [1-3], 530-537.

(10) Nowotny, J. Inteface defect chemistry and its impact on properties of oxide ceramic materials. In Science of Ceramic Interfaces; Nowotny, J., Ed.; Elsevier Science Publishers B.V., (1991); pp 79-204.

(11) Baumard, J. F.; Tani, E. "Thermoelectric-Power in Reduced Pure and Nb-Doped TiO_2 Rutile at High-Temperature". Physica Status Solidi a-Applied Research (1977), 39 [2], 373-382.

(12) Baumard, J. F.; Tani, E. "Electrical-conductivity and charge compensation in Nb doped TiO_2 rutile ". J. Chem. Phys. (1977), 67 [3], 857-860.

(13) Nowotny, J. Oxide Semiconductors for Solar Energy Conversion; CRC Press, 2012.

(14) Atanacio, A. J.; Bak, T.; Nowotny, J. "Effect of Indium on the Surface versus Bulk Chemistry for Indium-Doped TiO_2". Applied Materials and Interfaces (2012), In Print.

(15) Akiyama, K.; Toyama, N.; Muraoka, K.; Tsunashima, M. "Configurational observation of titanium oxide pigment particles". Journal of the American Ceramic Society (1998), 81 [4], 1071-1073.

(16) Atashbar, M. Z.; Sun, H. T.; Gong, B.; Wlodarski, W.; Lamb, R. "XPS study of Nb-doped oxygen sensing TiO_2 thin films prepared by sol-gel method". Thin Solid Films (1998), 326 [1], 238-244.

(17) Tsunashima, M.; Muraoka, K.; Akiyama, K.; Toyama, N. "Relationships between particle properties and pigment characteristics of nb containing TiO_2". Shikizai kyokaishi (In Japanese) (1998)[71], 297-304.

(18) Zaitsev, S. V.; Moon, J.; Takagi, H.; Awano, M. "Preparation and characterization of nanocrystalline doped TiO_2". Advanced Powder Technology (2000), 11 [2], 211-220.

(19) Ruiz, A. M.; Dezanneau, G.; Arbiol, J.; Cornet, A.; Morante, J. R. "Insights into the structural and chemical modifications of Nb additive on TiO_2 nanoparticles". Chemistry of Materials (2004), 16 [5], 862-871.

(20) Pang, Y.; Wynblatt, P. "Correlation between grain-boundary segregation and grain-boundary plane orientation in Nb-doped TiO_2". Journal of the American Ceramic Society (2005), 88 [8], 2286-2291.

(21) Black, J. R.; Kingery, D. W. "Segregation of Aliovalent Solutes Adjacent Surfaces in MgO". Journal of the American Ceramic Society (1979), 62, 176-178.
(22) Sikora, I.; Stolze, F.; Hirschwald, W. "Segregation of chromium in CoO-Cr_2O_3 solid-solutions and $CoCr_2O_4$ spinel phases studied by SIMS and ESCA ". Surface and Interface Analysis (1987), 10 [8], 424-429.
(23) Bernasik, A.; Rekas, M.; Sloma, M.; Weppner, W. "Electrical surface versus bulk properties of Fe-doped TiO_2 single crystals". Solid State Ion. (1994), 72 [Part 2], 12-18.
(24) Sheppard, L. R.; Bak, T.; Nowotny, J.; Nowotny, M. K. "Effect of Oxygen Activity on Niobium Segregation in Niobium-Doped Titanium Dioxide". Journal of the Australian Ceramic Society (2008), 44 [2], 42-46.
(25) Diebold, U. "The surface science of titanium dioxide". Surface Science Reports (2003), 48, 53-229.
(26) Sheppard, L. R.; Dittrich, T.; Nowotny, M. K. "The Impact of Niobium Surface Segregation on Charge Separation in Niobium-Doped Titanium Dioxide". Journal of Physical Chemistry C (2012), 116 [39], 20923-20929.
(27) Bak, T.; Nowotny, J.; Sucher, N. J.; Wachsman, E. "Effect of Crystal Imperfections on Reactivity and Photoreactivity of TiO_2 (Rutile) with Oxygen, Water, and Bacteria". The Journal of Physical Chemistry C (2011), 115 [32], 15711-15738.
(28) Solid State Physics; Kröger, F. A.; Vink, H. J., Eds.; Academic Press: New York, (1956); Vol. 3, pp 307.
(29) Stoneham, M. "Theory of Defect Processes". Physics Today (1980), 33, 34-37.
(30) Nowotny, M. K.; Bak, T.; Nowotny, J. "Electrical properties and defect chemistry of TiO_2 single crystal. IV. Prolonged oxidation kinetics and chemical diffusion". Journal of Physical Chemistry B (2006), 110 [33], 16302-16308.
(31) Magneli, A. "The Crystal Structures of Mo9O26 (Beta'-Molybdenum Oxide) and MO8O23 (Beta-Molybdenum Oxide)". Acta Chemica Scandinavica (1948), 2 [5-6], 501-517.
(32) Atanacio, A. J.; Nowotny, J.; Prince, K. E. "Effect of Oxygen Activity on Surface Composition of In-Doped TiO_2 at Elevated Temperatures". Journal of Physical Chemistry C (2012), 116 [36], 19246-19251.
(33) Valderrama-N, J.; Jacob, K. T. "Vapor pressure and dissociation energy of (In_2O)". Thermochimica Acta (1977), 21 [2], 215-224.
(34) Kamegashira, N.; Matsui, T.; Harada, M.; Naito, K. "Vaporization of Niobium Dioxide by Mass-Effusion and Mass-Spectrometric Methods". Journal of Nuclear Materials (1981), 101 [1-2], 207-216.
(35) Yang, J.; Zhang, X.; Wang, C.; Sun, P.; Wang, L.; Xia, B.; Liu, Y. "Solar photocatalytic activities of porous Nb-doped TiO_2 microspheres prepared by ultrasonic spray pyrolysis". Solid State Sciences (2012), 14 [1], 139-144.
(36) Nowotny, J.; Bak, T.; Nowotny, M. K.; Sheppard, L. R. "TiO_2 surface active sites for water splitting". Journal of Physical Chemistry B (2006), 110 [37], 18492-18495.

CHAPTER 11

Summary of Conclusions

The present thesis studied the phenomenon of segregation in TiO_2 for In^{3+} and Nb^{5+} as acceptor-type, and donor-type dopants, respectively. Specifically, it assessed the effect of the processing conditions, in terms of time, temperature and oxygen activity, on the enrichment of In^{3+} and Nb^{5+} dopants at the topmost- and near-surface layers of TiO_2 using the range of complementary analysis techniques XPS, SIMS, RBS and PIXE. The comprehensive study, reported as a series of 5 papers, can be summarised by the following key points:

- The minimum time required to establish equilibrium concentration at the surface of In-doped TiO_2 under oxidising conditions, $p(O_2)$ = 21 kPa, at 1273 K, was determined to be 20 h.
- It has been established that under the highly reducing gas phase conditions, $p(O_2) = 10^{-10}$ Pa, gas/solid equilibrium conditions cannot be established in In-doped TiO_2 due to a substantial amount of indium evaporation from the surface.
- The results of XPS, SIMS, and RBS analysis demonstrated that indium segregation to the surface in oxidising gas phase conditions, (pO_2) = 21 kPa and 10 Pa, is very substantial. It results in the removal of indium from titanium sites in the bulk phase where they are acceptor-type centres, and transports them to the surface where they are incorporated into interstitial sites, resulting in the formation of donor-type centres at the surface.
- The predominant driving force for the segregation of positively charged indium ions in In-doped TiO_2 was postulated in a derived model to be a negative surface charge caused by titanium vacancies formed within the surface layer in an oxidising gas phase environment.

- The derived model indicates that the segregation-induced surface concentration of In in In-doped TiO_2 in oxidising conditions is so high that interaction between the predominant point defects, titanium vacancies and indium interstitial ions, form negatively charged defect complexes which result in the formation of a low-dimensional surface structure and sub-surface layer. This structure exhibits outstanding properties.
- In the case of Nb, unlike indium it was established that Nb does not evaporate and equilibrium can therefore be established in both oxidising and reducing gas phase environments.
- It has been shown that in oxidising gas phase conditions, substantial Nb surface enrichment occurs in Nb-doped TiO_2. However, in reducing conditions Nb is instead transported from the surface into the bulk phase. This effect has been termed desegregation.
- The driving force for Nb desegregation under highly reducing gas phase conditions is a positive surface charge related to a Magneli-type surface structure. The resulting electrostatic interactions drive the departure of positively charged niobium ions toward the bulk phase. The experimental data indicate that annealing in the gas phase of controlled oxygen activity may be used to modify the surface composition and related properties of Nb-doped TiO_2 in a controlled manner.

The outcomes of this project, presented as a series of five individual but interrelated manuscripts contribute significantly to the understanding of segregation, particularly of In^{3+} and Nb^{5+}, on the surface vs. bulk chemistry of TiO_2. The results of this well-defined segregation study may be utilised for selecting the optimal processing conditions, in terms of temperature, time and oxygen activity, to generate specimens with specific acceptor- or donor-type surface vs. bulk compositions and related properties for improved performance in applications such as solar energy conversion or water purification.

APPENDIX 1

List of Refereed Publications

The following table provides the full list of my publications to date. The asterisks denote publications related to this thesis research area and published during this PhD candidature from 2006-2013.

		Year	Publication
1.		2002	Latella, B. A.; Atanacio, A. J.; Liu, T. S. "Fatigue damage mechanisms in CeO_2 stabilized tetragonal ZrO_2". J. Mater. Sci. Lett. (2002), 21 [11], 879-882.
2.		2002	Latella, B. A.; Liu, T.; Atanacio, A. J. "Effect of grain size on hertzian contact damage in 9 mol% Ce-TZP ceramics". J. European Ceram. Soc. (2002), 22 [12], 1971-1979.
3.		2005	Atanacio, A. J.; Latella, B. A.; Barbe, C. J.; Swain, M. V. "Mechanical properties and adhesion characteristics of hybrid sol-gel thin films". Surf. Coat. Technol. (2005), 192 [2-3], 354-364.
4.		2006	Losic, D.; Triani, G.; Evans, P. J.; Atanacio, A.; Mitchell, J. G.; Voelcker, N. H. "Controlled pore structure modification of diatoms by atomic layer deposition of TiO_2". J. Mater. Chem. (2006), 16 [41], 4029-4034.
5.	*	2006	Sheppard, L. R.; Atanacio, A.; Bak, T.; Nowotny, J.; Prince, K. E. Effect of niobium segregation on the surface properties of titanium dioxide. In Solar hydrogen and nanotechnology; Vayssieres, L., Ed.; Spie-Int Soc Optical Engineering: Bellingham, (2006); Vol. 6340; pp U298-U306.
6.	*	2007	Sheppard, L. R.; Atanacio, A. J.; Bak, T.; Nowotny, J.; Prince, K. E. "Bulk diffusion of niobium in single-crystal titanium dioxide". Journal of Physical Chemistry B (2007), 111 [28], 8126-8130.
7.		2007	Low, I. M.; Wren, E.; Prince, K. E.; Atanacio, A. "Characterisation of phase relations and properties in air-oxidised Ti_3SiC_2". Mater. Sci. Eng. A-Struct. Mater. Prop. Microstruct. Process. (2007), 466 [1-2], 140-147.
8.	*	2007	Sheppard, L. R.; Zhou, M. F.; Atanacio, A.; Bak, T.; Nowotny, J.; Prince, K. E. "Determination of niobium diffusion in titania and zirconia using secondary ion mass spectrometry". Adv. Appl. Ceram. (2007), 106 [1-2], 89-94.
10.		2007	Roest, R.; Atanacio, A. J.; Latella, B. A.; Wuhrer, R.; Ben-Nissan, B. "An investigation of sol gel coated zirconia thin films on anodized titanium substrate by secondary ion mass spectrometry and scanning electron microscopy". Materials Forum (2007), 31, 160-163.
11.		2008	Tsen, G. K. O.; Sewell, R. H.; Atanacio, A. J.; Prince, K. E.; Musca, C. A.; Dell, J. M.; Faraone, L. "Incorporation and activation of arsenic in MBE-grown HgCdTe". Semicond. Sci. Technol. (2008), 23 [1], 1-6.

12.	*	2008	Wang, X. D.; Mitchell, D. R. G.; Prince, K.; Atanacio, A. J.; Caruso, R. A. "Gold nanoparticle incorporation into porous titania networks using an agarose gel templating technique for photocatalytic applications". Chemistry of Materials (2008), 20 [12], 3917-3926.
13.		2008	Johnson, B. C.; Atanacio, A. J.; Prince, K. E.; McCallum, J. C. Boron enhanced h diffusion in amorphous si formed by ion implantation. In Doping engineering for front-end processing; Pawlak, B. J., Pelaz, M. L., Law, M., Suguro, K., Eds., (2008); Vol. 1070; pp 211-216.
14.		2009	Chuong L. Nguyen, Armand Atanacio, Wei Zhang, Kathryn E. Prince, Margaret M. Hyland, James B. Metson. Phase-oriented surface segregation in an aluminium casting alloy. Applied Surface Science (2009), 225, 4880-4885.
15.		2009	Sabri, Y. M.; Ippolito, S. J.; Tardio, J.; Atanacio, A. J.; Sood, D. K.; Bhargava, S. K. "Mercury diffusion in gold and silver thin film electrodes on quartz crystal microbalance sensors". Sens. Actuator B-Chem. (2009), 137 [1], 246-252.
16.		2009	Johnson, B. C.; McCallum, J. C.; Atanacio, A. J.; Prince, K. E. "Intrinsic and boron-enhanced hydrogen diffusion in amorphous silicon formed by ion implantation". Appl. Phys. Lett. (2009), 95 [10], 101911-101913.
17.	*	2009	Sheppard, L. R.; Atanacio, A. J.; Bak, T.; Nowotny, J.; Nowotny, M. K.; Prince, K. E. "Niobium diffusion in niobium-doped titanium dioxide". J. Solid State Electrochem. (2009), 13 [7], 1115-1121.
18.		2009	Partridge, J. G.; Field, M. R.; Sadek, A. Z.; Kalantar-zadeh, K.; Du Plessis, J.; Taylor, M. B.; Atanacio, A.; Prince, K. E.; McCulloch, D. G. "Fabrication, structural characterization and testing of a nanostructured tin oxide gas sensor". IEEE Sens. J. (2009), 9 [5-6], 563-568.
19.		2009	Jisheng Han, Sima Dimitrijev, Fred Kong, and Armand Atanacio. "SIMS investigation on the 3C-SiC on Si". Journal of Material Science and Engineering (2009) 3[8], 15-17.
20.	*	2011	Atanacio, A. J.; Nowotny, J.; Prince, K. E. "Reactivity between In_2O_3 and TiO_2 (rutile) studied using secondary ion mass spectrometry (sims)". Sep. Purif. Technol. (2012), 91, 96-102.
21.		2012	Cohen, D. D.; Crawford, J.; Stelcer, E.; Atanacio, A. "A new approach to the combination of iba techniques and wind back trajectory data to determine source contributions to long range transport of fine particle air pollution". Nuclear Instruments & Methods in Physics Research Section B-Beam Interactions with Materials and Atoms (2012), 273, 186-188.
22.		2012	Ionescu, M.; Winton, B.; Wexler, D.; Siegele, R.; Deslantes, A.; Stelcer, E.; Atanacio, A.; Cohen, D. D. "Enhanced biocompatibility of pdms (polydimethylsiloxane) polymer films by ion irradiation". Nuclear Instruments & Methods in Physics Research Section B-Beam Interactions with Materials and Atoms (2012), 273, 161-163.
23.		2012	Cohen, D. D.; Crawford, J.; Stelcer, E.; Atanacio, A. J. "Application of positive matrix factorisation, multi-linear engine and back trajectory techniques to the quantification of coal-fired power station pollution in metropolitan sydney". Atmospheric Environment (2012), 61, 204.

24.		2012	Sabri, Y. M.; Ippolito, S. J.; Atanacio, A. J.; Bansal, V.; Bhargava, S. K. "Mercury vapor sensor enhancement by nanostructured gold deposited on nickel surfaces using galvanic replacement reactions". J. Mater. Chem. (2012), 22 [40], 21395-21404. (This paper was featured as the journal cover image)
25.	*	2012	Atanacio, A. J.; Nowotny, J.; Prince, K. E. "Effect of oxygen activity on surface composition of in-doped TiO_2 at elevated temperatures". Journal of Physical Chemistry C (2012), 116 [36], 19246-19251.
26.	*	2012	Atanacio, A. J.; Bak, T.; Nowotny, J. "Effect of indium on the surface versus bulk chemistry for indium-doped TiO_2". Applied Materials and Interfaces (2012) DOI: 10.1021/am301729z
27.	*	2013	Atanacio A. J., Bak T., Nowotny J., Prince K. E. "Diffusion Kinetics of Indium ion TiO_2 Single Crystal". Journal of the American Ceramic Society (2013) DOI: 10.1111/jace.12244
28.	*	2013	Atanacio, A. J., Bak, T., Nowotny, J. "Effect of Niobium Segregation on Surface Chemistry and the Related Electric Field Light-Induced Charge Carrier Separation in Nb-Doped TiO_2". Journal of the American Chemical Society (2012) In submission.